Application-Specific Calibration of Condensation Particle Counters under Low Pressure Conditions

Oliver Bernhard Felix Bischof

Energie & Umwelt / Energy & Environment
Band / Volume 579
ISBN 978-3-95806-629-8

Mitglied der Helmholtz-Gemeinschaft

JÜLICH
Forschungszentrum

Schriften des Forschungszentrums Jülich
Reihe Energie & Umwelt / Energy & Environment Band / Volume 579

Forschungszentrum Jülich GmbH
Institut für Energie- und Klimaforschung
Troposphäre (IEK-8)

Application-Specific Calibration of Condensation Particle Counters under Low Pressure Conditions

Oliver Bernhard Felix Bischof

Schriften des Forschungszentrums Jülich
Reihe Energie & Umwelt / Energy & Environment Band / Volume 579

ISSN 1866-1793 ISBN 978-3-95806-629-8

Bibliografische Information der Deutschen Nationalbibliothek.
Die Deutsche Nationalbibliothek verzeichnet diese Publikation in der
Deutschen Nationalbibliografie; detaillierte Bibliografische Daten
sind im Internet über http://dnb.d-nb.de abrufbar.

Herausgeber und Vertrieb:	Forschungszentrum Jülich GmbH Zentralbibliothek, Verlag 52425 Jülich Tel.: +49 2461 61-5368 Fax: +49 2461 61-6103 zb-publikation@fz-juelich.de www.fz-juelich.de/zb
Umschlaggestaltung:	Grafische Medien, Forschungszentrum Jülich GmbH
Titelbild:	© Dr. Julie Cozic, September 2005 „Fascinating cloud formations on Jungfraujoch, Switzerland.“
Druck:	Grafische Medien, Forschungszentrum Jülich GmbH
Copyright:	Forschungszentrum Jülich 2022

Schriften des Forschungszentrums Jülich
Reihe Energie & Umwelt / Energy & Environment, Band / Volume 579

D 82 (Diss. RWTH Aachen University, 2021)

ISSN 1866-1793
ISBN 978-3-95806-629-8

Vollständig frei verfügbar über das Publikationsportal des Forschungszentrums Jülich (JuSER)
unter www.fz-juelich.de/zb/openaccess.

Abstract

Condensation Particle Counters (CPC) are research instruments that are commonly used to measure fine, airborne particles. They are able to determine the particle number concentration of both, the smallest nanoparticles and also larger particles in the accumulation mode, which cannot be measured with optical methods at all or with sufficient accuracy. In the last four decades, CPCs have been increasingly used to determine particle number concentrations also at non-standard atmospheric pressure in both scientific research as well as for regulatory purposes. Measurement conditions at reduced pressure require a dedicated calibration of the CPCs to ensure correct results. The aim of my thesis was to investigate the performance of CPCs at various levels of low-pressure by means of a comprehensive and detailed calibration study.

In the first part, this thesis reviews details of the CPC technology, explains applications with a need for low-pressure calibration and presents an extensive literature review of the field. It provides a critical analysis of the papers most relevant to this research, building on a survey of more than 60 peer-reviewed publications from the past forty years. The literature review points to contradictions in the understanding of the behavior of CPCs at low pressure and highlights opposing findings. In a subsequent section, a numerical model is applied to investigate how reduced pressure conditions impact CPC performance in theory. The model delivers a prediction of CPC counting efficiencies as well as d_{90}, d_{50} and d_{10} cut-sizes at various levels of reduced pressure.

The second part of this thesis describes extensive laboratory experiments and provides a detailed analysis of the performance at reduced pressure. Two different CPC models were calibrated for their particle counting efficiency, smallest particle size detection limit, and concentration linearity. The calibrations were performed with test aerosols of two very different particle sources. One of the calibration aerosols is representative of inorganic particles in ambient air not impacted by anthropogenic activity. The other aerosol is freshly generated soot from an inverted-flame burner, which serves as a proxy for combustion emissions found in urban environments. Additionally, all counting efficiency experiments were done with the relative humidity of the calibration aerosol varied from almost dry to moderate levels of humidity. This aspect was included to consider that humidity might play a role in the activation of particles inside a CPC.

This thesis provides new insights into the experimental method, operating parameters and effective practices to calibrate CPCs for their use under low-pressure conditions. Results demonstrate that in general CPCs work as specified down to a threshold pressure. Below that point, their performance depends on the exact measurement conditions and the specific CPC design. These findings are an important advancement in understanding the behavior of CPCs at low pressure and can serve as guidance when correcting the reported number concentration for the impact of reduced pressure. They also show that a dedicated calibration of CPCs is advisable for every type of low-pressure application that requires highly accurate particle number concentration data.

Zusammenfassung

Kondensationspartikelzähler (CPC) sind hoch entwickelte Messgeräte zur Messung feiner, luftgetragener Partikel. Sie können die Partikelanzahlkonzentration sowohl kleinster Nanopartikel als auch größerer Partikel im Akkumulationsmodus bestimmen, die mit optischen Methoden überhaupt oder nicht mit ausreichender Genauigkeit gemessen werden können. In den letzten vier Jahrzehnten wurden CPCs zunehmend in der Forschung sowie für regulatorische Zwecke zur Bestimmung von Partikelanzahlwerten bei Bedingungen auch unterhalb des Normluftdrucks verwendet. Um korrekte Messergebnisse sicherzustellen, erfordern derartige Messbedingungen eine entsprechende Kalibrierung. Ziel dieser Arbeit war es, die Leistungsfähigkeit von CPCs bei Niederdruckbedingungen mittels einer umfassenden Studie zu untersuchen.

Der erste Teil meiner Arbeit befasst sich mit den Details der CPC-Technologie, erläutert Anwendungen bei denen eine Niederdruck-Kalibrierung erforderlich ist und präsentiert eine umfassende Literaturrecherche von mehr als 60 für diese Forschung relevanten wissenschaftliche Publikationen aus den letzten vierzig Jahren. Die Literaturrecherche zeigt Widersprüche im Verständnis des Verhaltens von CPCs bei Niederdruck auf und betrachtet die zum Teil gegensätzlichen Ergebnisse. In einem weiteren Abschnitt wird ein numerisches Modell angewendet, um zu untersuchen wie sich ein reduzierter Druck auf das Verhalten von CPCs theoretisch auswirkt. Das Modell liefert eine Prognose der Zähleffizienz sowie der d_{90}, d_{50} und d_{10} Kenngrößen bei verschiedenen Niederdruckniveaus.

Der zweite Teil dieser Arbeit beschreibt ausführliche Laborexperimente zum Verhalten von CPCs bei reduziertem Druck. Zwei verschiedene CPC-Modelle wurden hinsichtlich ihrer Zähleffizienz, unterer Nachweisgrenze und Konzentrationslinearität untersucht. Die Kalibrierungen wurden mit Prüfaerosolen aus zwei unterschiedlichen Quellen durchgeführt. Das erste Aerosol ist repräsentativ für Umgebungsluft, die nicht durch anthropogene Aktivität beeinflusst wird. Das andere ist frisch-erzeugter Ruß aus einem Brenner, der hier stellvertretend für Verbrennungsemissionen im städtischen Raum steht. Des Weiteren wurden Experimente durchgeführt, bei denen die relative Luftfeuchte des Kalibrieraerosols von fast trocken bis zu moderaten Werten variiert wurde. Dieser Aspekt wurde einbezogen, um zu untersuchen, ob geringe Feuchte eine Rolle bei der Aktivierung von Partikeln in einem CPC spielen kann.

Diese Arbeit liefert neue Erkenntnisse zu den Betriebsbedingungen und empfohlenen Vorgehensweisen zur Kalibrierung von CPCs für deren Einsatz bei Drücken unterhalb der Normluftdrucks. Die Ergebnisse zeigen, dass CPCs bis zu einem bestimmten Druckniveau wie spezifiziert messen, ihr Verhalten unterhalb dessen aber von den genauen Messbedingungen und dem CPC-Modell abhängt. Diese Ergebnisse sind ein wichtiger Fortschritt für den Einsatz von CPCs bei Niederdruck und können für Korrekturen der gemessenen Anzahlkonzentration dienen. Sie zeigen auch, dass eine anwendungsspezifische Kalibrierung von CPCs für Niederdruckanwendungen immer dann ratsam ist, wenn eine hochgenaue Partikelanzahlkonzentration erforderlich ist.

Acknowledgements

I am deeply grateful to everyone that supported me in pursuing a PhD as a part-time external doctoral researcher at this advanced stage of my career. I received a great deal of support throughout my research and the writing of this thesis. First of all, I would like to thank my advisors, Professor Dr. Astrid Kiendler-Scharr and Professor Dr.-Ing. Reinhold Kneer, for all their guidance and for letting me do this work at their respective institutes. I appreciate the opportunity very much and am indefinitely grateful for it!

I would also like to express my sincere gratitude to Dr. Andreas Petzold and Dr. Ulrich Bundke, who acted as my tutors at Forschungszentrum Jülich, for all their valuable guidance throughout my dissertation. You provided me with the knowledge, tools, space and academic backing that I needed to successfully complete my research. I also want to thank my lab colleagues Patrick Weber, Benno Fischer and Marcel Berg who helped with many practical aspects of my experiment and accepted my frequent comings and goings. I would also like to thank the entire Global Observations research group in Jülich for adopting me and being my PhD family.

A big thank you goes to many colleagues at TSI in Aachen and Minnesota who were indispensable during the 25+ years of my professional career. First and foremost, I am indebted to Dr. Hans-Georg Horn, who not only hired me and taught me much of what I know about aerosol measurement but also was an outstanding mentor in many ways. I am still deeply sad that he passed away much too early in April 2019. Another early mentor at TSI was Gilmore Sem, from whom I learnt much about CPCs and aerosol instrumentation in general. For their assistance with my PhD research I would like to thank Brian Osmondson who granted me the use of various TSI instruments, Dr. Ryan Han for all his guidance on CPC modeling, and to Maynard Havlicek for sharing so much of what he knows about CPCs with me. I am particularly grateful to Dr. Thomas Krinke for 17+ years of great collaboration, friendship and many lively discussions. There are many excellent colleagues on his Particle Instruments team that are too many to mention. Lastly, I would like to thank Steve Buerkle for being a fantastic boss and for giving me the opportunity to do this research next to my full-time job at TSI.

In addition, I am thankful for the encouragement and advice of various members of the European and international aerosol science community. I really appreciate the work of the Gesellschaft für Aerosolforschung (GAeF), was proud to serve along a unique group of people on the organization committee of the European Aerosol Conference (EAC) 2020 and have learnt a lot from the CLOUD project ever since its start in 2008.

Last but not least, I would like to thank my family. My parents Astrid and Bernhard Bischof have been my true North for as long as I can think and are still always there for me. I could not have wished for more love, better values, wiser counsel and encouragement. Finally, I could not have completed this dissertation next to a full-time job without making sacrifices at home. I am grateful that my children not only tolerated this but were as thrilled for me to being able to do this as I was. Thank you, Marie, Tom and Arne, for being the wonderful children that you are!

Contents

Table of Nomenclature

Constants

e	Elementary unit of charge	$1.602 \cdot 10^{-19}$ C
k	Boltzmann constant	$1.381 \cdot 10^{-23}$ J/K
M	Molecular weight of dry air	28.965 g/mol
R	Universal gas constant	8.314 J/(mol · K)
μ	Viscosity of air	$1.807 \cdot 10^{-5}$ Pa · s

Latin symbols

C_c	Cunningham slip correction	-
D	Diffusion coefficient of a particle	m^2/s
D_{con}	Condenser diameter	mm
d_{50}	Lower detection limit or cut-off size of a CPC	nm
d_d	Droplet diameter	µm
d_k	Kelvin diameter	nm
d_p	Particle diameter	nm
F_v	Volume fraction of dissolved solid material	-
GSD	Geometric standard deviation	-
L_{con}	Condenser length	mm
N_{AEM}	Number concentration of an AEM	P/cm^3
N_{CPC}	Number concentration of a CPC	P/cm^3
N_{ref}	Reference concentration	P/cm^3
n_p	Number of elementary charges per particle	-
P	Penetration of a particle	%
$PM10$	Particulate matter of particles <10 µm	$µg/m^3$
$PM2.5$	Particulate matter of particles <2.5 µm	$µg/m^3$
PN	Particle number	P/cm^3

p_{sat}	Saturation vapor pressure	Pa
p_v	Vapor pressure of working fluid	Pa
q_{ae}	Aerosol sample flow rate of a CPC	L/min
q_e	Volumetric aerosol flow rate into AEM filter	L/min
S	Saturation ratio	-
R^2	Coefficient of determination	-
RH	Relative humidity	%
T_{con}	Condenser temperature of a CPC	°C
T_{opt}	Optics temperature of a CPC	°C
T_{sat}	Saturator temperature of a CPC	°C

Greek symbols

β	Dimensionless diffusion coefficient	-
δ_s	Surface tension	N/m
η_{CPC}	Counting efficiency of a CPC	-
$\xi(d_p)$	Multiple-charge correction factor	-
ρ_L	Density of working fluid	Kg/m^3
τ_p	Nominal time of particle in viewing volume	µs

Abbreviations

AEM	Aerosol electrometer	
AS	Ammonium sulfate	$(NH_4)_2SO_4$
CAST	Combustion aerosol standard	
CCN	Cloud condensation nuclei	
CEN	European Committee for Standardization	
CNC	Condensation nucleus counter	

CPC	Condensation particle counter	
DC	Diffusion Charger	
DEG	Diethylene glycol	$C_4H_{10}O_3$
DEHS	Di-ethyl-hexyl sebacate	$C_{26}H_{50}O_4$
DMA	Differential mobility analyzer	
DMPS	Differential mobility particle sizer	
EECPC	Engine exhaust CPC	
EEPS	Engine exhaust particle sizer	
ELPI	Electrical low-pressure impactor	
FCE	Faraday cup electrometer	
FMPS	Fast mobility particle sizer	
HEPA	High efficiency particulate air	
IAGOS	In-service aircraft for a global observing system	
IPA	Isopropyl alcohol	C_3H_8O
MFC	Mass flow controller	
MFM	Mass flow meter	
MOUDI	Micro-orifice uniform deposit impactor	
OPC	Optical particle counter	
PID	Proportional integral derivative controller	
PM	Particulate matter	
PMP	Particle measurement programme	
PSL	Polystyrene latex (beads)	
RMS	Root mean square	
SCPM [i]	Standard cubic centimeter per minute	10^{-6} m_N^3/min
SLPM [i]	Standard liter per minute	10^{-3} m_N^3/min
SMPS	Scanning mobility particle sizer	

[i] At a temperature of 273.15 K and an absolute pressure of 100 kPa.

TDMA	Tandem differential mobility analyzer
UFP	Ultrafine particles
UTLS	Upper troposphere and lower stratosphere
VOC	Volatile organic compounds
WCPC	Water-based CPC
WMO	World Meteorological Organization

Publications

This dissertation builds on the following, previously published research papers:

Bischof, O. F. (2015). Recent Developments in the Measurement of Low Particulate Emissions from Mobile Sources: A Review of Particle Number Legislations. *Emiss. Control Sci. Technol.*, 1: 203-212, 2015. https://doi.org/10.1007/s40825-015-0016-9.

Bischof, O. F., Weber, P., Bundke, U., Petzold, A., & Kiendler-Scharr, A. (2019). Characterization of the Miniaturized Inverted Flame Burner as a Combustion Source to Generate a Nanoparticle Calibration Aerosol. *Emiss. Control Sci. Technol.*, 6: 37-46. https://doi.org/10.1007/s40825-019-00147-w.

Hermann, M., Wehner, B., Bischof, O. F., Han, H.-S., Krinke, T. J., Liu, W., Zerrath, A. F., & Wiedensohler, A. (2007). Particle counting efficiencies of new TSI condensation particle counters. *J. Aerosol Sci.,* 38: 674-682. https://doi.org/10.1016/j.jaerosci.2007.05.001.

Kupc, A., Bischof, O. F., Beeston, M., Tritscher, T., Krinke, T. J., & Wagner, P. E. (2013). Laboratory Characterization of a New Nano Water-Based CPC 3788 and Performance Comparison to an Ultrafine Butanol-Based CPC 3776. *Aerosol Sci. Technol.* 47:2, 183-191. https://doi.org/10.1080/02786826.2012.738317.

Liu, W., Osmondson, B. L., Bischof, O. F., & Sem, G. J. (2005). Calibration of Condensation Particle Counters. *SAE Transactions,* Paper 2005-01-0189. https://doi.org/10.4271/2005-01-0189.

Sem, G. J., Bischof, O. F., & Kittelson, D. B. (2010). Review of Particle Size Distribution Measurements of Engine Exhaust Before 1985. Chapter in: “Aerosol Science and Technology: History and Reviews” (Edited by David S. Ensor), RTI Press. https://doi.org/10.3768/rtipress.2011.bk.0003.1109.

Verheggen, B., Cozic, J., Weingartner, E., Vana, M., Aalto, P., Hirsikko, A., Kulmala, M., Bischof, O. F., & Baltensperger, U. (2006). Observations of Atmospheric Nucleation Events in the Lower Free Troposphere. Poster EGU06-A-07606. *Geophysical Research Abstracts*, Vol. 8, 07606.

1. Introduction

The objective of this thesis is to improve on the understanding of the performance of aerosol particle detection by Condensation Particle Counters (CPC) under low-pressure conditions. CPCs are the instrument of choice for accurate measurements of submicrometer particles as all other methods struggle to detect particles that small or cannot determine their concentration without making assumptions. From several previous studies it is known that the performance characteristics of a CPC change when operated at low pressure. Until a few years ago this aspect was of interest only to a small group of aerosol researchers. Yet in recent years the use of CPCs at non-standard ambient pressures has gained in importance, with more CPCs being used e.g. on mountaintop research sites as well as onboard aircraft. Another factor was the emergence of particle number limit values for vehicle emission regulations and the corresponding tests also being done at high elevation, with some engine technologies being close to current not-to-exceed limits (NTE). These two groups of use cases lead to an interest in application specific CPC calibrations. CPCs used to measure a background aerosol not impacted by anthropogenic activity are ideally calibrated by inorganic particles as commonly found in ambient air. CPCs predominately used for the measurement of vehicle emissions or of urban air impacted by various combustion sources are better calibrated using freshly generated soot from a laboratory flame burner. Both of these quite different calibration aerosols are used in the extensive low-pressure laboratory experiments in this work. Key details of the experimental set-up, methodology and best practices to calibrate CPCs for their use under low-pressure conditions will be explained. The performance of two different CPC models is characterized at various levels of low-pressure down to 200 hPa. In addition, all calibration experiments are done at different levels of relative humidity, ranging from almost dry conditions to moderate levels of humidity. The result is a comprehensive study of two butanol-CPCs that also considers the key ambient parameters that can impact their performance at low pressure. The calibrations provide the CPC counting efficiency curves for the two calibration aerosols, with their smallest particle size detection limit as well as their concentration linearity at each of the low-pressure levels.

This thesis is structured as follows. Following the introduction, chapter 2 lays the foundation for this work. It provides relevant background on the subject of aerosols in general and then gives an overview of several measurement technologies suitable for the measurement of physical aerosol characteristics. CPC instruments and their technology are described in great detail. Key aspects of their calibration are examined and the need for application-specific calibrations is explained based. In the following chapter, chapter 3, a comprehensive review of the existing literature is presented. Out of more than 60 peer-reviewed papers, the findings from studies most relevant to this work are explained. In chapter 4, a numerical model is applied to find out how low-pressure conditions impact the performance of CPCs in theory. The model provides

simulated condenser saturation ratio profiles and theoretical counting efficiency curves for several levels of reduced pressure.

Chapter 5 focuses on the experimental set-up to achieve stable conditions for all parameters. Subsequently the instruments used in the experiment are explained and the two aerosol generators are characterized to determine their optimum operation conditions for CPC calibrations. Details on the data analysis procedure are given and all corrections made are described in detail. Chapter 6 presents the results of the calibration experiments, which represent the most comprehensive part of this work. At first the response of CPCs to selected monodisperse sizes at low-pressure is reported. Then the counting efficiency curves obtained during the measurements with two particle calibration materials at several low levels of relative humidity and discrete levels of reduced pressure are presented and discussed. The impact of low-pressure on the total particle concentration is considered and basic impact estimates are given for two practical scenarios. Finally, chapter 7 summarizes the findings of this work and gives an outlook on further research opportunities.

2. Background

This chapter provides some general background on the topic of aerosols and information on specific aerosols of interest for this work. It gives a brief overview of measurement techniques used for the physical characterization of aerosols, before providing detailed explanations on the history, working principle and types of Condensation Particle Counters (CPC). Further, key aspects of calibrating a CPC are presented and the need for application-specific calibrations of a CPC is explained.

2.1 Aerosol and measurement techniques

The word aerosol has attracted various meanings and even different pronunciations during its existence. In everyday language, it has been commonly used to describe a paint, household cleaning or personal care product delivered in the form of a spray. We also use it for medical nebulizers that deliver medicines to the respiratory tract of a patient for therapeutic purposes. Since 2019 it gained much wider public recognition with the emergence of the SARS-CoV-2 coronavirus and the discussion on aerosol transmission. An important milestone in this context was the position paper on the current state of knowledge on the transmission of the coronavirus through aerosols and the recommendations for efficient protection against it that the *Gesellschaft für Aerosolforschung* published (Association for Aerosol Research; GAeF, 2020).

The scientific definition of an aerosol is that of a system of solid and/or liquid particles dispersed in air or another carrier gas. That definition thus includes naturally occurring fogs, mists, (sea) sprays, and (volcanic) dusts but also anthropogenic emissions, smoke, smog and a variety of aerosols made for technological applications. Aerosols can be classified by how they are formed, typically into primary aerosols that are generated directly and into secondary aerosols that are produced through gas-to-particle conversion processes, for instance in the atmosphere from organic precursors. Another perspective is the one of “good” aerosols versus “bad” aerosols that V. H. Vincent used in his textbook on Aerosol Science for Industrial Hygienists (1995). Here the terminology “good” aerosols include those that offer an advantage or positive effect such as aerosols made for medical purposes, those used in biotechnology or aerosol particles engineered for specific material properties. By that same definition, “bad” aerosols are the ones that produce unwanted results or have an adverse effect on key aspects like human health, visibility or the climate.

The atmospheric background aerosol in much of Central Europe consists largely of ammonium sulfate ($(NH_4)_2SO_4$), ammonium nitrate (NH_4NO_3), sodium chloride (NaCl) and organics. In this work ammonium sulfate was therefore chosen as proxy for non-urban ambient aerosol. Under typical ambient conditions, ammonium sulfate largely forms as a secondary inorganic aerosol. Its precursors are ammonia emissions that originate mainly from the agricultural sector and sulfur dioxide (SO_2) or sulfuric acid (H_2SO_4). In the atmosphere, airborne ammonium sulfate particles can get coated with

secondary organic aerosol and also act as ice nuclei (Penner et al., 2018), which makes it climatically very relevant. In urban areas, however, and especially in locations close to major roads, most of the particles are produced as emission from diesel vehicles but also other by-products from the incomplete combustion of fossil fuels. In the past decade residential wood combustion used for comfort and as supplemental heating source has also increased in residential areas. The solid particles emitted by motor vehicles and other combustion sources are largely of a carbonaceous nature. Vehicle emissions typically consist of nanometer-sized soot particles as well as various organic and inorganic components. Consequently, it was decided to use a soot aerosol generated in the laboratory as proxy for the solid particles from combustion sources found in urban environments.

An important feature of aerosols is that they can span a very wide range of particle diameters, from the cluster size below 1 nm (0.001 µm) at which some of them are *born* to several hundreds of micrometers. The extent of that range is illustrated by the idealized aerosol size distribution in Fig. 1. As shown, an atmospheric aerosol can also have a number of distinct modes, although they rarely occur all at the same time.

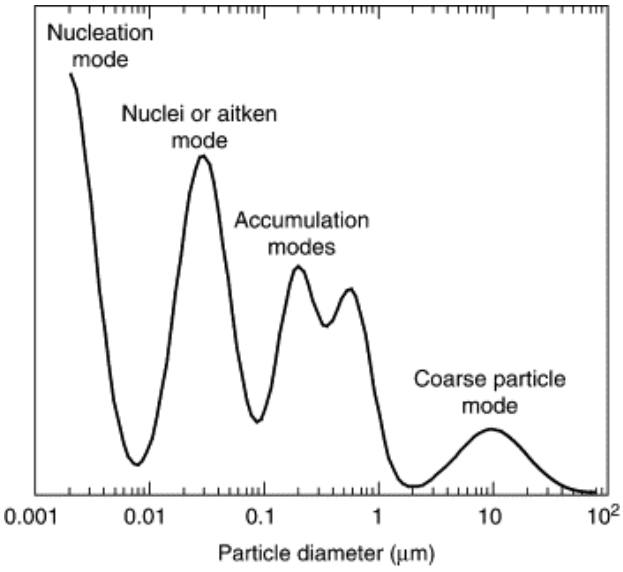

Fig. 1: Idealized number size distribution of an atmospheric aerosol (McMurry, 2003).

Aerosols are often classified by their particle size, using pre-fixes like nano, ultrafine, submicron, supermicron and coarse. Incidentally, particle size is also the salient property that defines how we can observe aerosols and characterize them by aerosol measurement techniques. A wide range of methods exists for the measurement of aerosols, which are described in great detail in the textbook edited by Kulkarni, Baron

and Willeke (2011) as well as in review papers by Pui and Lui (1998), McMurry (2000) and Pelzer et al. (2010). In a first instance, these methods can be divided into the measurement of chemical aerosol variables and the measurement of physical properties of the aerosol. There is a still growing choice of instruments that enable the chemical characterization or speciation of aerosols and probably an even wider choice of instruments that determine the physical characteristics of aerosols, such as their particle concentration, mass, surface area, size distribution and optical properties. The latter define how aerosol particles can absorb or scatter radiation in the atmosphere, which is especially important for understanding their direct effect on our climate. This work deals with the number concentration, so one of the physical characteristics of the aerosol. Therefore, only related measurement technologies are considered in the following brief overview.

There is no single instrument that is able to measure physical properties of airborne particles over the entire size range that aerosols can span, in other words the five decades from 1 nm to approximately 100 µm. Typically, the different measurement technologies are suitable for either submicron and nanoparticles or for coarse, supermicron particles with little overlap between them. In consequence, my personal preference is to group them into methods that are suitable for the measurement of nanoparticles and all other particles that are less than 1 µm in diameter, and those best suited to measure particles of sizes predominately larger than that size. The various measurement techniques also deliver different information about the aerosol, which is why often a combination of measurement instruments is needed. If we limit our consideration to submicrometer-sized particles, of which nanoparticles form a subset, then it is important to realize that this size fraction of the aerosol is the one that is the most difficult to measure. One reason for that is the small size of these aerosol particles, which means that they possess very little mass and also do not scatter much light. Yet these are precisely two of the common properties utilized to measure larger particles. For that reason, submicron particles require a unique set of tools for conditioning, sampling and the actual aerosol measurement. In other words, what is needed for their measurement are techniques that can deal with the challenging optical detection and low mass of submicron particles but also their typically high mobility.

Already since the 1800s a family of instruments that relies on the inertial separation and classification of particles has been used for offline measurements (Marple, 2004). Nevertheless, it was only the Berner impactor that made them an appropriate choice also for nanometer-sized particles. In Berner's design, a pressure drop was implemented in the lowest impactor stages to facilitate the collection of submicrometer particles as small as 82 nm (Berner et al., 1979). More refined versions of such low-pressure impactors were introduced some ten years later. The Micro-orifice Uniform Deposit Impactor (MOUDI) uses 2,000 micro-nozzles in its final stages to collect particles as small as 56 nm (Marple et al., 1991; MSP Corp., Shoreview, MN, USA). In parallel, Hillamo and Kauppinen (1991) compared different

units of the Berner impactor and found significant differences between supposedly identical impactors caused by manufacturing tolerances. Once optimized, their impactor version could achieve a collection of particles down to a lower limit of 32 nm, which resulted in the commercial Finnish low-pressure impactor design (Dekati Oy, Tampere, Finland). The drawback of this technique for atmospheric measurements is that a sufficient mass of particles has to be collected typically over several hours, so the resulting size distribution represents an average over the measurement period.

If nanoparticles are to be examined in real-time, then a great variety of measurement techniques are available as well. One way of further classifying them is into techniques used for detecting particles of that size and into those methods that enable the measurement of complete particle size distributions, as shown in Fig. 2. In this overview chart, the techniques used in this work have been identified by the blue frames. All other measurement techniques and their acronyms will be briefly explained later in this chapter.

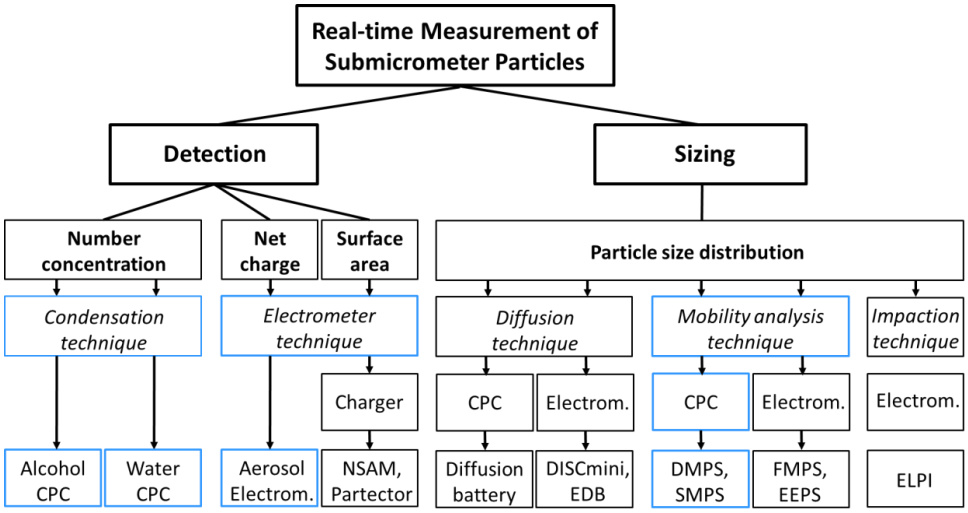

Fig. 2: Measurement techniques for the real-time measurement of submicrometer particles and overview of some corresponding instruments (O. F. Bischof, own classification).

The group of “detectors” can be classified into instruments that measure the number concentration of the aerosol, its surface area or total net charge. The first is accomplished by the condensation growth technique implemented in the Condensation Particle Counter (CPC) that is the very subject of this study, which is undoubtedly the most important instrument for measuring nanoparticles and explained in great detail in chapter 2.2. The surface area and total net charge can be measured by instruments based on the electrometer technique, either with or without

an additional charger. Aerosol electrometers that measure the total net charge can be used as a particle number concentration reference when the charge of the particles is known, as will be explained in chapter 5.2.3. When combined with a diffusion charger, they can be used to measure the lung deposited surface area (LDSA) of nanoparticles (Shin et al., 2007; Fierz et al., 2014) as realized in the Partector device (Naneos Particle Solutions GmbH, Windisch, Switzerland).

As regards the group of submicron “particle sizers”, they always rely on a combination of size classifying the particles first and then measuring the concentration of the classified particles with one of the aforementioned detection techniques afterwards. If the size classification of the particles is done by the diffusion technique, then the underlying mechanism is the Brownian motion that nanoparticles undergo and the collisions caused by an increasing number of diffusion screens. If combined with a CPC as the detector, it becomes a classic diffusion battery as it has been used since the 1970s (Knutson and Sinclair, 1979). The diffusion technique can also be used with an electrometer detector, which requires that particles are first charged by attaching ions to them (Fierz et al., 2002). A very common instrument of this type is the miniature diffusion size classifier, which utilizes a unipolar diffusion charger, a diffusional precipitator and a two-stage electrometer detector (Fierz et al., 2011; DiSCmini, Testo SE & Co. KGaA, Lenzkirch, Germany).

Instruments that rely on the electrical mobility classification of particles became commercially first available in 1967, when the Whitby Aerosol Analyzer (WAA, TSI Inc.) was developed. In 1974, it was replaced by the much more compact electrical aerosol analyzer (EAA, TSI Inc.). The EAA was originally intended for atmospheric aerosol measurements but quickly found its use also in engine exhaust research (Sem et al., 2010). The EAA is the immediate predecessor of the Differential Mobility Particle Sizer (DMPS) and Scanning Mobility Particle Sizer (SMPS) systems that are used very widely today. Especially the SMPS has become the most important instrument for measuring size distributions of submicrometer particles from as small as 1 nm and up to 1 µm. Both the DMPS and the SMPS use the same hardware, which is a combination of an aerosol neutralizer, a differential mobility analyzer (DMA) and a CPC as the detector. In the aerosol neutralizer, a sealed radioactive or soft X-ray source is commonly used to produce both positive and negative air ions that are attracted to the oppositely charged aerosol particles while these pass through. Provided the residence time inside the neutralizer is sufficient, the particles acquire a well-defined equilibrium charge level, which is a pre-condition for their size classification in the electric field in a DMA. Inside the DMA, the particles initially follow the sample flow until, depending on the voltage applied to the central electrode and their electrical mobility, a well-defined part is extracted through a slit in the center electrode (Pelzer et al., 2010). The difference between DMPS and SMPS is the mode of operation and the size resolution, as in a DMPS the voltage is changed step-wise while in the SMPS it is scanned continuously (Wang and Flagan, 1990). The scanning mode of operation reduces the measurement time from typically 5 to 10 min down to

practical scan times of 45 to 90 sec. Even faster high size resolution measurements of as little as 3 to 5 sec have been possible since the introduction of the newest generation of Nano-SMPS (Tröstl et al., 2015; TSI Inc., Shoreview, MN, USA).

Lastly, there is a group of fast sizers that have gotten much attention with the increasing interest in the measurement of vehicle emissions during transient test cycles as are standard in the automotive industry. One group of them is based on an “inside-out” DMA, in which the size-classified particles are not attracted to a center rod and classified there, but rather repelled outward. The concentration per size class is then measured by a stack of parallel, insulated electrometers that surround the DMA column. This enables the measurement of nanoparticle size spectra with a size resolution of 16 channels per decade and a high time resolution of 1 Hz as in the Fast Mobility Particle Sizer (FMPS, TSI Inc.) or even 10 Hz as in the Engine Exhaust Particle Sizer (EEPS, TSI Inc.) and the Differential Mobility Spectrometer (DMS500, Cambustion Ltd., Cambridge, UK). The fundamental difference between the EEPS and the DMS500 is the operation at ambient pressure versus low pressure, which is of importance for volatile particles and also results in a different size range.

The Electrical Low-Pressure Impactor (ELPI, Dekati Oy) also belongs to the category of fast sizers as it can report second by second size distributions of transient particle emissions (Maricq et al., 2000). Its measurement principle is based on the inertial classification in a 12 to 14 stage low-pressure impactor and the detection by an equal number of electrometers that are one-by-one connected to the impactor stages.

2.2 Condensation Particle Counter

A Condensation Particle Counter or CPC for short is a scientific instrument that is used to measure the number concentration of aerosol particles smaller than a few micrometers. It enables the measurement of single particles with a lower particle size detection limit between 3 and 10 nanometers in diameter for the most common models. The original name *Condensation Nucleus Counter* comes from cloud physics where condensation nuclei are precursors to the formation of cloud droplets. Its operational principle is based on the condensation technique that makes tiny, nanometer-sized particles physically larger for an easier optical detection.

In principle, any CPC utilizes these three steps:

1) Saturation: Supersaturated vapor is formed inside the CPC instrument from its working fluid;
2) Condensation: The vapor is made to condense on the surface of the tiny particles that are to be measured. Hereby they act as nuclei in the formation of optically much larger droplets;
3) Detection: The enlarged particles scatter light when they pass a laser beam inside the instrument optics. A photodetector detects pulses generated by the

scattered light each time a particle passes through the laser beam. Lastly, a signal processor converts that signal into particle counts.

The steps of the CPC measurement technique can be visualized as shown in Fig. 3.

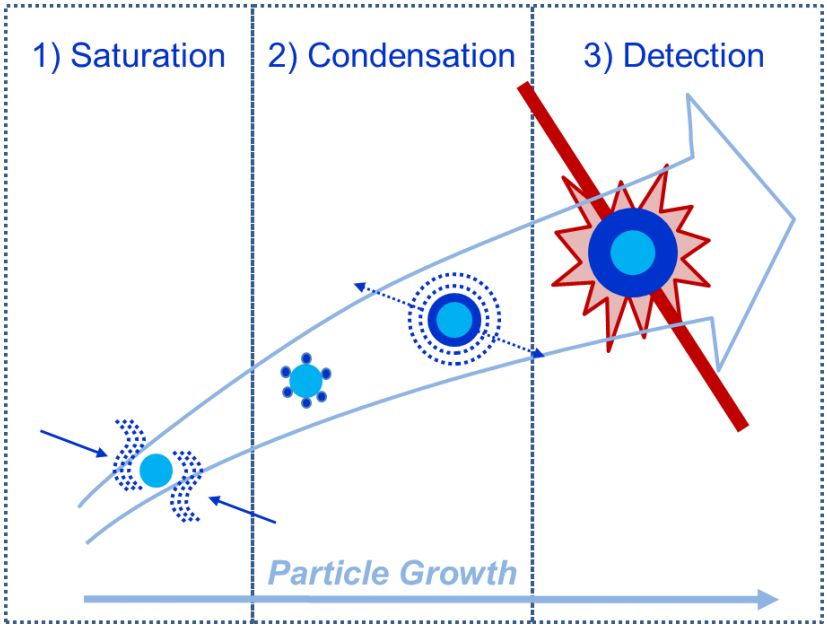

Fig. 3: Visualization of the growth of a small aerosol particle into a larger droplet as implemented in the CPC technique (adapted from internal material of TSI Inc.).

In an actual CPC instrument, this process is implemented as follows. The aerosol sample flow enters the CPC and then passes through the saturator where it is exposed to a vapor that is generated from the CPC's working fluid in a controlled manner. In butanol- or isopropanol-based CPCs that saturator is heated to a precisely controlled temperature, so the liquid alcohol forms a vapor that diffuses into the sample flow. Subsequently the aerosol particles and the surrounding alcohol vapor enter the condenser section where they are cooled so the vapor gets supersaturated. The vapor then condenses heterogeneously onto the aerosol particles, which in a butanol CPC happens at very high supersaturations of approximately 100 to 200%. The operating parameters are chosen carefully to remain below the critical supersaturation (typically around 300%) at which droplets would form by homogeneous nucleation. Hereby the thermal diffusivity of the working fluid vapor is

important and its ratio to the vapor diffusivity must be high so condensation of the vapor occurs on the particles rather than on the cold walls of the instrument.

In an ideal CPC, the vapor condenses on all particles larger than the CPC's lower detection limit. The critical particle diameter at which condensation takes place at the present supersaturation level, which equals the smallest particle size detection limit or d_{50} cut-off size of the CPC, should correspond to the Kelvin diameter d_k from activation theory:

$$d_k = \frac{4\,M * \delta_s}{R * \rho_L * T} * \frac{1}{ln\,S} \tag{2.1}$$

where M is the molecular weight, δ_s the surface tension and ρ_L the density of the working fluid; R the universal gas constant, T the temperature and S the saturation ratio. The Kelvin diameter d_k is thus assumed to be the diameter of a *pure* droplet of the working fluid that is in equilibrium with the vapor of that fluid at the saturation ratio. Particles with a size below the Kelvin diameter d_k remain inactivated while particles of that very size or greater grow into much larger droplets. The grown droplets are of a nearly uniform size in the small micrometer range that is largely independent of the original particle diameter. The outright validity of the Kelvin equation to determine the critical activation diameter has been questioned over the years (Kulmula et al., 2007; Winkler et al., 2008) and it has been shown to have a shortcoming as it does not consider the role of a particle's chemical composition (Giechaskiel et al., 2011b). Nevertheless, it is still widely used as it is a convenient descriptive method.

Once the particles are grown into droplets they are easily detectable with conventional optics. In an alcohol-based CPC the instrument optics are typically heated as well. They consist of a laser diode light source, a collimating and a focusing lens, a measurement zone, and receiving optics with a photodetector. As the droplets pass through the laser light, each droplet scatters light as it passes through the laser. The scattered light is focused onto the photodetector that converts the light-scattering signal into an electrical pulse. Each of the pulses corresponds to an individual particle and is counted, which is recorded and processed into the particle number concentration of the aerosol by the instrument's firmware. An example for how this operation is implemented in an actual CPC is given in the schematic in Fig. 4.

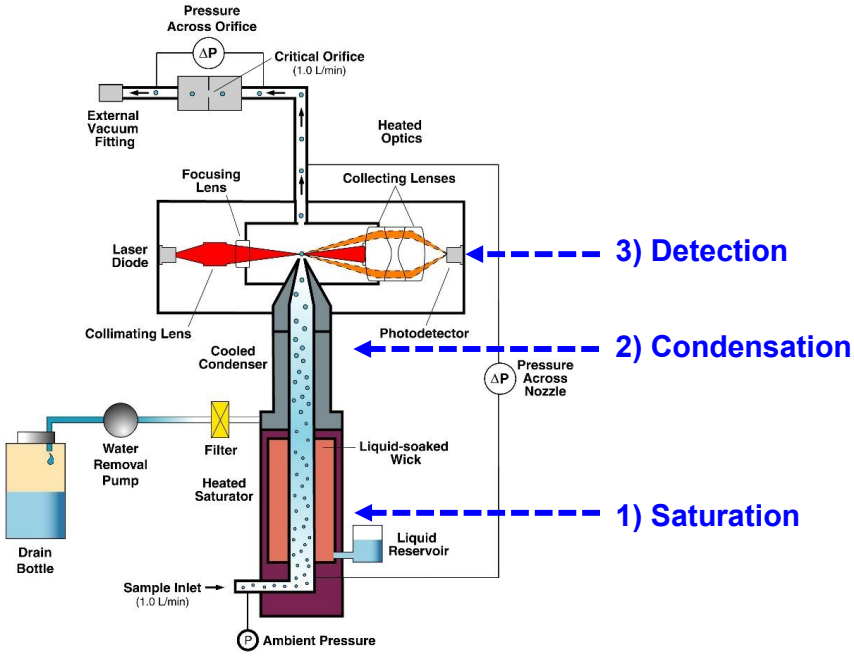

Fig. 4: Operating principle of a typical laminar flow, butanol CPC (Schematic courtesy of TSI Incorporated, Model 3790 EECPC Operation and Service Manual).

In a single-particle counting CPC, this is everything that is needed to determine the particle number concentration. However, at higher concentrations particle coincidence leads to undercounting. The exact concentration at which this occurs depends on the CPC model but typically it will happen between 10,000 to 50,000 P/cm^3. Some CPC models apply a continuous, live-time coincidence correction but it is also possible to make manual coincidence corrections as explained in chapter 5.4.1. It should be noted that some CPC models switch into an additional photometric mode for high concentrations. Such models are not considered in this work as that mode is fundamentally less accurate.

In each CPC instrument, there are a number of critical parameters that ensure an accurate measurement, which are the operating temperatures of saturator T_{sat}, condenser T_{con} and optics T_{opt}; the sample flow rate q_{ae} as well as the threshold setting for optical detection. The performance of the CPC is typically characterized by its counting efficiency curve. That curve displays its lower detection limit, which is the d_{50} cut-off size of the CPC, and the asymptotic maximum efficiency. More recently also its characteristic d_{10} and d_{90} diameters have gained importance. Last but not least

also the particle concentration linearity is considered to ensure there are no concentration-dependent effects that impact the accuracy of the CPC measurement.

2.2.1 History of CPCs

The technique that eventually formed the basis for the measurement of the smallest aerosol particles was originally developed for another purpose. Already in 1875 Paul-Jean Coulier described his experiments in a chamber that demonstrated that condensation of water onto airborne dust particles occurs when the air is expanded. Five years later, John Aitken described experiments with water-saturated air that he conducted independently of Coulier's work that were in fact almost the same. Aitken then went on to implement his findings in an experimental set up primarily designed to measure dust particle concentrations in outdoor atmospheres. His invention used a pump to cool the air saturated with water by adiabatic expansion, and counted the resulting droplets as they fell onto a counting grid. This work resulted in the first very basic expansion-type condensation nucleus counter (CNC) in 1890, which he kept refining over the years. It took almost five decades for adiabatic-expansion CNCs to undergo additional developments of significance. These included the inventions of Bradbury and Meuron (1938) as well as of Nolan and Pollak (1945) that introduced light sources and electrical photodetectors to measure the light attenuation.

CPCs as we know them today are diffusional, thermal-cooling instruments that first saturate the sample flow with alcohol vapor as it passes over a heated pool of liquid alcohol. The design of modern-day instruments is credited to the work of Bricard et al. (1976) at the Laboratory of Aerosol Physics of the University Paris VI and a landmark paper presented by Agarwal, Sem, and Pourprix at the International Conference on Atmospheric Aerosols, Condensation and Ice Nuclei, in Galway, Ireland, in 1977 (Agarwal et al., 1981). The instrument they designed was capable of counting single aerosol particles larger than approximately 20 nm in diameter in real time. Their instrument design was implemented in the world's first continuous-flow CNC that was no longer a research project but an effortlessly usable instrument, which became commercially available from 1979 onwards (CNC Model 3020, TSI Inc.). Later papers by Agarwal and Sem (1980) and Agarwal et al. (1981) provided further details. It should be noted that around the same time Kousaka and co-workers at the University of Osaka Prefecture in Japan introduced another continuous-flow technique, which they referred to as mixing type condensation nucleus counter (Kousaka et al., 1982). In this design, two vapor-saturated flows undergo turbulent mixing. Here, one of the flows is heated while the other one is cold, in order to rapidly cool and supersaturate the vapor. Mixing CNCs found far less widespread use but are still built and used today.

The choice of commercially available diffusional thermal CNC models grew in 1988 with the introduction of the model 3022 and in 1989 with the model 3025 (both by TSI Inc.). The latter was the first ultrafine CNC and based on Stolzenburg's PhD thesis

work (1988). It was also in 1988 that TSI Incorporated started changing the name of its products from condensation *nucleus* counter to condensation *particle* counter or CPC, as the company wanted to emphasize that these instruments count all particles in their specified size range instead of only the nuclei. This is an important distinction from devices used to study atomic nuclei in the field of nuclear physics as well as from instruments that measure atmospheric cloud condensation nuclei (CCN). Credit for promulgating this change in terminology goes to Pat Keady and her presentation at the AAAR Annual Meeting in Chapel Hill, NC, in 1988. With the launch of the CPC model 3010 in 1992, TSI started to use the term CPC exclusively. Since then it has de facto become the only name for this instrument class and one that is used by all manufacturers, researchers and industrial users today. Aside from the above historic references, I will therefore only refer to these instruments as condensation particle counters or CPCs in this thesis.

2.2.2 Alcohol-based CPC instruments

The design of alcohol-based CPCs has been largely described in the beginning of chapter 2.2 already. While it may seem that a number of alcohols could be used in theory and are occasionally promoted as options in so-called “flexible working fluid type” CPCs, only two alcohols are commonly used in practice. N-butyl alcohol (C_4H_9OH), better known as butanol, is by far the most frequent one. It is a colorless, neutral liquid of medium volatility at room temperature. The advantage of butanol is that inside a CPC it achieves supersaturations above 100% at moderate temperatures of 35 to 40°C. Butanol offers the benefit of a mass diffusivity of just 0.081 cm^2/s, which is considerably smaller than the 0.215 cm^2/s for the thermal diffusivity of air. Depending on CPC geometry, flow or model, that supersaturated butanol vapor can be made to condense heterogeneously onto the particles inside the condenser at moderate temperatures of 10 to 25°C. The disadvantages of this working fluid are its disagreeable odor and that extended exposure to butanol vapor may result in ocular irritation, mild soreness of the nose and slight headaches. For this reason, it is good measurement practice to vent the CPC exhaust to the outside air during laboratory experiments. However, butanol vapor might disturb any measurement of Volatile Organic Compounds (VOC) conducted simultaneously in its proximity, e.g. in an atmospheric monitoring station. In such cases it is recommended to use either activated carbon or catalytic vapor filters to adsorb the butanol vapor.

The other alcohol that is frequently used as CPC working fluid is isopropyl alcohol (C_3H_8O), which is more commonly referred to as isopropanol or IPA for short. Isopropanol is a colorless liquid that forms supersaturated vapor at saturator temperatures of about 30°C and condenses onto the particles at condenser temperatures of about 15 to 20°C. Moreover, it is a volatile liquid, so it evaporates quickly in ambient air. One of the main downsides of isopropanol is that it is infinitely hygroscopic, so it has the tendency to absorb water from the humidity of the air over

time. It should in consequence not be used as the working fluid of choice when sampling humid air over extended periods without proper sample conditioning.

2.2.3 Water-based CPC instruments

In fact, the best working fluid to measure atmospheric aerosols would be water. Water offers the advantage of being odorless, non-flammable, and non-toxic, making it a promising candidate to be used in the condensation-based measurement technique for particle counting. Water-based CPC instruments (WCPC) also offer the benefit that they can be used in locations such as schools, homes, workplaces, and even manufacturing clean rooms. Yet it took more than one hundred years from the work of Coulier and Aitken in the late 19th century until water found a wide-spread use in continuous flow CPC instruments. It was only in 2004 that Susanne Hering and Mark Stolzenburg patented a method for producing a diffusive, continuous laminar flow for particle growth via condensation of water vapor (U.S. Patent 6,712,881). In actual WCPC instruments, their idea was implemented as presented in Fig. 5.

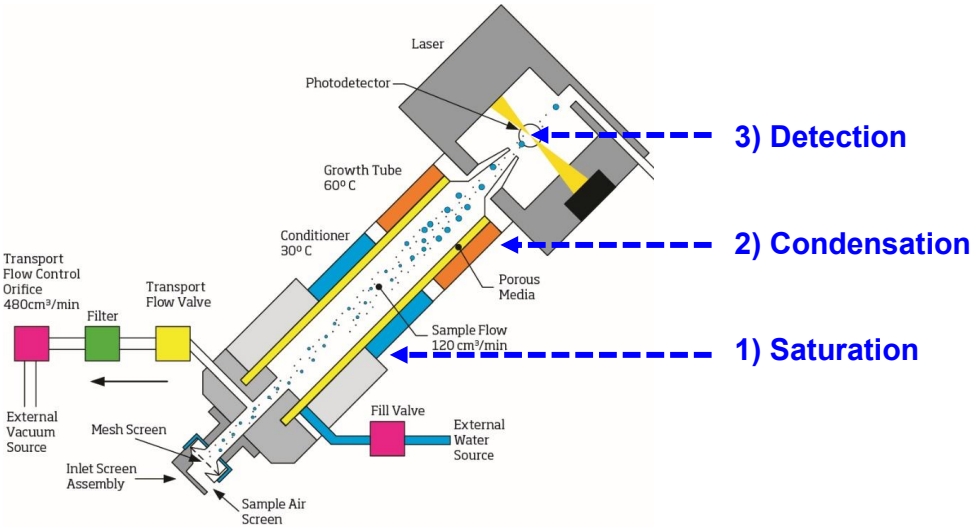

Fig. 5: Operating principle of a water-based CPC (Schematic courtesy of TSI Incorporated, Model 3783 Manual).

The invention of Hering and Stolzenburg permits the use of water as the working fluid in a continuous flow device without having to rely on mixing or adiabatic expansion. In their design, it is the saturator that is cooled, followed by a warm growth tube acting as condenser – so the temperatures are reversed from how they are used in a

conventional alcohol-based CPC. Their work led to the first generation of commercially available water-based CPCs, the WCPC 400 (Quant Technologies LLC, Blaine, MN, USA), and the subsequent first generation WCPC models 3782, 3785, and 3786 from TSI Inc.

In the original WCPC design, a single wick covers the internal walls of both the saturator and the condenser section, which were called the conditioner and the growth tube at that time. The wick consists of a porous medium that is hygroscopic in order to wet the inner walls with water. After entering the conditioner, the aerosol sample flow is saturated with water vapor to nearly 100% relative humidity and is equilibrated to temperatures in the range from 10 to 20°C, depending on the WCPC model. The sample flow then passes to the subsequent growth tube where the wet inner wall is heated to elevated temperatures between 50 to 80°C in order to raise the vapor pressure for condensational growth. The WCPC thereby utilizes one fundamental characteristic of water vapor, which is its high mass diffusivity of 0.265 cm^2/s. Indeed, the diffusion of the water vapor to the centerline of the sample flow is faster than the heat flux from the walls. The result is a maximum supersaturation condition in the centerline of the aerosol stream. The aerosol particles in the flow then act as nuclei and grow through heterogeneous condensation into larger droplets as they continue through the growth tube. After the growth area, the now enlarged droplets enter the optics section where they pass through the laser beam generated by a laser diode. Each time a droplet passes through the laser it scatters light, which is detected by a silicon photodetector. As described earlier, the photodetector then converts that signal into an electrical pulse that is counted. This approach has been implemented in the second generation of WCPCs that have been used for approximately the past twelve years (Models 3783, 3787 and 3788; TSI Inc.).

In the paper by Kupc et al. (2013) a group of researchers from University of Vienna and TSI determined a d_{50} cut-off diameter of 2.7 nm for a model 3788 Nano-WCPC when measuring an atomized NaCl aerosol versus a 2.8 nm cut-off size for an equivalent ultrafine butanol CPC (Model 3776, TSI Inc.). The counting efficiency of the WCPC was also only slightly different for electrosprayed proteins (albumin, ubiquitin, and ferritin). Yet, they also observed a different response of the WCPC for laboratory-generated candle aerosol, clean emery oil (EO) and silver particles. These are all substances with a lower affinity for water that have also resulted in a much larger cut-off diameter in water-based CPC instruments previously (Hermann et al., 2007). These results have demonstrated that particle composition can have a significant influence specifically on the smallest particle size detection limit, the instrument's counting efficiency, and also the linearity response of a WCPC. Nonetheless, water-based CPCs have been shown to perform very similarly to equivalent butanol CPC models for salt (NaCl), ammonium sulfate and sucrose aerosols. In particular when used for the measurement of ambient aerosols they are equivalent and often preferable to butanol. This is for example the case when WCPCs

are operated in routine monitoring networks such as the one of the South Coast Air Quality Management District (SCAQMD) in Southern California, USA.

More recently, Susanne Hering et al. (2014) introduced a 3-stage measurement approach for laminar-flow WCPCs that they called the *moderated* design. In this new concept the conditioner stage is unchanged but the original growth tube that was heated by one defined temperature has been replaced by a new growth section that consists of two stages. The first of these stages is a short section that is warm and wet-walled. It is called the *initiator*, which determines the supersaturation of water vapor at the center flow line. It is followed by a longer stage called the *moderator* that is cool and wetted, which can be set to a temperature that provides a desired dew point. This 3-stage design is approximately of the same total length as the wick in the original WCPC. This approach results in much less water vapor contained in the flow passing through the optics. Another key benefit is that the flow leaving the moderator is noncondensing at temperatures equal to and greater than 18°C, making the instrument more resistant to pressure changes and less prone to water condensation in subsequent sections of the instrument. This third generation was first implemented in the “Moderated, Aerosol, Growth with Internal water Cycling” or in short “MAGIC” CPC (Model 210, Aerosol Devices Inc.). In 2020, a custom design developed by Hering and co-workers at Aerosol Dynamics Inc. for NASA has even flown into space and provided five months of continuous measurement data from the International Space Station (ISS). The moderated design is also used in the aptly called versatile WCPC (vWCPC, Model 3789, TSI Inc.), which features a selectable lower cut-off diameter. Under laboratory conditions, the vWCPC can be operated so it can detect particles that are less than 2 nm in diameter (Hering et al., 2017). Unfortunately, these third-generation models only became commercially available just before the end of this experimental work and were therefore not included in this study.

2.3 CPC calibration

From a metrology perspective, a calibration is defined as an operation that takes place in two steps under well-specified conditions. “In a first step, it establishes a relation between the quantity values with measurement uncertainties provided by measurement standards and corresponding indications with associated measurement uncertainties. In a second step, it uses this information to establish a relation for obtaining a measurement result from an indication” (JCGM, 2012). In order to calibrate a CPC, it is critical to determine its counting efficiency curve, lower detection limit and sometimes also the efficiency at additional cut-sizes. Instrument manufacturers generally perform the initial calibration in order to assure and certify that each new instrument they manufacture meets the published specifications and other performance criteria for the specified use. The manufacturer will also calibrate instruments after service and maintenance work to recertify the instruments’ performance. In addition, qualified third parties such as national metrology institutes

and calibration centers conduct calibrations as well. As importantly, experienced users have an interest in conducting calibrations before measurement campaigns or in order to validate the performance of their instruments under specific operating conditions. The latter is the subject of this thesis in which the performance of Condensation Particle Counters at reduced pressure is investigated.

2.3.1 CPC calibration guidelines and standards

Less than 25 years ago the Verein Deutscher Ingenieure (VDI, Association of German Engineers) published a particulate matter measurement guideline that stated that a Condensation Particle Counter “is an absolute counter” and that “its count mode needs no calibration” (VDI 3489, 1995). While there were reasons for making such a statement at the time based on the robustness and relative independence of that measurement compared to other methods, the accuracy of a CPC especially close to its detection limit depends strongly on a variety of ambient parameters that can influence its activation parameters and optical detection performance. In 2008 VDI considered this when they replaced their original CPC guidance with the newer guideline VDI 3867, part 2. In 2015, the International Organization for Standardization published an international standard that describes the calibration of CPCs from a metrology perspective (ISO 27891). This standard describes two main calibration methods: 1) by comparison with a reference aerosol electrometer and 2) by comparison with a reference CPC instrument. The lengths of the sample tubing to either of these instruments must be identical or be adjusted proportionally to any differences in flow rate to keep diffusional losses the same. For experiments in this thesis, it was decided to use the comparison against an aerosol electrometer as the primary calibration method as it represents a reference method that itself is independent of the CPC. This can be considered as the most accurate procedure when making sure all necessary corrections have been made. The electrometer was used to measure reference concentrations from a few hundred up to one million particles per cubic centimeter. Since at least two CPCs were always used simultaneously, it provided the additional possibility to also compare the CPCs against one another. Interestingly, ISO 27891 allows the use of a wide range of particle calibration materials and primary aerosol generation methods, even though it recognizes differences in CPC detection efficiency between different calibration materials. Instead, ISO 27891 puts an emphasis on possible differences in particle losses between the CPC under calibration and the reference instrument as well as the potential effect of multiply-charged particles.

2.3.2 Fundamentals of CPC calibration

In principle, a CPC calibration is always done by generating a well-defined test aerosol that provides a stable particle number concentration over the calibration

interval and then measuring simultaneously with the instrument under calibration and a reference instrument. While the Scanning Mobility Particle Sizer (SMPS) introduced in chapter 2.1 might seem to be a possible reference due to its ability to directly measure complete size distributions in the required size range, it is not used for several reasons. One of these is that for particle sizes below 20 nm, the fraction of charged particles in the charge equilibrium required for its operation is very low (Wiedensohler, 1988). This results in very poor counting statistics at these small sizes at scan times used in SMPS operation. Another is the significant length that particles have to travel inside an SMPS until they are detected, resulting in diffusion losses of again the smallest particles that would introduce elevated uncertainties during the calibration. Moreover, the SMPS includes a CPC as its concentration detector, so it is not an independent method and could not serve as a primary aerosol standard.

Liu and Pui (1974) first described a detailed method for the primary calibration of CPCs in their landmark paper on a submicrometer aerosol standard. Their calibration system provided the first universal technique to produce calibration aerosols of known particle size, composition, and number concentration. In their method, they generated the challenge aerosol by first atomizing a salt (NaCl) solution to form a polydisperse aerosol. This aerosol is subsequently dried, brought into charge equilibrium by passing through an aerosol neutralizer and size-classified by a Differential Mobility Analyzer (DMA) to produce monodisperse particles in a range from 0.01 to 0.5 µm in diameter. A flow splitter divides the aerosol downstream of the DMA, so that the CPC under calibration and a sensitive aerosol electrometer are measuring the same calibration aerosol side by side. The aerosol electrometer's number concentration N_{AEM} is then determined using the following equation:

$$N_{AEM} = \frac{I}{n_p * q_e * e} \tag{2.2}$$

where I is the current measured by the electrometer, n_p the number of elementary charges per particle, q_e the volumetric aerosol flow rate into the electrometer filter, and e the elementary unit of charge of 1.6×10^{-19} coulomb.

The main benefit of this calibration method, and likely the reason why Liu and Pui referred to it as "primary, absolute calibration", is that it provides a procedure that is independent from the measurement method utilized in a CPC in the first place. A limitation of the method by Liu and Pui is the presence of multiple charges in the DMA-classified aerosol as explained in chapter 2.4.3. The aerosol is thus not truly monodisperse across the entire size range, which requires corrections to the electrometer's number concentration. An equally important aspect is the particle concentration range obtained after size selection by a DMA during the aerosol generation. Concentrations of around one hundred particles per cm^3 (P/cm^3) are too

low for electrometer measurement due to its inherent signal-to-noise ratio. On the other hand, high particle concentrations in the hundred thousand particles per cm^3 can exceed the upper concentration limit of a CPC and lead to coincidence errors that also require correction as explained in chapter 5.4.1.

2.4 Traceable CPC calibration

As explained before, a calibration ensures the measurement accuracy of a CPC compared to a known standard or reference. A fundamental improvement on the method introduced by Liu and Pui is the consideration of traceability, especially for regulatory measurements. The traceability of the calibration method described in the previous chapter largely depends on the accuracy of the DMA to produce truly monodisperse particles and the precision of the particle concentration measurement by the aerosol electrometer. I was part of a team at TSI that has demonstrated the traceability of a CPC calibration 17 years ago. We published our method in an SAE paper (Liu et al., 2005), in which an electrospray aerosol generator in combination with a Nano-DMA was introduced to the calibration setup, see Fig. 6.

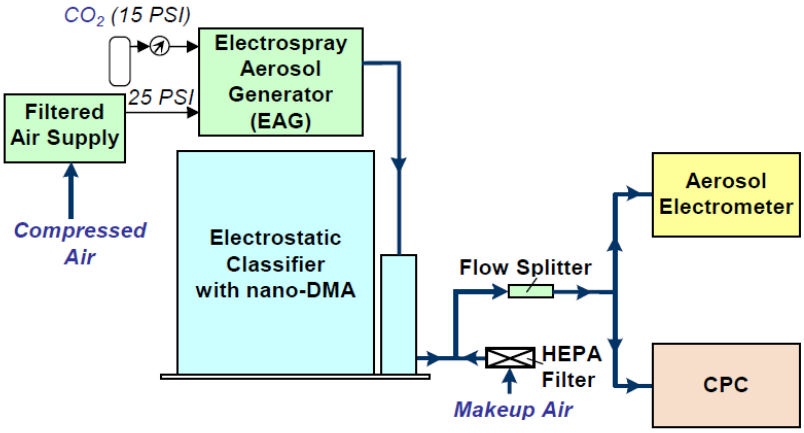

Fig. 6: Experimental setup for the traceable calibration of CPCs using an electrospray aerosol generator and an electrostatic classifier with a Nano-DMA (Liu et al., 2005).

In that study it was shown that CPCs can be calibrated with a very high accuracy so they meet even the rigorous performance demands of regulations for the automotive industry. We successfully demonstrated the traceability of that calibration method to the standards of the United States National Institute of Standards and Technology (NIST). The advantage of an electrospray for aerosol generation is that it can produce high concentrations of uniform, already monodisperse particles down to sizes as

small as 2 nm and up to 150 nm. Varying the particle size that gets produced is difficult, however, so the Nano-DMA (Model 3085, TSI Inc.) was included to select the monodisperse size of choice. An important additional benefit of generating calibration particles by electrospray and size-selecting them with a Nano-DMA is that the resulting size distributions lead to the fraction of multiply-charged particles being negligible. It was demonstrated that the traceability of the Nano-DMA depends on its geometric dimensions, the flow rates used and the voltage applied to its center electrode. The Nano-DMA's geometric parameters were measured with a NIST traceable micrometer and bore gauge, and its sheath and monodisperse flow rates with a NIST traceable flow meter. Finally, a NIST traceable kilovolt divider was used to calibrate the high voltage provided to the center rod of the DMA. The uncertainty analysis of the Nano-DMA resulted in combined uncertainties of 1.45% ± 0.02% for small-sized calibration particles between 16 and 37 nm in diameter.

In the same study the traceability of the aerosol electrometer used as reference (Model 3068B, TSI Inc.) was also determined. Firstly, the aerosol flow rate entering the electrometer was measured with a NIST traceable flow meter. Secondly it was shown that the size-classified calibration particles were singly-charged by performing a size distribution scan using a Scanning Mobility Particle Sizer (SMPS) system. Thirdly, the number concentration N_{AEM} of the aerosol electrometer was derived from the current signal by using the resistance of an embedded high-gain amplifier (R) to convert it into a voltage. Lastly, it was verified with the manufacturer that the embedded resistor R was measured using a NIST traceable standard, ensuring that its resistance was within ± 1% of its nominal value.

Although this traceable CPC calibration method is used globally in the automotive industry to calibrate Particle Number Counters (PNC) for tailpipe emission measurements today, it does have some limitations for other applications. The main constraint is that the electrospray was designed to generate particles from conductive, low-concentrated aqueous suspensions. Emery oil or polyalphaolefin (PAO, C_nH_{2n+2}) by its chemical name, which is widely utilized for PNC calibrations, consists mainly of C30 and C40 polyolefins. It is thus typical of compounds found in the lubricating oil used in combustion engines, but not of particles commonly found in ambient air. Additionally, the annual calibration of automotive PNC instruments is limited to the counting efficiencies at only two particle sizes of 23 nm (± 1 nm) and 41 nm (± 1 nm) as well as a linearity measurement for a minimum of six concentrations across the instrument's single particle counting range (UN-ECE, 2015).

2.4.1 CPC counting efficiency and smallest size detection limit

The particle size-dependent counting efficiency is one of the key characteristics of a CPC. It is calculated as the ratio of the corrected number concentration of particles detected by the CPC under calibration to the corrected number concentration measured by a reference instrument. This is done for all representative particle sizes

across a specified size range. In an ideal CPC, the counting efficiency would be 100% or 1 for all diameters, yet the CPC detection efficiency varies with particle size in real instruments. In particular, it drops steeply at smaller particle sizes, resulting in a sigmoid response. That characteristic S-shaped counting efficiency curve is presented in Fig. 7., with the dotted lines visualizing the size of particles having 50% activation efficiency. The best performance compared to the reference is seen for particle sizes of 12 nm and larger, while it is poorer for particles nearer and below the CPC's lower detection limit. The reason for that is that the smallest particles are more difficult to activate for condensational growth and are also more strongly impacted by diffusion losses. The precise shape and the slope of the counting efficiency curve depends on the specific CPC's internal design. Factors like full versus split or capillary flow models, the difference between the operational temperatures, optical detection settings and the type of working fluid all influence it.

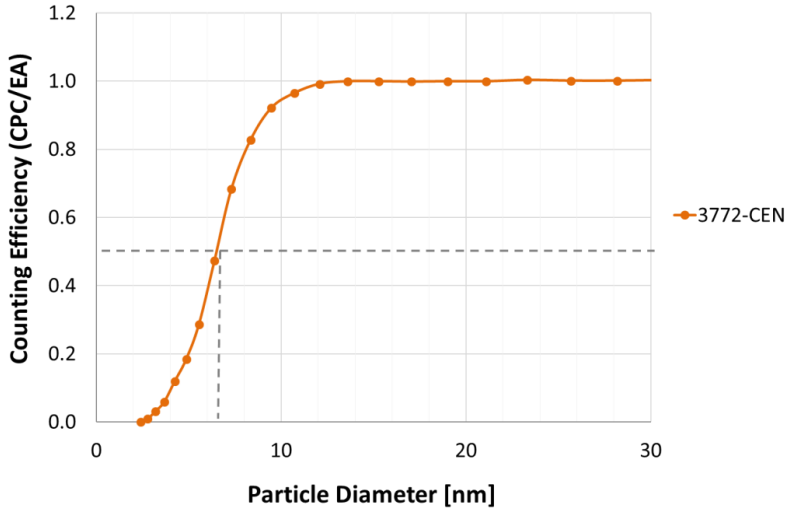

Fig. 7: Example of the counting efficiency curve of a butanol CPC (Model 3772-CEN, TSI Inc.) for ammonium sulfate particles (data from this work).

An equally important characteristic of a CPC is its smallest size detection limit. This characteristic diameter is defined as the particle size at which the counting efficiency is precisely 50%, so the data point on the efficiency curve where exactly half of all particles present are detected. For that reason, a CPC's lower detection limit is typically referred to as its d_{50} cut-off diameter. It is important to understand that the detection efficiency at or near this cut-off size can be influenced by the chemical composition of the particles being measured (Hermann et al., 2007; Kangasluoma et al., 2014), which should have consequences for the particle material selected for calibration. It is for this reason that two rather different calibration aerosols were used in this work to take a possible material dependence into account: inorganic, polar

ammonium sulfate and freshly-generated, nonpolar soot. These choices and the corresponding calibration methods will be explained in chapter 5.3 in more detail.

While only the lower detection limit is always determined during a CPC calibration, the detection efficiency at other diameters can be of importance as well. The need to calibrate a CPC at additional diameters is specified in standard operating procedures or specific regulations. One example is UN-ECE Regulation 83 which determines the measurement of the particle number (PN) emission during the type approval of passenger cars in Europe (UN-ECE, 2015; Bischof, 2015). This regulation mandates the measurement of the total number of all particles greater than 23 nm ± 1 nm in diluted exhaust emissions over a drive cycle, which effectively can only be measured with a CPC. In addition to this increased cut-off diameter, it also specifies a counting efficiency limit for particles with a diameter of 41 ± 1 nm, the so-called "d_{41}". CPCs used for measurements complying with this regulation therefore also need to be calibrated at 41 nm and demonstrate an efficiency of greater than 0.90 at that size.

2.4.2 Concentration linearity

The concentration linearity of a CPC represents its measurement response to changes in the total particle number concentration when comparing it to a reference instrument. The interrelated proportionality of a CPC over a defined concentration range can be verified by producing a calibration aerosol at several concentration levels, which is then measured simultaneously with the CPC under calibration and the concentration reference. In this work that reference is an aerosol electrometer. The reference concentrations obtained are then used for a linear regression, so that the slope or the R^2 value expresses the CPC's linearity response. Depending on the CPC model, the proportional counting performance of the instrument can be verified without the need for dilution over a typical concentration range from a few 100 to 10^4 or even 10^5 P/cm^3. Above these concentrations, dilution with HEPA-filtered air normally becomes necessary. As can be seen in Fig. 8, CPCs are highly linear devices when operated in their count mode at ambient conditions.

In this example graph, the CPC 3772-CEN follows the linear regression very well between about 0 and 25,000 P/cm^3, with an almost ideal R^2 value of 0.9998 and a slope of 1.0178. A common approach to determine the linearity of a CPC is to either vary the concentration of a monomodal polydisperse aerosol or of only one specific particle size by using a proportional dilution bridge. UN-ECE Regulation 83 actually is an example for the latter method as it mandates that the linearity test is done with a particle size of 50 nm or larger for six or more particle concentration levels spaced uniformly across the CPC's concentration range. This followed the recommendations of Marshall and Sandbach (2007) who in their work explained that linearity checks should be done with particles between 50 and 100 nm, so a size where a CPC's counting efficiency has already achieved its maximum.

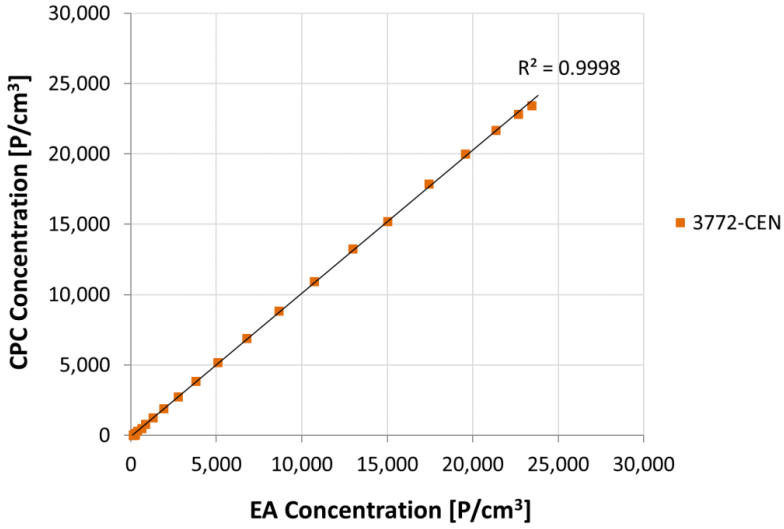

Fig. 8: Linearity response of a butanol CPC (Model 3772-CEN, TSI Inc.) for ammonium sulfate particles (data from this work).

In this thesis, the linearity test is taken one step further as the entire data set is used to determine the linearity behavior as shown in Fig. 8. Although the concentration linearity was looked at for each and every measurement, not all of the data are reported. That is because the response in the single particle counting region of the CPCs used in this work has been very linear as has also been demonstrated in numerous studies previously.

2.4.3 Multiple charge effects

One of the largest errors that can occur when aerosol electrometers are used as the reference is caused by multiply-charged particles in the calibration aerosol. Whenever a Differential Mobility Analyzer (DMA) is used to size classify a polydisperse aerosol, it relies on an aerosol neutralizer to standardize the charge distribution of the polydisperse aerosol prior to size classifying it. Most often either a radioactive or a soft X-ray source are used to attain the Boltzmann equilibrium charge distribution. This results in a defined charge probability as a function of particle diameter as shown for some example sizes in Tab. 1. So, it is not only the desired monodisperse, singly charged particles that exit the DMA. Instead, the aerosol leaving it is only of a mono-mobility, as the particles can carry a certain number of multiple charges which are statistically different depending on their size. Larger particles carrying 2 or 3 charges with the same electrical mobility as the singly charged particles that are classified by the DMA in the ideal case will introduce a bias when the total net charge is used as

basis for the reference concentration for the CPC calibration. That fraction of multiply charged particles increases the larger the chosen particle diameter gets. In consequence, the relationship between the reference number concentration and the current that is measured by the aerosol electrometer gets more complicated and can lead to large errors when the reference concentration is not corrected accordingly.

Tab. 1: Fraction of the total concentration that carries a certain number of charges as a function of the particle diameter calculated according to Wiedensohler et al. (1986).

Particle Diameter [nm]	**Fraction of Particles That Carries This Number of Charges**						
	-3	-2	-1	0	1	2	3
2.6	0	0	1.1%	98.0%	0.9%	0	0
5.2	0	0	2.4%	95.6%	2.0%	0	0
10.8	0	0	5.6%	90.0%	4.5%	0	0
19.1	0	0	10.5%	81.4%	8.1%	0	0
29.4	0	0.2%	15.5%	72.3%	11.9%	0.1%	0
39.2	0	0.5%	19.3%	65.3%	14.7%	0.3%	0
69.8	0	2.8%	25.8%	50.3%	19.6%	1.6%	0
107.5	0.5%	6.3%	28.1%	39.7%	21.6%	3.6%	0.2%
143.3	1.5%	9.1%	28.0%	33.8%	21.6%	5.3%	0.7%
191.1	3.1%	11.7%	26.7%	28.8%	20.7%	6.9%	1.4%

An experimental way of determining the fraction of multiply charged particles per particle diameter of interest is by Tandem DMA (TDMA), which is a setup that consists of two Differential Mobility Analyzers used in series. The classified aerosol leaving the first DMA is subsequently scanned with a second DMA. Since the classification in any DMA is by the particle's electrical mobility rather than by its physical size, the aerosol leaving the first DMA will contain singly-charged particles of the chosen size but, depending on the physical size of the particles, might also include a number of larger particles that carry two or more charges with the same electrical mobility. These will be detected and reported at their actual size when passing through an aerosol neutralizer and subsequent scanning with the second DMA. The probability of particles carrying more than one charge can then be determined by comparing the two spectra. Mamakos (2016) proposed a simplified methodology to quantify the ratio of multiple to single charge fractions by calculating them directly from the raw signal of a single measurement. Another, quite different approach to determine the fraction of multiply charged particles, is to perform a size distribution scan of the polydisperse

test aerosol using an SMPS system. The DMA used for the size classification is then set to a voltage that selects a particle size that is larger than the mode of the size distribution. There will be no significant percentage of multiply charged particles present in that shoulder as larger particles carrying more than one charge will have a higher electrical mobility and thus appear only as particles of a smaller diameter.

In this thesis, the interest is in the smallest particles of the size distribution near to the CPC cut-off diameter. In that size range of interest, particles generally carry single charges and depending on their size also a small share of double charges, while triple charges are already negligible. In order to correct for the presence of these multiply-charged particles, the elegant but not widely-known method introduced by Bundke et al. (2015) was applied, which is described in greater detail in chapter 5.4.2.

2.5 Application-specific CPC calibration

CPCs have been used as general-purpose instruments in basic aerosol research ever since diffusional, thermal-cooling CPCs became available. Nonetheless until about 25 years ago, only the aerosol science community was well aware of them and there were no specific demands as to their calibration. It has been a much more recent development that CPCs are also used in continuous measurements that serve regulatory or near-reference purposes. It is especially for such usage that a reliable, highly accurate calibration is required. As a matter of fact, CPCs are the most commonly used instruments to measure the concentration of airborne nanoparticles today, e.g. during the continuous monitoring of clean rooms, in industrial R&D, and routine air quality measurements, to name just a few.

There are various applications in both academia and industry in which CPCs are operated below the standard pressure of 101.3 kPa. Common low-pressure applications of specific interest are the use of CPCs in mountain top measurement stations, onboard research aircraft and at high elevation vehicle emission test centers. Almost all of the commonly available CPC models have not been designed to work at reduced pressure. As a result, some of them visibly malfunction already when the ambient pressure drops by about 70 or 100 hPa, depending on the CPC model. In consequence, CPCs that are to be operated at low pressure often require modifications of their hard- and firmware. In addition, they should always be custom-calibrated for such usage. A reduced atmospheric pressure due to high elevation or other low-pressure situations can impact the slope of the counting efficiency curve and the smallest size still detected by the CPC. A dedicated calibration ensures that either the pressure dependence of the instruments' counting efficiency is considered during the measurement or that the data obtained can be corrected after the measurements are completed.

CPCs remain the corner stone of fundamental aerosol science due to their suitability for measuring the number concentration of airborne particles down to small

nanometer sizes in a wide range of applications. There is growing interest in characterizing important physical processes in the atmosphere to study and predict global climate change. The role that airborne particles play in the atmosphere is of great importance, which is why more measurements are needed to advance our understanding of their origin and formation, as well as of short-term events and long-term concentration trends. For this reason, a variety of measurement sites with ambient pressures well below standard atmospheric conditions are used in order to get as complete a picture as possible, ranging from high-altitude research stations on summits of great elevation, to airborne measurements on aircraft and even satellites, which are explained in the following chapters.

2.5.1 High-altitude aerosol research

There are growing efforts in high-altitude climate research on mountaintop stations as these locations are considered to be of special interest for climate studies due the distance to most anthropogenic air pollution sources as well as the direct impact that climate change has on mountains and glaciers on a global scale. Hundreds of CPCs are currently used for long-term measurements of the particle number concentration in global research networks. This includes the Global Atmosphere Watch (GAW) program of the World Meteorological Organization (WMO); the Aerosol, Clouds, and Trace gases Research InfraStructure (ACTRIS) and similar research programs.

Tab. 2: Atmospheric research stations measuring particle number concentration currently operational within the Global Atmosphere Watch program (from GAWSiS website).

	Station name	Country	GAW ID	Altitude asl [m]	Atmospheric Pressure [hPa]
1	Chacaltaya	Bolivia	CHC	5,340	516
2	Pyramid (NCO)	Nepal	PYR	5,079	535
3	Mt. Waliguan	China	WLG	3,810	632
4	Mt. Kenya	Kenya	MKN	3,678	643
5	Jungfraujoch	Switzerland	JFJ	3,580	651
6	Mauna Loa	USA	MLO	3,397	666
7	Steamboat Springs	USA	SPL	3,220	682
8	Sonnblick	Austria	SNB	3,100	692
9	BEO Moussala	Bulgaria	BEO	2,925	708
10	Pic du Midi	France	PDM	2,877	712

Tab. 2 provides a list of the ten environmental research stations with the highest altitude currently operational in the GAW network, complemented by a nominal calculation of the corresponding atmospheric pressure. Many CPCs are operated at one of the two dozen worldwide research stations that are located at elevations above 2,000 m asl. The GAW regional station at Chacaltaya in Bolivia is currently the station with the highest elevation at 5,340 m asl, an altitude that corresponds to a reduced atmospheric pressure of just 516 hPa. The high-altitude research station on Jungfraujoch in Switzerland has been a site where aerosol measurements have been done continuously since the 1990's. At 3,580 m asl it is an ideal location to study nucleation events in the lower free troposphere and also how aerosol particles interact with clouds (Verheggen et al., 2006). Even the Schneefernerhaus alpine research station on Mt. Zugspitze in Germany with its elevation of 2,670 m asl and an ambient pressure of 730 hPa poses an, albeit lesser, challenge to the measurement instrumentation. Since measurement data from atmospheric observations at high altitude come with unknown uncertainties, a calibration corresponding to the prevalent atmospheric pressure should always be performed.

2.5.2 Airborne climate research

Scientific research aircraft are regularly used for airborne measurements but due to the high costs involved they are typically limited to a few extended measurement campaigns rather than routine measurements. In Europe alone, there are currently about 45 research aircraft in operation that fly campaigns for atmospheric and climate research. These include the Citation II of the Netherlands Aerospace Centre (NLR), the Falcon 20 of the German Aerospace Center (DLR) and the BAe146 of the Facility for Airborne Atmospheric Measurements (FAAM) based on the Cranfield University campus in the UK. The number of aircraft available for measurements in the upper troposphere and lower stratosphere (UTLS) is much smaller, with the Russian high-altitude research aircraft M-55 Geophysica and the "High-Altitude and Long-Range Research Aircraft" (HALO) of DLR being two of the more prominent examples.

An approach to obtain fast number-based size information in the small nanometer size range during airborne measurements was first described by Stein et al. (2001). They developed an instrument that they named Condensation Particle Size Analyzer (CPSA), which made use of the impact of different operating parameters on the smallest particle size detected by a CPC. The CPSA essentially consisted of four CPC engines operated in parallel, each with a different lower detection limit. They purposely varied the temperature difference between the CPCs' saturators and condensers by 9 to 30 K, which resulted in different supersaturations and hence different cut-off diameters. For an ammonium sulfate test aerosol, they were able to purposely vary the instrument's d_{50} between 4 and 13 nm.

A notable alternative to dedicated but costly research flights is the use of commercial long-distance passenger aircraft for global atmospheric observations. The Global

Observations research group at Forschungszentrum Jülich operates research instruments routinely on commercial passenger aircraft as part of the “In-Service Aircraft for a Global Observing System” (IAGOS) research infrastructure (Petzold et al., 2015). The IAGOS research infrastructure builds on two decades of experience acquired in two earlier projects that deployed instruments for atmospheric measurements onboard a fleet of passenger aircraft: MOZAIC (Measurement of Ozone and Water Vapour on Airbus In-service Aircraft) and CARIBIC (Civil Aircraft for the Regular Investigation of the Atmosphere Based on an Instrument Container). Like both of these earlier research projects, IAGOS also relies on commercial passenger aircraft as the measurement platform. IAGOS uses custom-built, autonomous high-tech instrumentation for the in-situ measurement of atmospheric chemical species and aerosol particles. IAGOS-CORE could be regarded as the continuation of MOZAIC, as it offers the same high quality of measurement data. The IAGOS-CORE aerosol package P2c that is used for these measurements includes two CPC units that measure aerosol particle numbers in the UTLS. One of the CPCs in the P2c aerosol package measures the total particle number concentration and the other CPC determines the concentration of non-volatile particles that remain after passing through a thermodenuder, which is a device that can be used to remove the volatile compounds of the aerosol (Bundke et al., 2015).

The operation of CPCs onboard an aircraft presents a truly unique set of challenges. Firstly, all technical issues that come with operating research instruments on a commercial aircraft have to be addressed. This includes aspects such as dedicated sampling probes, a suitable enclosure, fire protection and the physical location of the measurement package, to name just a few. Secondly, operating conditions onboard an aircraft greatly deviate from standard conditions, especially with respect to the rapid changes in outside ambient pressure and temperature. It takes an Airbus A330 aircraft about 2.5 min to reach an initial altitude of 5,000 ft after take-off, which corresponds to an ambient pressure of approximately 840 hPa, and about 10 min to climb to 16,000 ft (550 hPa). An A330 reaches its maximum cruising altitude of 41,000 ft, corresponding to 180 hPa, about 30 min after take-off. The sampling inlet is thus exposed to a range of ambient pressures, with air pressure changes as high as 100 hPa per minute. Thirdly, the aerosol package P2c had to be designed for fully autonomous measurement periods of two months without user intervention, which added further requirements. One key aspect here are the data acquisition and the transfer to making them available in near real-time (Petzold et al., 2015). Finally, special requirements regarding compliance with aircraft safety regulations and the high-quality management standards of civil aviation have to be fulfilled. Safety regulations require for instance the safe handling of the CPC’s working fluid, which resulted in the development of two double-walled containments for the butanol supply and its reservoir in the P2c aerosol package (Bundke et al., 2015).

2.5.3 Continuous monitoring of particle number in urban air

At present, no binding international or national ambient air quality standard requires the routine monitoring of the number concentration of fine and ultrafine particles, while environmental authorities in most parts of the world have been required to measure the PM2.5 and PM10 particulate mass already for many years. At the same time, the public awareness of local air pollution and the impact on the climate keeps increasing. In particular, people living in close proximity to emission sources such as power plants and incinerators, but also airports, busy roads and waterways have become active in the fight against harmful levels of ultrafine particles on a local level. In the United States, the Environmental Protection Agency (US EPA) was the first governmental agency that at least added the measurement of ultrafine particles as an optional metric to the measurements done in its near-road monitoring networks. In consequence, some regional agencies like the Bay Area Air Quality Management District (BAAQMD) started to monitor particle number concentrations. The BAAQMD currently does so at nine sites in the San Francisco Bay Area using CPCs. In Europe, the National Air Pollution Monitoring Network (NABEL) monitoring network in Switzerland (EMPA, 2000) and the German Ultrafine Aerosol Network (GUAN; Birmili, 2015) also added particle number concentration as a metric to their routine monitoring efforts. In 2016, the European Committee for Standardization (CEN) published a technical specification that harmonizes the continuous measurement of particle number concentration of atmospheric aerosol by CPCs (CEN/TS 16976:2016). It determined that only CPCs with identical cut-off diameters and working fluids should be used under well-defined operating conditions.

The same CEN guideline does not specifically determine a valid range of atmospheric pressure, although it does refer to the measurement being made “above 900 hPa” and that “instrument inlet temperature, pressure and relative humidity” should be reported with the data. This makes complete sense in Europe, which only has a dozen mid-sized cities above 1,000 m asl across the continent, of which Davos in Switzerland (1,560 m) and Briançon in France (1,326 m) are at the highest elevation. The situation is quite different globally, however, as many cities with more than 100,000 inhabitants can be found at high altitude in several countries in Central and South America such as Bolivia, Colombia, Ecuador, Mexico and Peru. In Asia the same can be said for China and India. Of these larger cities the aptly named El Alto in Bolivia has the highest elevation at 4,150 m, which corresponds to a barometric pressure of just 604 hPa at 15°C.

2.5.4 Vehicle exhaust emission certification

The earliest near real-time measurements of particles emitted by vehicle exhaust were made by David Kittelson and co-workers around 1974. They were the first to use the Electrical Aerosol Analyzer (EAA) for their research on engine exhaust (Sem et al., 2010). In 1980, the first CPC was introduced as a detector to the measurement

of diesel exhaust aerosol, at the time still in combination with a diffusion battery. While CPCs found an increasing use for the measurement of vehicle exhaust emissions over the years, it took almost three decades until they were considered for regulatory use. This was the direct result of the Particle Measurement Programme (PMP), which was established as a Working Group of the United Nations Economic Commissions for Europe (UN-ECE) Working Party on Pollution and Energy (GRPE) in August 2001. The purpose of the PMP was to develop a measurement system with good sensitivity for measuring nanometer-sized particles in heavy and light duty vehicle emissions, so they could be regulated and type approval legislation amended in order to reduce the particle emissions from these vehicles. Phase 1 of PMP investigated the repeatability of several potential candidate instruments during steady-state and transient laboratory tests at a single site. This was followed by a comparison study of the best-performing measurement systems during PMP phase 2, which subjected a total of 21 different particle instruments to even more diligent tests. The final report (Mohr and Lehmann, 2003) came to the far-reaching conclusion that the solid particle number method achieved the objective of the program, which effectively lead to CPCs becoming the method of choice for this use by the automotive industry. During PMP phase 3, a “Golden” solid particle number measurement system was then used as a reference that was circulated to the different sites that participated in an interlaboratory test program (Andersson et al., 2007). After more than seven years of work, PMP agreed on a robust test procedure, which became known as the “PMP method”. It specifies all aspects of the measurement of the number of solid particles in vehicle exhaust emissions in great detail. The European Commission followed the findings and recommendations of the PMP group and a new vehicle emission standard came into force in early 2009 (UN-ECE, 2015). This was also the first time that particle number (PN) was included in a regulation anywhere in the world (Bischof, 2015). Effectively since September 2011, Euro 5b and subsequent Euro 6 light-duty vehicle emission standards required the measurement of the number of solid particles for the type approval of all new diesel vehicles sold in the European Union. Since 2014, the Euro 6 standard also limits the PN emissions from gasoline direct injection (GDI) light-duty vehicles. Today, a PN limit value of 6×10^{11} particles/km cannot be exceeded in the exhaust of all new light-duty diesel and gasoline vehicles during type approval. This regulation for light-duty vehicles was complemented by the on-road PN measurement of vehicle emissions with the so-called Portable Emissions Measurement Systems (PN-PEMS) in September 2017, which also involves CPCs, although not exclusively. For heavy-duty vehicles such as trucks and buses, PN emission limits were introduced with the Euro VI standard that went into effect in 2013 for new type approvals and in 2014 for all registrations. The PN limit value in the Euro VI standard is 6×10^{11} particles/ kWh under the conditions of the World Harmonized Transient Cycle (WHTC) test.

All of the above regulations specify the use of a PNC instrument that is in fact a full-flow CPC with a well-defined cut-off diameter and counting accuracy, see the salient

performance criteria in Tab. 3. The CPCs that are used for these legislative emission measurements must be properly calibrated by the manufacturer preceding their first use and be supplied with a corresponding calibration certificate. Prior to using a CPC for such an emissions test, the user needs to make sure that the CPC has been calibrated against a traceable calibration standard within the past twelve months. This requires calibration against either an aerosol electrometer or another CPC that was calibrated against an electrometer acting as a reference (Giechaskiel et al., 2009).

Tab. 3: Salient performance criteria of a CPC used as PNC detector in legislative vehicle emission testing (UN-ECE, 2015).

Parameter	**Criterion**	**Specification**
Counting efficiency	d_{50} (50% ± 12%)	23 nm (± 1 nm)
	d_{90} (>90 %)	41 nm (± 1 nm)
Counting accuracy	from 1 to 10,000 P/cm^3	±10%
Readability	below 100 P/cm^3	0.1 P/cm^3
Concentration linearity		linear over full range
Measurement mode		single particle counting
Reporting frequency of data		≥ 0.5 Hz
Response time (T90)		< 5 s
Coincidence correction		≤ 10%

This legislative use of CPCs drove the development of a corresponding traceable calibration method (UN-ECE, 2015). Yet it still raises questions when emission tests in this highly regulated environment are performed at ambient conditions significantly different from the specified atmospheric pressure conditions of 100 kPa ± 7.5% due to the geographical location. In the EU, the highest elevation of an emissions test facility is about 800 m asl but in the United States, Tier 3 standards introduced a definition of high-altitude conditions that require a test altitude that corresponds to 1,620 m asl. This criterion has been included as the decrease in oxygen supply at high elevations has a notable effect on internal combustion engines, in particular on their engine power. The reduced air density leads to the fuel-air mixture becoming richer, which also results in increased fuel consumption and hence higher tailpipe emissions. Testing of engines and vehicles at high altitude locations is therefore regularly performed at locations in e.g. Colorado (USA) as well as Mexico. China has nine provinces with an elevation higher than 1,500 m, which is why their government changed its regulatory requirements for testing to altitudes. Although emissions

testing in North America will only require the use of CPCs for the type approval of vehicles that are exported, the new China 6 emissions regulations require the same PN limit value as the corresponding Euro 6 regulations since January 2021. The Chinese regulation also has a specific altitude requirement that the particle number counter must work up to 2,400 m asl. So, despite the fact that there are several test centers globally that operate at a reduced pressure, as well as on-road tests that are also being done on mountain roads, there is currently no specification for the calibration of CPCs used at high elevation or correction for lower ambient pressure.

2.5.5 Aircraft emissions testing

The potential of particles emitted by aircraft engines to impact cloud formation in the atmosphere was investigated during large studies such as the PartEmis experiment reported in Petzold et al. (2003). The outcome of their research was detailed information on the particle size distribution, thermal stability, mixing state, and CCN activation of aircraft emission. All of these parameters are needed to advance the understanding of the contribution of global aviation to climate change. Environmental conditions to test aircraft emissions during actual in-flight operation are challenging to say the least. Airplanes are flown at altitudes of up to 12,000 m which results in very different conditions than on the ground. Most importantly, the atmospheric pressure at such high altitude can drop to 200 hPa and even below. In practice, there is no reasonable way of routinely testing the emissions from aircraft under in-flight conditions. Consequently, the relevant SAE Aerospace Recommended Practice (ARP) is an aircraft *engine* method instead of one for the aircraft in its entirety. It describes the recommended sampling conditions, measurement instrumentation, and procedures for the measurement of non-volatile particle concentrations from the exhaust of aircraft engines. It is performed at dedicated test beds for aircraft gas turbine engine emissions measurement on the ground. During these emission tests, the engines are operated at atmospheric conditions with corrections made for a reference temperature of 15°C and an air pressure of 101.3 kPa.

During the SAMPLE project, Petzold et al. (2011) performed an experimental comparison of particle measurement techniques with the aim to assess their suitability for standardized measurement of the particulate emission from aircraft engines. They used three different models CPC side-by-side to measure the particle number concentrations from a simulator that generated an emission that was found to be representative of aircraft exhaust. The importance of the calibration was highlighted when the CPCs were first utilized in the project. Initially there were large discrepancies as the different model CPCs were used without the cut-off size being specified or considered, which created an uncertainty of the measurement that was not acceptable for legislative purposes (Crayford et al., 2011). Specifically, in the size range below 23 nm where volatile particles are typically found, number concentrations showed large differences of up to 30%. After testing a great variety of aircraft engine

types and sizes, the measurement uncertainty could be reduced by agreeing on specifications for CPCs employed for the dedicated measurement of aircraft emissions. The results from this project demonstrated that CPCs are robust and accurate instruments, but also that the lower cut-off diameter and proper sample conditioning must be well-defined to achieve reliable and reproducible results.

The project concluded with the recommendation to measure the non-volatile particle number by combining a volatile particle remover and a CPC (Petzold et al., 2011). This recommendation ultimately found its way into the new international aircraft emission regulation. In February 2019, the International Civil Aviation Organization (ICAO) agreed on the new, more stringent standard for the certification of aircraft and aircraft engines that for the first time limit the emissions of non-volatile Particulate Matter (nvPM) by their number concentration. The ICAO requires that this measurement is done by a CPC with a 10 nm cut-off diameter as most of the non-volatile particles from aircraft turbine engines are in the particle size range from 15 to 60 nm. Nonetheless, the new standard only requires a manufacturer's calibration of the CPC's d_{50} and d_{90} diameters, as well as a linearity test, which are to be done at ambient conditions.

3. Review of prior research

This chapter describes a thorough review of existing peer-reviewed literature on the operation of CPCs at low pressure. It is intended to document the current state of knowledge before describing the experimental aspects of this work. After reviewing the literature, the previous research is grouped into three categories and the findings are evaluated. This chapter does not attempt a complete overview of all literature published on this subject as only few studies were extensive characterizations done at several levels of operating pressure and for various particle sizes. Instead it focuses on those papers that can be considered relevant benchmark studies.

3.1 Historic context of low-pressure experiments

Already more than 80 years ago G. Schlarb studied the use of an adiabatic-expansion CNC under non-standard conditions. During his experiments he observed a drop in the total counting efficiency when he operated his device at lower than atmospheric pressure. Schlarb (1940) reported his observation yet he did not provide any theoretical analysis of its occurrence. This so-called Schlarb effect has been largely forgotten since it was investigated at that time and I am very grateful to François Gensdarmes of IRSN in France who made me aware of its existence. Twenty years later than Schlarb, Pollak and Metnieks (1960) showed in experiments with their model 1957 photoelectric CNC that the difference they measured for a given total concentration was the larger, the lower the pressure. They also found that for a given pressure the discrepancy increased with the amount of the number concentration. Their discovery is in contrast to the classic activation theory as the Kelvin equation does not include the number concentration as a contributing factor.

In 1976 Philippe Mulcey published his PhD thesis on work he did under the guidance of Professor Jean Bricard, the father of French aerosol science. During his studies, Mulcey investigated the vertical distribution of condensation nuclei in the stratosphere using balloons. For this work, he used a new type of continuous-flow CNC developed at the Saclay Nuclear Research Centre of the French Atomic Energy Commission (CEA) near Paris. This design was one of the two immediate predecessors of the first commercial continuous flow CPC (Model 3020, TSI Inc.; Agarwal and Sem 1980), which later found very wide use globally. Mulcey adapted his prototype for measurement at UTLS conditions and conducted tests in a low-pressure simulation chamber. He declared that one should be able to derive the theoretical number concentration N_T of an aerosol contained in a chamber at reduced pressure from the concentration N_0 at atmospheric pressure and the ratio of the reduced pressure p to the atmospheric pressure p_0:

$$N_T = \frac{N_0 * p}{p_0} \tag{3.1}$$

Mulcey stated that the measured number concentration N of the aerosol in his chamber will be less than the expected theoretical number concentration N_T when the pressure is lowered. He found that under certain conditions the concentration difference could be eliminated when he increased the supersaturation inside the CNC. He accomplished this by using a higher saturator temperature, while he maintained the condenser at a constant temperature. He concluded that besides the operating pressure, the main parameters contributing to the Schlarb effect are the supersaturation applied to the mixture of aerosol and saturated vapor - and the magnitude of the aerosol number concentration.

3.2 Early research in the 1980's and 1990's

Heintzenberg and Ogren published one of the earliest noteworthy studies on the operation of a modern-day CPC at reduced pressure in 1985. Their paper focuses on the use of a CPC onboard the DLR's Falcon 20 aircraft during experiments in the Arctic troposphere, with measurements conducted between sea level and about 10,000 m altitude. In their work they used the commercial model 3020 CPC (TSI Inc.), which was only introduced a few years before their experiments. As this model CPC cannot be operated under reduced and varying pressure conditions as is, they made two simple modifications: 1) they replaced the built-in pump and mass flowmeter by an external pump and needle valve, and 2) they replaced a few gaskets and the automatic butanol refill systems to make the instrument leak-tight.

Additionally, they also calibrated their CPC using an aerosol ageing and expansion technique. They used a polydisperse laboratory aerosol that was aged for some time in a glass vessel and evacuated it down to 100 Torr (133 hPa). They then increased the pressure by adding filtered air through a needle valve into the vessel. As a result, they found that the model 3020 "counts most of the particles in the vessel above 300 Torr" (400 hPa). Beyond this rather qualitative observation, they also made a correction of the number concentration reported by their CPC to account for the actual volume flow. Based on this correction they concluded that this model CPC worked well down to a pressure of about 200 Torr (267 hPa). It is important to note that Heintzenberg and Ogren commented that a better approach to calibrate a CPC for use at reduced pressure "is a calibration with monodisperse, singly charged particles at a range of pressures", but that they did not have the necessary instruments available at the time. It is for this reason that their work does not include any counting efficiency curves or reports changes in the CPC's lower detection limit.

Zhang and Liu conducted two studies that investigated the performance of CPCs at reduced pressure, one for the model 3020 in 1990 and the other for the model 3760 (TSI Inc.) in 1991. The first was a theoretical study that looked at the heat and mass transfer processes inside the condenser section of the CPC 3020. They explained that a lower operating pressure and a lower flow rate will increase the thermal cooling

effect, and simultaneously result in enhanced losses of the butanol vapor to the walls of the condenser section. By contrast, a higher operating pressure and flow rate will result in less depletion of the butanol vapor onto the walls of the condenser but simultaneously lead to a weaker thermal cooling effect. Both of these opposing effects are competing, which is the process that ultimately determines the CPC's performance. Their numerical analysis showed that the cut-off diameter of a model 3020 CPC is the smallest at standard atmospheric pressure, and that it shifts by several nanometers to larger sizes when the pressure is reduced to one tenth of it.

In their 1991 paper, Zhang and Liu describe the experimental work on the performance of a CPC 3760 over the range from 1,000 to 100 hPa. To my knowledge this was the first study that experimentally determined the counting efficiency of a CPC for different levels of operating pressure depending on particle size. In their setup they used an atomizer to produce particles from a NaCl solution, which they subsequently vaporized in a furnace heated to 900°C and finally nucleated to form primary particles by rapid cooling. Their aerosol generation system was completed by a DMA to size select monodisperse particles. The low-pressure section, which contained the CPC under test and a reference aerosol electrometer, was separated by a pressure control valve and pumped to the desired pressure level. Although the size resolution of their counting efficiency curve is limited, it reveals that the overall counting efficiency of a CPC 3760 diminishes only a little when the operating pressure is lowered to levels of 200 to 300 hPa. Their data also show a significant shift of the CPC's lower cut-off diameter towards larger particle sizes with decreasing pressure. This agrees with their theoretical work for the CPC 3020. They also found that the maximum counting efficiency at larger sizes drops to only about 10% of the value at standard conditions when the pressure is reduced further to 100 hPa.

A few years later Cofer III et al. (1998) presented a paper that describes a laboratory calibration before their field experiments. Once again, the purpose of their work was the use of CPCs onboard an aircraft, which in their case was NASA's T-39 Sabreliner jet. They also calibrated four different CPC instruments rather than just one, of which two were model 3025A ultrafine CPCs and two were models 3760 (both TSI Inc.). Following Heintzenberg and Ogren, they replaced the CPC's built-in pumps and flow controllers by a different pump and external mass flow controllers. Cofer III et al. generated a calibration aerosol by the Scheibel and Porstendörfer method (Scheibel & Porstendörfer, 1983), which couples a constant temperature tube furnace to produce a polydisperse primary aerosol and a DMA for electrostatic classification of discrete particle sizes. As a result, they got a monodisperse, non-volatile NaCl aerosol with diameters ranging from 4 to 180 nm. At ambient conditions, their model 3025A UCPCs counted between 91% and 97% of the total number of particles measured by a reference electrometer. Efficiencies for the model 3760 CPCs were not determined at ambient conditions.

The main focus of their work was to characterize the CPC performance for the aircraft system at a constant 160 Torr (213 hPa), which corresponded to the pressure of their internal flight-system. In order to mimic airborne conditions, the calibration aerosol was drawn directly from a manifold controlled to the reduced pressure level via critical orifice. Cofer III et al. found that at 160 Torr the total measurement efficiency of the ultrafine CPCs in the range from 10 nm to 180 nm was about 75%, while it was about 55% for the model 3760 CPCs in the range from 20 nm to 180 nm, see Fig. 9. They also concluded that both CPC models started to undercount particles “as concentrations rose into the mid 10^4 P/cm^3 range” and that this “behavior could be calibrated for and corrected over the range of our tests”.

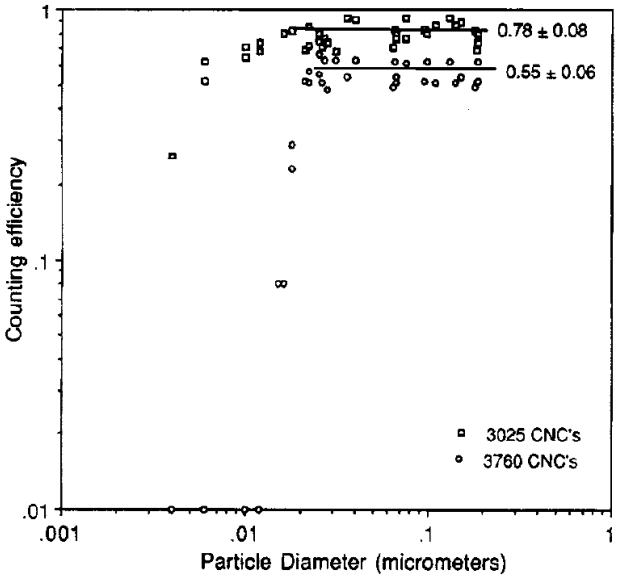

Fig. 9: Counting efficiencies of two CPCs at 160 Torr, taken from Cofer III et al. (1998).

Although Cofer III et al. reported a change in the total counting efficiency for both CPC models and that the lower cut-off diameters changed as well, the precise impact of an ambient pressure of 160 Torr on the counting efficiency curve cannot be clearly seen. One can speculate from their graph in Fig. 9 that basically the slope of the counting efficiency curve drops more sharply and that the d_{50} or lower cut-off diameter increases from the nominal 3 nm to about 6 nm for the ultrafine CPC. At the same time, it seems to indicate an increase from 14 nm to about 20 nm for the CPC 3760.

3.3 Work by Hermann in the 2000's

A very important milestone in the performance characterization and calibration of CPCs at aircraft pressures was the research of Markus Hermann and co-authors published in the early 2000's (Hermann, 2000; Hermann and Wiedensohler, 2001, Hermann et al., 2005). Their work was done during the "Civil Aircraft for Remote sensing and In-situ measurements in the troposphere and lower stratosphere Based on the Instrumentation Container concept" (CARIBIC) project. The goal of CARIBIC were aerosol and trace gas measurements in the upper troposphere and lower stratosphere using scientific instruments in an air-freight container flown on board commercial aircraft. The CARIBIC aerosol system included CPCs 7610 (TSI Inc.), which were introduced in 1992 along with a remote processor that allowed for them to be used in semiconductor manufacturing environments. The model 7610 was thus the industrial cleanroom monitoring variant of the CPC 3760, with an initially identical geometry and operating parameters. Hermann modified his CPCs 7610 to meet aviation requirements and designated them as model 7610lp. The main modifications were replacing materials not permitted for commercial flights, improving the mechanical stability and changing to a 28 V DC power supply.

The calibration setup of Hermann and co-workers was similar to the one of Cofer III et al. It also relied on the Scheibel and Porstendörfer method to produce a primary, polydisperse aerosol, a DMA to size-select particle diameters and an aerosol electrometer as the concentration reference. The main difference is that in Hermann's setup at the Leibniz Institute for Tropospheric Research (TROPOS) also the DMA was operated at reduced pressure. The pressure in this setup could be reduced from ambient level down to 160 hPa, once again by manually adjusting a needle valve. For the CARIBIC aerosol system, the CPC 7610lp was characterized at six discrete pressure levels of 160, 200, 300, 400, 700 and 1,000 hPa. The particle sizes of the calibration aerosol were varied from 3 to 50 nm for silver and from 5 to 90 nm for salt (NaCl) particles. This work is the first that thus provided detailed counting efficiency curves at several pressure levels with high size resolution.

In Hermann's study, detailed counting efficiency curves were determined for his modified model 7610lp CPC based on up to 12 particle sizes below 15 nm, as shown in Fig. 10. The results show a slight decrease of the lower detection limit from 14 nm at standard conditions to about 11.5 nm for pressures between 160 and 300 hPa. Along with that shift in the cut-off diameter there is also a notable change in the counting efficiency curves below 400 hPa. The curves increase their slope with reducing pressure and decrease the maximum counting efficiency to as low as 80%, with the latter value being the one determined at the lowest pressure of 160 hPa.

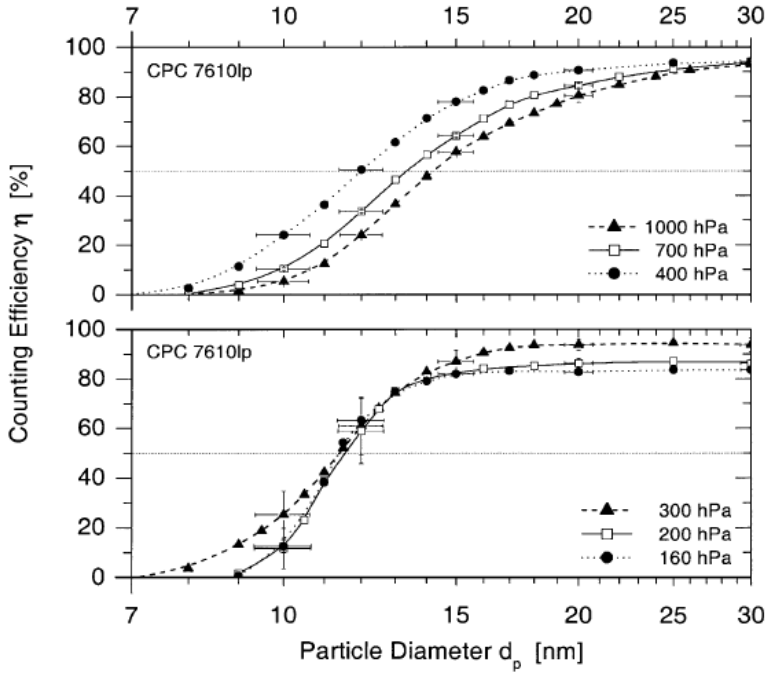

Fig. 10: Counting efficiencies of a modified CPC 7610lp for silver particles at 160, 200, 300, 400, 700 and 1,000 hPa, taken from Hermann and Wiedensohler (2001).

In his PhD thesis, Hermann (2000) concludes that there is no obvious explanation for the decrease he observed in the maximum counting efficiency of the CPC. He surmises that it might be caused by changes occurring in the focusing nozzle just before the CPC optics due to the reduced volume flow at decreasing pressure. Improper focusing of the detected flow could in principle result in a weaker scattering signal below the CPC's threshold setting for optical detection, but this theory was later dismissed by Takegawa and Sakurai (2011).

3.4 More recent work

In 2011 Takegawa and Sakurai investigated the performance of a model 3771 CPC (TSI Inc.) for use under airborne measurement conditions. Their CPC model of choice was another laminar-flow, butanol-based instrument, which succeeded both the CPC 3760A and the model 3762 in 2006. The manufacturer specified this CPC model for an ambient range from 1,050 to 750 hPa. Unlike in other studies, no modifications for use at low pressure were mentioned by the authors. Their experimental setup relied on an electrospray aerosol generator (Model 3480, TSI Inc.) to produce small sucrose particles up to 50 nm and in addition on a Combustion Aerosol Standard (CAST) to

produce flame soot particles of 50 nm and larger. The aerosol generators as well as a DMA, a reference CPC and the supply of make-up air were all operated at standard conditions. Only the CPC and the reference aerosol electrometer were placed in the low-pressure section, which was separated from the aerosol generation section by an orifice. Instead of using a needle valve to reduce the pressure, Takegawa and Sakurai made use of orifices with different diameters to avoid contamination caused by particles possibly being produced when adjusting the valve. They performed their experiments at five discrete pressure levels ranging from 1,010 hPa to 300 hPa. One interesting difference compared to the work of Hermann et al. was that they repeated their 60 second measurements five times, with the DMA's high voltage being set to 0 V before, in between and after the actual measurements, so that a total sampling time of 11 min was needed for each pressure level and particle size. In their study they found essentially no differences in the counting efficiency curves for sucrose particles between 1,010 hPa and 800 hPa. Only after lowering the pressure further to 600 hPa, they observed a slight shift of the curve to *larger* particles, as can be seen in Fig. 11.

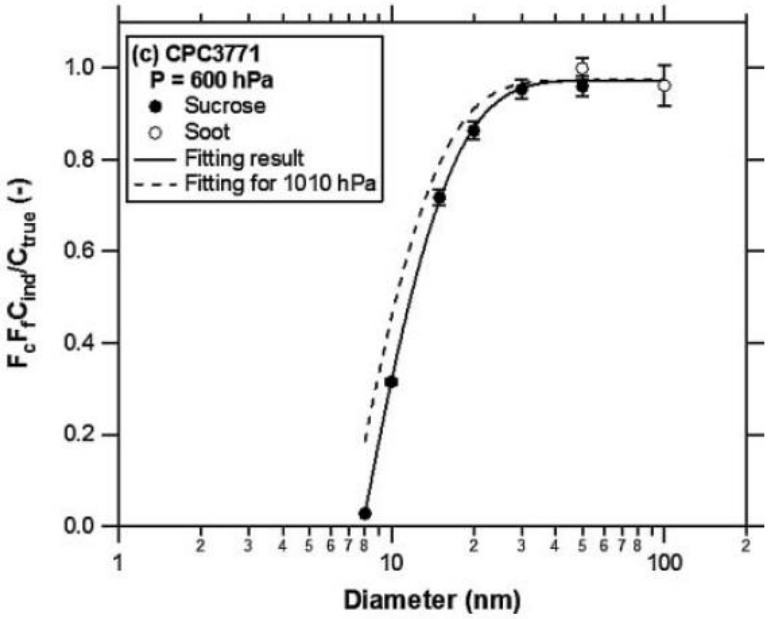

Fig. 11: Counting efficiency of a CPC 3771 for sucrose and soot particles at 600 hPa compared to 1,000 hPa (dashed line), taken from Takegawa and Sakurai (2011).

That shift to a larger particle diameter got even more pronounced the more they lowered the pressure. Finally, at 300 hPa, which was the lowest pressure they tested, the counting efficiency curve had shifted substantially to larger particle sizes as shown

in Fig. 12. The curve also exhibited a flatter slope and it is clearly visible that only a much lower maximum counting efficiency of about 85% is achieved.

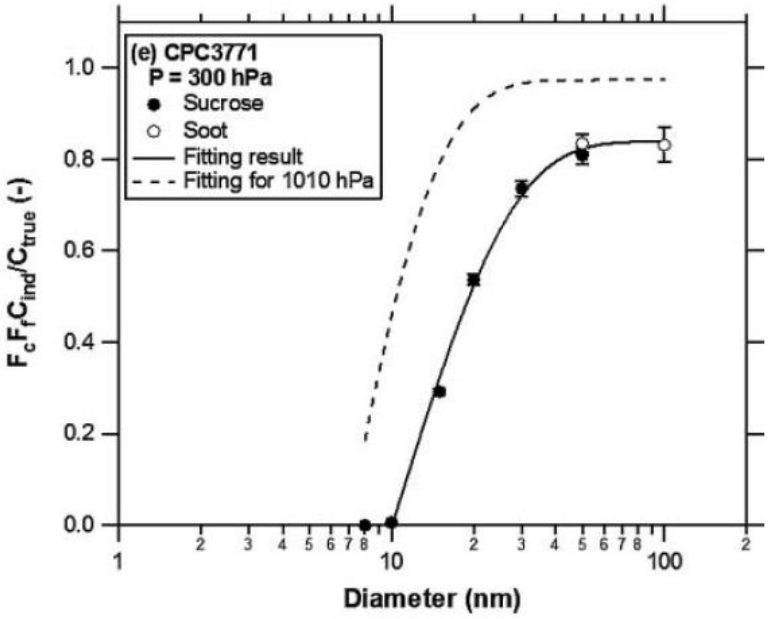

Fig. 12: Counting efficiency of a CPC 3771 for sucrose and soot particles at 300 hPa compared to 1,000 hPa (dashed line), taken from Takegawa and Sakurai (2011).

The data in the Takegawa and Sakurai (2011) paper seem to suggest that between 1,010 and 600 hPa the CPC's cut-off diameter for sucrose particles increased only slightly from the nominal 10 nm to an actual value of approximately 10.5 nm, while it shifted significantly to about 20 nm when decreasing the pressure further to 300 hPa. The authors hypothesized that their observed effects were due to a diminished saturation ratio, caused by rapid losses of butanol vapor to the condenser walls at very low pressure. An additional effect of a lower saturation ratio would be less condensational growth, which could also result in the lower maximum detection efficiency observed at 300 hPa.

An even more recent study is the one conducted by Bundke et al. (2015), which was driven by the increasing interest in long-term atmospheric and climate research realized in the IAGOS research infrastructure described in chapter 2.5.2. Their CPC model of choice was a Sky-CPC 5.411 (Grimm Aerosol Technik GmbH & Co. KG, Ainring, Germany), which is a CPC core unit without pump or display that is optimized for operation at low pressure according to the manufacturer. In their initial calibration they characterized and calibrated the Sky-CPC for pressure levels of 170, 200, 600 and 900 hPa in a laboratory experiment; see Fig. 13.

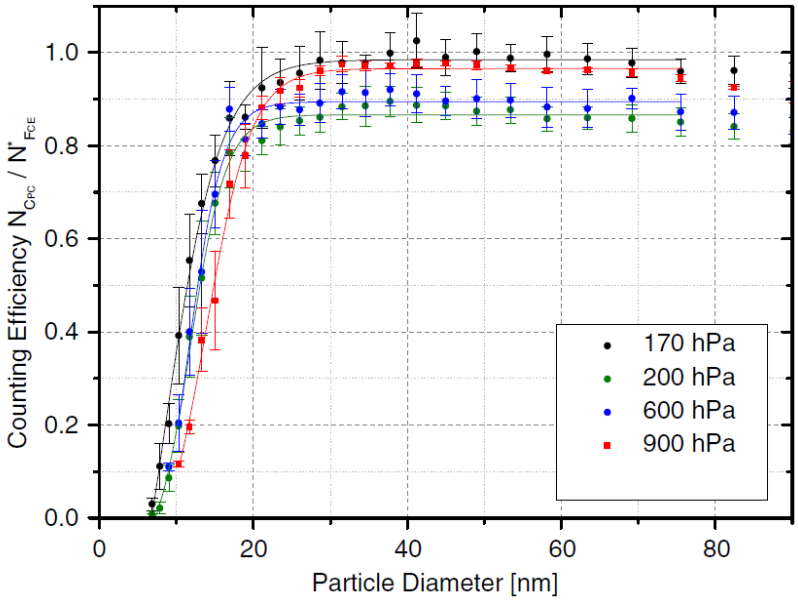

Fig. 13: Counting efficiency of a Sky-CPC 5.411 for ammonium sulfate particles at 170, 200, 600 and 900 hPa pressure levels, taken from Bundke et al. (2015).

Their experimental setup consisted of an atomizer aerosol generator followed by a diffusion drier and a DMA to size select particle for the calibration. The outlet of their DMA was connected to the low-pressure section by means of a critical orifice. In that section, the test aerosol was conditioned and diluted before it was subsequently split into the CPC under test and a reference aerosol electrometer. They used ammonium sulfate as their calibration aerosol and challenged the CPC with two dozen particle sizes, of which nine below 20 nm. With this approach, they determined a lower size detection limit of 15 nm at 900 hPa and one of about 11.5 nm at 170 hPa. Their data imply that the Sky-CPC's d_{50} cut-off size shifts only slightly to smaller diameters when going to greatly reduced pressure. Interestingly, at larger particle sizes the asymptotic detection efficiency of that CPC does not follow the same trend as the CPC's cut-off. The data of Bundke et al. exhibit a continuous decrease of the maximum detection efficiency when lowering the pressure from 900 to 200 hPa. At 200 hPa, they observed a counting efficiency of greater than 86% for particles with a diameter of about 25 nm and larger. When further reducing the operational pressure to 170 hPa that trend reverts and the counting efficiency increases again to values close to 100% for all particles larger than about 30 nm. This phenomenon was not explained further.

3.5 Summary of previous work

This literature study analyzed about two dozen peer-reviewed publications that investigated the performance of various CPCs at reduced atmospheric pressure which were published in the past 35 years. An overview of the key technical specifications of the previously characterized CPC models is given in Tab. 4.

Tab. 4: Summary of main specifications of the butanol CPC models used in previous studies.

Study	Model	Manufacturer	Nominal cut-off, d_{50} [nm]	Detected flowrate [cm^3/min]	Operating temp. T_{sat}, T_{cond}
Heintzenberg & Ogren (1985), Zhang & Liu (1990)	3020	TSI Inc.	10	300 (full-flow)	35°C, 10°C
Zhang & Liu (1991), Cofer III et al. (1998)	3760	TSI Inc.	10	1410 (full-flow)	ΔT= 17°C
Cofer III et al. (1998)	3025A	TSI Inc.	3	30 ± 3 (split-flow)	37°C, 10°C
Hermann (2000), Hermann & Wiedensohler (2001)	7610lp	TSI Inc., modified	14	1410 (full-flow)	ΔT= 17°C
Takegawa & Sakurai (2011)	3771	TSI Inc.	10	1000 ± 50 (full-flow)	39°C, 22°C
Bundke et al. (2015)	5.411 Sky-CPC	Grimm	13	600 (full-flow)	36°C, 10°C

Essentially all of the previous studies employed butanol CPCs, with all but the 3025A model used by Cofer III et al. being of a full-flow design where the sample flowrate equals the detected aerosol flowrate. All but one of the CPCs previously characterized are out of production today, with the most recently characterized Sky-CPC 5.411 being the exception.

When comparing the previous literature, the apparent implication is that there is no consensus on how a CPC can be expected to perform at reduced pressure overall. This can also be seen in the overview provided in Tab. 5. On the one hand, a number of studies concludes that the d_{50} lower detection limit of a CPC shifts towards slightly *smaller* particle diameters (-) when the operating pressure is reduced. Wilson, Hyun, and Blackshear (1983) were the first to report such a shift in the cut-off size of a CPC towards smaller particle diameters for a pressure shift from 400 to 187 hPa.

Tab. 5: Overview of approximate values from previous key studies on full-flow CPC models.

Study	Lower cut-off size d_{50} at reduced p	Direction of d_{50} shift	Maximum detection efficiency N_{max}	Shift of N_{max}
Heintzenberg & Ogren (1985), CPC 3020	NA	NA	100% at ≥400 hPa	<10% at 267 hPa
Zhang & Liu (1991), CPC 3760	23 nm at 200 hPa	++	99% (100 nm) at ≥200 hPa	<15% at 100 hPa
Cofer III et al. (1998), CPC 3760	20 nm at 213 hPa	++	NA	55% (100 nm) at 213 hPa
Hermann (2000), CPC 7610 (3760)	12 nm at 200 hPa	-	93% (30 nm) at ≥400 hPa	<83% at 160 hPa
Hermann & Wiedensohler (2001), CPC 7610 (3760)	12 nm at 200 hPa	-	95% (30 nm) at ≥300 hPa	<85% at 160 hPa
Takegawa & Sakurai (2011), CPC 3771	20 nm at 300 hPa	++	75% (30 nm) at ≥600 hPa	<85% at 300 hPa
Bundke et al. (2015), Sky-CPC 5.411	12.5 nm at 200 hPa	-	95% (30 nm) at ≥600 hPa	<87% at 200 hPa

More recently, Wiedensohler et al. (1997) as well as Schröder & Ström (1997), Hermann (2000) and Hermann & Wiedensohler (2001) all described an at least similar behavior in their trend, where the d_{50} cut-off sizes of their CPCs 7610/3760 shifted to *smaller* diameters at lower pressures. Hermann was the first to report that this is the case until an apparent minimum is reached at a certain pressure threshold. This critical pressure seems to be at a different level for the different CPC models. Hermann (2000) also stated that there is likely an enhanced heat transfer inside the condenser section of the CPC at reduced pressure, which is larger than the mass transfer of the working fluid to the walls of the condenser. On the other hand, four papers by Zhang and Liu (1990, 1991), Cofer III et al. (1998), and Takegawa and Sakurai (2011) show both theoretically and experimentally a shift towards notably *larger* cut-off diameters (++) with decreasing pressure. Takegawa and Sakurai (2011) suggest that the CPC design and losses of butanol vapor to the wall of the condenser section might influence how the d_{50} of a CPC changes.

In summary, the comparison of these previous studies on the operation of several CPC models at reduced pressure leaves us with several questions. The results reported in these peer-reviewed papers seem to be inconsistent, even for identical CPC models. This could be due to the fact that some of the studies were restricted to only one specific model, as the different CPC models come with different geometries

and operating parameters such as the temperatures of their condenser and saturators or their flow rates. The studies also varied in their detail, as some only looked at a small number of pressure levels, a limited number of particle sizes, and only one specific calibration material. Another likely cause of the discrepancies observed might be due to the precise calibration methods used. Previous studies used quite different experimental methods, especially with regards to the actual low-pressure section of the experiments. However, the combined results could also point to another reason: Maybe, in some cases, the precise performance of a CPC near its cut-off diameter *should be expected* to vary during its operation at reduced pressure.

4. Modeling of CPC performance at low-pressure

This chapter describes a two-dimensional numerical model for the activation of particles in a CPC. It is applied to initially determine the performance characteristics of a CPC under low-pressure conditions through numerical work. The model provides condenser saturation ratio profiles and theoretical counting efficiency curves for various low-pressure conditions. The modeling data help to gain insight into how the operating parameters impact the performance of a CPC at reduced pressure in theory.

4.1 Description of the numerical model

The theoretical prediction of the CPC counting efficiency curves in this chapter has been calculated based on the established analytical model developed by Stolzenburg (1991). A corresponding modeling tool had previously been implemented in MATLAB by Dr. Ryan Han at TSI headquarters, who also ran the model and provided the resulting raw data. My contribution was to define the modeling objective, select the operational parameters, generate the graphs in this chapter unless stated otherwise as well as all of the analysis provided here. This model could only be run for the CPC 3772-CEN but not for the Sky-CPC 5.411, as there are no constructive details available for the latter model since instrument manufacturers do not like to provide information on their exact CPC design for proprietary reasons.

The two-dimensional model of Stolzenburg (1991) determines the activation efficiency based on the sample flow going through the saturator and condenser sections of a thermal-cooling, laminar, continuous-flow CPC. As explained in chapter 2.2, in an alcohol-based CPC the aerosol sample is first saturated with alcohol vapor in the heated saturator section. The vapor is supersaturated once the vapor-aerosol sample flow mixture enters the thermally-cooled condenser section, where it condenses onto the aerosol particles and thereby forms much larger droplets. In the numerical model, the condenser is simplified to one uniform segment as illustrated in Fig. 14.

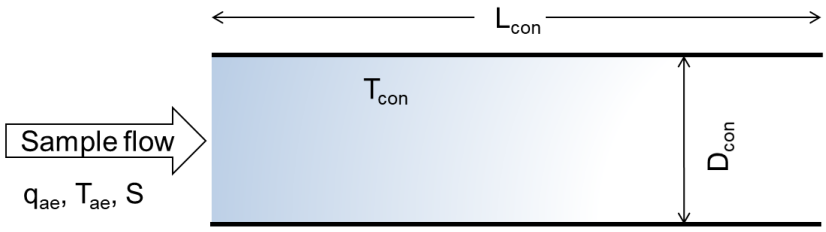

Fig. 14: CPC condenser section as assumed by the mathematical model.

In the model, the sample flow passes through the condenser, which is the section where particle activation and growth occurs. The sample flow is assumed to consist of particles dispersed in air, which provides the thermal and mass properties used for calculation. The operational parameters used by the model are thus the aerosol sample flow q_{ae}, the aerosol temperature after the saturator section T_{ae}, the saturation ratio S defined as being 1 at condenser entrance, as well as the length L_{con}, temperature T_{con}, and tube diameter D_{con} of the condenser section. The model treats the flow as fully laminar throughout the condenser section. Air density, thermal diffusivity, and the mass diffusivity of both the butanol vapor as well as the particles are all considered to be constant.

At first, the model considers convective and diffusive heat as well as mass transfer to derive profiles of temperature, vapor pressure and saturation ratio through the condenser section. The activation of particles depends on the spatial profile of the saturation ratio S of the condensing vapor, which is defined as the ratio of the fluid's vapor pressure p_v to the saturation vapor pressure, p_{sat}:

$$S = \frac{p_v}{p_{sat}(T)} \tag{4.1}$$

The activation efficiency of the CPC is then calculated by combining these profiles with the Kelvin equation (2.1) and the aerosol transport model, which assumes diffusional losses of particles to be insignificant. Further details and all equations used by the model are given in Stolzenburg (1991) and Hering & Stolzenburg (2005).

In a subsequent step, the theoretically predicted particle activation efficiencies at standard atmospheric pressure of 1,013 hPa were then compared to experimentally-determined counting efficiencies. Differences between the theoretical and experimental efficiency values arise from factors such as subsistent diffusional losses to the walls of the condenser, slight changes in residence time inside the CPC and non-uniform temperature profiles that can occur in reality. In addition, uncertainties of the modeling parameters can increase the disparity. This is especially true for properties like the mass and the thermal mass diffusivity, as well as the boundary layer effect. An effective *delta T* can be introduced to account for the difference between the aerosol temperature T_{ae} and the condenser temperature T_{con}, which is then used to adjust the calculation. The *delta T* is applied to the CPC modelling at both standard atmospheric pressure as well as the reduced pressure levels. In case of the CPC 3772-CEN, the deviation from actual to effective *delta T* turned out to be negligible.

4.2 Basic results of the numerical model

In the first stage the model was applied to a generic CPC model 3772 with a 10 nm lower cut-off diameter. This was done for two pressure levels, with the first pressure

being standard atmospheric condition of 1,013 hPa and the other a reduced pressure of 720 hPa, which corresponds to an altitude of approximately 2,840 m asl. This altitude is a good proxy for typical conditions found for example at the Pic du Midi or Schneefernerhaus mountaintop research stations.

The computed condenser centerline temperature for that CPC seems to behave very similar between standard and 720 hPa pressure, although it reaches up to 1.5°C difference before the peak saturation is reached. For the reduced pressure case, the condenser centerline temperature decreases faster, which can be attributed to the higher momentum diffusivity or kinematic viscosity and the thermal diffusivity at lower pressure. A lower condenser temperature results in a lower saturation vapor pressure as it is entirely dependent on the temperature. The vapor pressure in the condenser section is roughly the same at both 1,013 hPa and 720 hPa pressure as the working fluid's vapor pressure is essentially a function of the saturator temperature. As can be seen in equation (4.1), the saturation ratio *S* will increase at a lower saturation vapor pressure. This should lead to an increased activation efficiency at smaller particle sizes, as the Kelvin diameter is inversely proportional to the saturation ratio. In consequence, theory predicts that at a lower saturation vapor pressure a CPC should activate somewhat smaller particles and should be expected to have a lower cut-off diameter than at standard conditions.

As displayed in Fig. 15, the results of the model analysis indicate that the theoretical saturation ratio as a function of its dimensionless axial (z/R) coordinates peaks after passing about one quarter of the condenser tube along its axis.

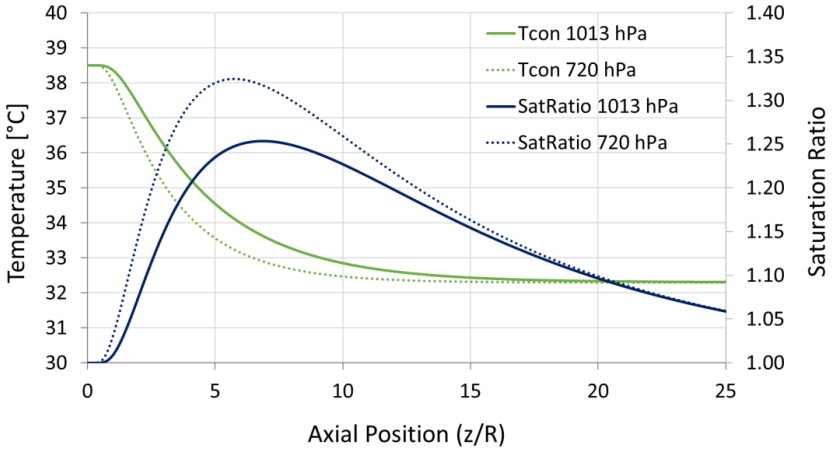

Fig. 15: Modelling results for centerline temperature and saturation ratio of the CPC condenser at standard pressure and a reduced pressure of 720 hPa.

This is the case for both standard and reduced pressures, with the differences being that there is a steeper slope in case of the reduced pressure and that its saturation ratio reaches a higher peak saturation value.

Although the Sky-CPC 5.411 could not be modeled in this work, it is possible to compare results with model data for the Grimm CPC model 5.41X that were publicly presented (Steiner et al., 2018). Fig. 16 shows the saturation ratio of that generic Grimm CPC model when operating it with standard temperatures of T_{sat}= 36°C for the saturator and T_{con}= 10°C for its condenser. As can be seen in the graph, the curve peaks much earlier along the axis of its condenser tube than the one of the CPC 3772. Notably, the saturation ratio of the CPC 5.41X also reaches a peak value that is approximately a factor of three higher than in the CPC 3772.

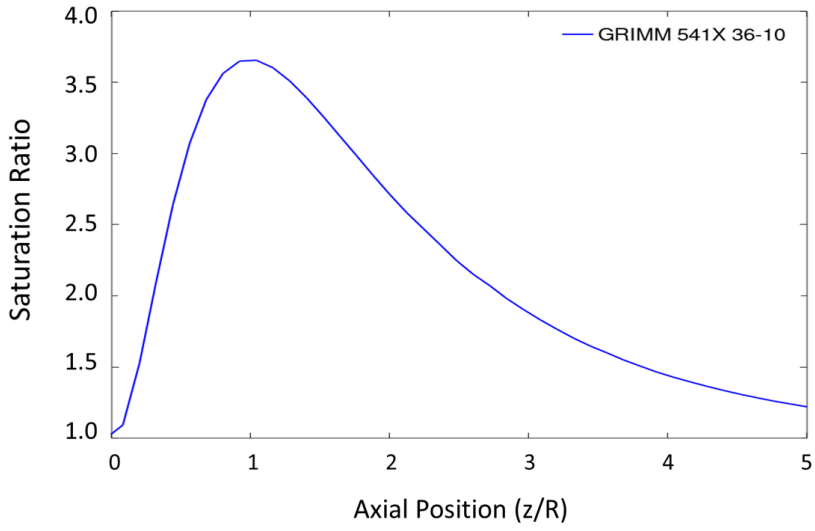

Fig. 16: Modelling results for the saturation ratio in a CPC 5.41X condenser along the axial position at standard pressure (Graph courtesy G. Steiner).

In a next step, the numerical model was used to calculate saturation ratio profiles for the generic CPC 3772 for the same two pressure levels of 1,013 hPa and 720 hPa as in Fig. 15. In the resulting contour plots, the condenser saturation ratio as the z dimension is expressed by different colors, with axial and radial positions being normalized by the condenser radius. The two contour plots in Fig. 17 show the saturation ratio *S* inside the CPC condenser versus dimensionless axial (z/R) and radial (r/R) coordinates, with a lateral flow direction. Cooler colors, starting with blue for the minimum value, represent lower saturation ratios and warmer colors, with red for the maximum value, represent higher saturation ratios. The largest changes in saturation ratio occur along the condenser's centerline, from an *S* of 1 at condenser

entrance until it rapidly peaks along the centerline. This maximum, expressed by the dark red color, is reached after about one quarter of the total length.

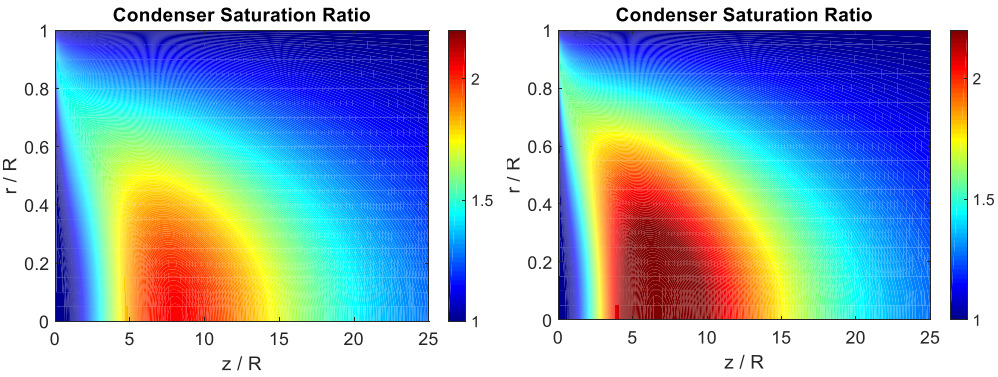

Fig. 17: Condenser saturation ratio profiles for 1,013 hPa (left) and 720 hPa (right) pressure (Unpublished data and graphs courtesy of R. Han).

The corresponding theoretical counting efficiency curve for a CPC 3772 were then calculated, which has a 10 nm lower detection limit. Results in Fig. 18 show a clear effect on that simulated curve already when reducing the ambient pressure from standard atmospheric pressure by a comparatively moderate drop of less than 300 hPa. As postulated by theory, the numerical model shows that the CPC activates smaller particles at lower saturation vapor pressure.

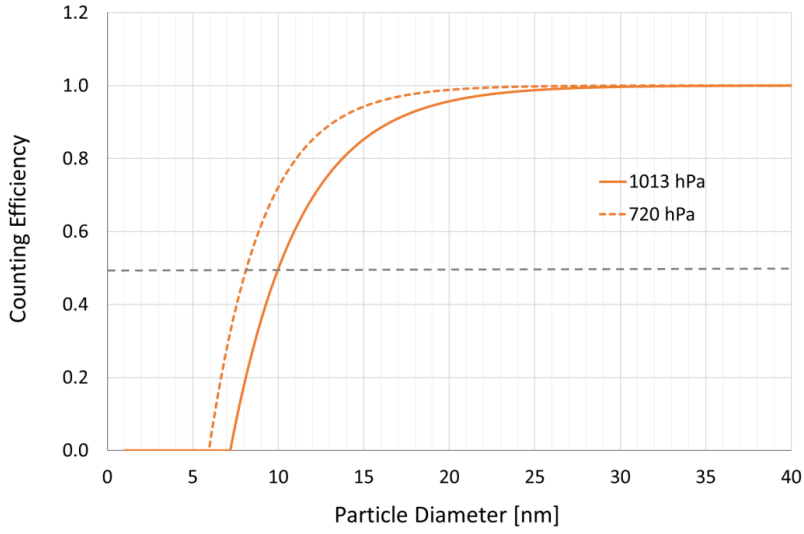

Fig. 18: Simulated counting efficiency curve for a generic CPC model 3772 with 10 nm detection limit at 1,013 hPa (solid line) and 720 hPa (dashed line) pressure.

There is a marked shift in the efficiency curve to a lower cut-off diameter and a slightly steeper slope as displayed. The modeled d_{50} cut-off diameter changes from 10 nm at ambient pressure to 8.1 nm at 720 hPa. The impact on the slope of the counting efficiency curve is less pronounced but it can be seen that there is a larger difference between the two curves at e.g. 80% detection efficiency compared to 40% efficiency. The numerical model also predicts a minor impact on the asymptotic detection efficiency, as a value of 99% efficiency is already reached at a smaller particle size for the reduced pressure.

4.3 Modelled counting efficiencies of the CPC 3772-CEN

Subsequently the model was applied to the exact geometry of the CPC 3772-CEN and operating parameters relevant for the experimental work of this thesis. At first, the model was compared to an experimentally determined efficiency curve as shown in Fig. 19. This calibration curve was measured by the World Calibration Centre for Aerosol Physics (WCCAP) at TROPOS in Leipzig, Germany. The measured efficiency curve was fitted using an empirical approach based on a four-parameter exponential function first described in Mertes et al. (1995) and later applied to different CPC models by Wiedensohler et al. (1997) and Banse et al. (2001). The function fitted to the measured efficiency also delivered the d_{50} value, so the CPC's cut-off diameter. In the experimental calibration presented here it corresponds to 7.1 nm for silver particles.

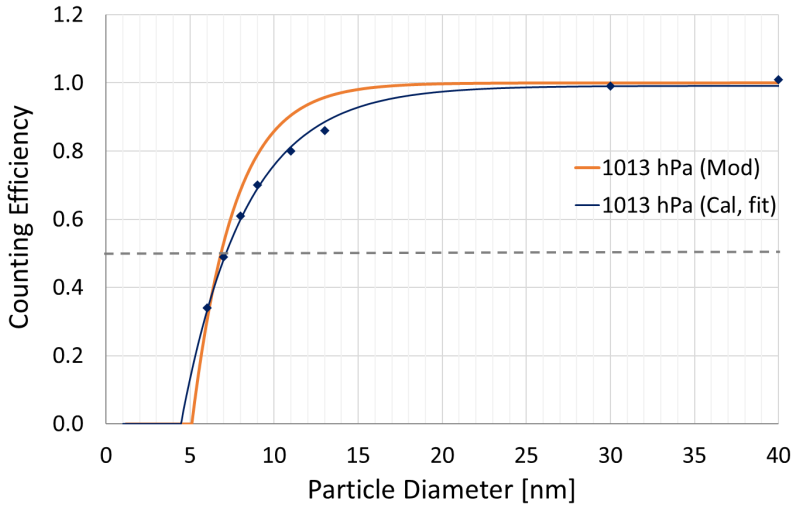

Fig. 19: Simulated and experimentally determined counting efficiency curves for the CPC 3772-CEN at 1,013 hPa.

The simulated efficiency curve and the curve fitted to the experimental calibration data agree well for the cut-off diameter and the maximum detection efficiency at particle sizes larger than 25 nm. The agreement is less than perfect for the d_{10} and d_{90} values of the efficiency curve, as is evidenced by the slightly more tilted slope for the measured calibration data. Reasons for the discrepancy between the experimental and the simulated curve are boundary layer effects near the wall of the condenser and phoretic particle losses, as well as diffusion losses for the smallest particles that the model does not consider.

Next three comparatively moderate values of reduced pressure were selected, that is to say levels of 900, 700 and 500 hPa. These pressures correspond to the ones where the CPC 3772-CEN performed well, e.g. during measurements of the total concentration for discrete, monodisperse particle sizes that are reported in the chapter 6.1. As can be seen in Fig. 20, the three efficiency curves generated by the model are of a very comparable shape with the cut-off sizes shifted to smaller diameters with decreasing pressure. The model calculates a very moderate decrease in the simulated activation efficiency and the resulting cut-off diameter of just 0.7 to 0.8 nm for each of the 200 hPa pressure steps. The slopes of the three counting efficiency curves are remarkably similar and the particle sizes where 99% detection efficiency is reached are still quite close to one another.

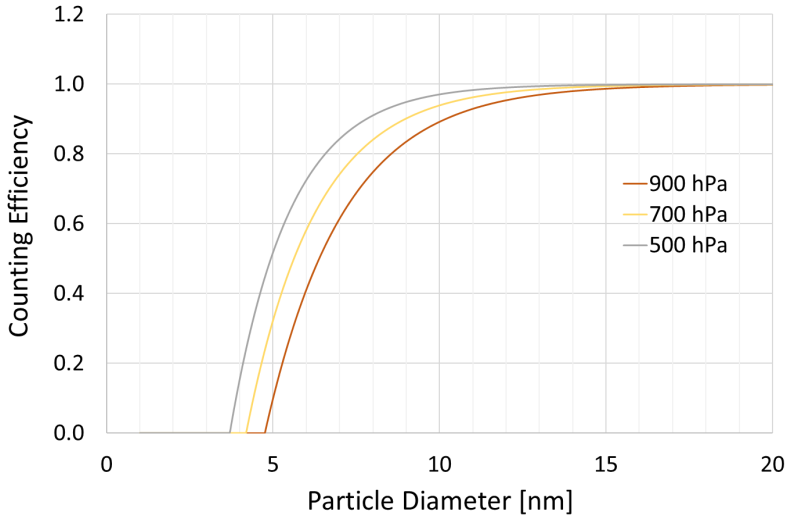

Fig. 20: Simulated counting efficiency curves of the CPC 3772-CEN for reduced pressures of 900, 700 and 500 hPa.

It is important to emphasize again that this two-dimensional model does not account for particle losses due to diffusional deposition. This is worth considering as particle

diffusion loss becomes the more important the lower the pressure and would therefore be a cause for a shift of the d_{50} to larger sizes. Yet diffusional losses of particles also mainly happen before the particles are activated. Once they are activated, the nanometer-sized particles grow very rapidly into micron-sized droplets, which are essentially immune to diffusion loss effects.

In the end the modeling analysis was concluded by looking at even lower levels of reduced pressure of 400, 300 and 200 hPa. The numerical model predicts a much lesser effect of these pressure levels on the counting efficiency curves, but nevertheless a continued shift to even smaller cut-off diameters as presented in Fig. 21. Interestingly, the shift subsides to a reduction in d_{50} by only 0.2 to 0.3 nm. The cut-off at 200 nm has shifted to 4.1 nm, from the 6.8 nm it had at standard atmospheric conditions. This effect could be due to the saturation vapor pressure and hence the Kelvin diameter not being linearly proportional to the pressure. There is even less impact on the slope of the curves at these levels of pressure, and almost none that separates the curves at 300 and 200 hPa.

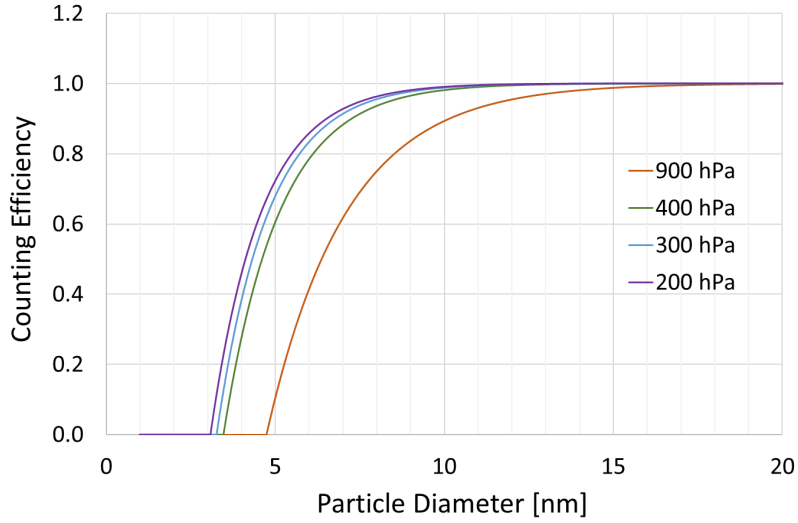

Fig. 21: Simulated counting efficiency curves of the CPC 3772-CEN for reduced pressures of 400, 300 and 200 hPa, with 900 hPa shown for comparison.

Although the Sky-CPC could not be modeled in this work, it is possible to make a very basic comparison of the reductions in the cut-off diameter calculated by the numerical model for the 3772-CEN with the experimentally determined values reported by Bundke et al. (2015). For the relatively moderate values of reduced pressure from 900 to 600 hPa, their calibration of the Sky-CPC seems to show an average reduction in the cut-off size on the order of 0.7 nm for each increment of 100 hPa, although this

change is smaller than the uncertainty of the measurement expressed by the error bars. Yet it might indicate that the changes are about twice the value predicted by the model for the CPC 3772-CEN for each of the 200 hPa pressure steps shown in Fig. 20. Interestingly, most of the shift to a smaller d_{50} size of the Sky-CPC seems to have happened until the 600 hPa pressure level. The change gets significantly smaller when the pressure is further reduced to 200 hPa. For the lower levels of reduced pressure, the experimental d_{50} values for the Sky-CPC indicate an average depletion of only 0.1 nm per 100 hPa, which compares to between 0.2 and 0.3 nm reported by the model for the CPC 3772-CEN for the same pressure increment as seen in Fig. 21. In other words, there does not appear to be a simple relationship between experimentally reported cut-sizes of the Sky-CPC and the ones determined for the 3772-CEN CPC by the analytic model. This gets even more complicated when considering that the experimental data reveal a reduction by a considerable 1.2 nm when further lowering the pressure by just 30 hPa down to 170 hPa.

Another metric to summarize the modeled results for the CPC 3772-CEN are the characteristic d_{90}, d_{50} and d_{10} diameters that represent the particle sizes detected with 90%, 50% and 10% efficiency. The d_{90} diameter with a counting efficiency of larger than 90% was introduced with the calibration requirements for the EURO emission legislations explained in chapter 2.5. The d_{10} is not frequently used but a characteristic value that provides insight into which of the very smallest particles are only just counted, with a 10% efficiency. The results for these three cut-sizes obtained by the model at the six levels of reduced pressure are compared to standard conditions of 1,013 hPa in Tab. 6.

Tab. 6: Pressure dependence of modeled characteristic diameters of the CPC 3772-CEN.

Pressure [hPa]	d_{90} [nm]	Cut-off, d_{50} [nm]	d_{10} [nm]
1,013	10.9	6.8	5.4
900	10.2	6.4	5.0
700	9.0	5.6	4.4
500	7.8	4.9	3.9
400	7.3	4.6	3.6
300	6.8	4.3	3.4
200	6.5	4.1	3.2

In conclusion, the numerical model delivered theoretical counting efficiency curves and d_{90}, d_{50} and d_{10} cut-sizes for all pressure levels that were considered to be of interest for this work. The results demonstrate a reasonable agreement between the modeled and experimentally determined counting efficiency curves for a CPC 3772 at standard

conditions of 1,013 hPa. When lowering the pressure gradually in discrete steps, three effects can be observed. Firstly, the model tells us that the counting efficiency curve will shift to smaller diameters, even though only very slightly. For this particular model CPC, the highest cut-off diameter of 6.8 nm is the one obtained at a pressure of 1,013 hPa. The lowest theoretical cut-off size of 4.1 nm is the one at the lowest pressure of 200 hPa used by the model. Secondly, the mathematical model predicts a minor change in the slope of the curves. Below the respective activation sizes, the counting efficiency decreases very rapidly at all pressures modelled, with the theoretical curves dropping more sharply to zero than experimental ones. The lowest pressure of 200 hPa modelled also yields the sharpest theoretical efficiency curve. Although differences in the shape of the efficiency curves for the different pressure levels are small overall, they are greater for the increment from 900 hPa to 700 hPa than for the increment at the lowest pressure from 400 hPa to 200 hPa. Thirdly, the model deduces no apparent decrease in the maximum asymptotic counting efficiency in the modelled results. This being said, there are bigger differences in the particle size at which a maximum counting efficiency of 99% is achieved. The corresponding diameter declines from 16.6 nm at 1,013 hPa to just 10.0 nm at 200 hPa.

As explained in the beginning, this particular numerical model makes several simplifications and uses assumptions that are not fully representative of what is happening during real-life operation of a CPC at reduced pressure. Nonetheless, it points to some trends and effects that will be interesting to compare to the outcomes of the various experiments done in this thesis.

5. Experimental set-up and characterization

This chapter provides a detailed description of the experimental set-up and explains the flow, pressure and RH control system required to achieve stable conditions of all parameters in depth. Subsequently, key features of the instruments used in the experiment are reported and the two aerosol generators are characterized to determine their optimum operational settings for the calibration of CPCs.

5.1 Calibration setup

In order to better understand the inconsistent findings of previous studies, an extensive experimental characterization of two different CPC models was carried out in this work. The calibration of the CPCs was done simultaneously at several discrete levels of reduced pressure with two, quite different particle materials that serve as proxy for the practical applications described in chapter 2.5. Ammonium sulfate serves as a calibration aerosol representative of atmospheric background and flame soot as an aerosol that is characteristic for combustion emissions. Lastly, the CPCs were calibrated using 38 different particle sizes, which resulted in a very high size resolution of the calibration from 2.4 nm to 136 nm. An additional interest was the role that modest amounts of relative humidity (RH) can play in the activation of the smallest sized particles in a CPC. All of the aforementioned low-pressure studies were conducted under essentially dry conditions. Nonetheless CPCs are known to exhibit some material dependence around their lower detection limit and for instance compounds condensed on the surface of soot particles will increase their activation. Therefore, the measurements were also performed at 4 to 5 discrete RH levels ranging from 1% to 40% for each pressure stage. The working hypothesis for this particular aspect was that the minimum particle size at which a CPC can activate condensation, the Kelvin diameter, is not only dependent on thermodynamic properties but that relative humidity could impact it e.g. due to surface effects.

In order to calibrate a CPC for its performance at both low pressure and different levels of relative humidity (RH) it is necessary to achieve a stable control of the absolute pressure as well as of the RH levels during the entire duration of the experiments. In Bundke et al. (2015) an advanced calibration setup was described in greater detail, which was also used for these experiments after some modifications were made. The main constructive changes are that a larger number of instruments could be included for simultaneous measurements and the corresponding larger sample flows could be accommodated even at low-pressure conditions. The modified setup also used an improved pressure and humidity control that allows for an automated measurement at variable pressure levels at pre-defined, stable values of relative humidity. This modified experimental setup is described in the following chapters in greater detail.

5.1.1 Flow control

The control system of the experiment was custom-designed in the aerosol laboratory at Forschungszentrum Jülich. It relies on a mixing chamber with well-defined input and output flows at its center. The output flow from that chamber represents the desired calibration aerosol at its chosen pressure set point and RH value. The required pressure level is controlled by a main input flow V_p, which enters the mixing chamber through a mass flow controller (MFC, Model F-201EV, Bronkhorst High-Tech B.V., Ruurlo, Netherlands), followed by a high efficiency particulate air (HEPA) filter. Two additional flows are used to achieve and maintain the desired level of relative humidity. Dry mixing air is added by an input flow V_t, while humidified air is added by a flow V_f until the setpoint value of RH is reached. This humid airflow can be saturated with up to 100% relative humidity by passing it through a bubbler column that is partially filled with distilled, particle-free water. Both flows are controlled by identical MFCs and pass through subsequent HEPA filters before they are combined prior to entering the mixing chamber. The resulting combined flow V_m is held constant so that the control of pressure and the control of relative humidity are independent of each another. The basic flow schematic of the pressure and RH control system is presented in Fig. 22.

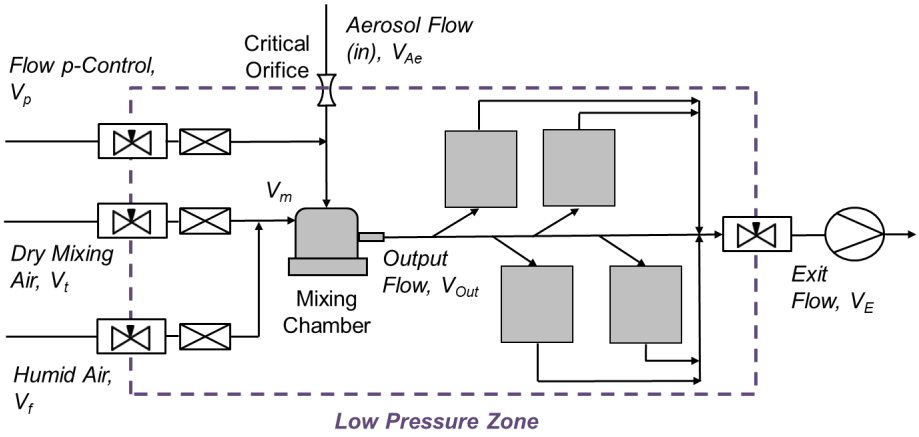

Fig. 22: Basic flow schematic of the pressure and humidity control system.

One additional flow also enters the mixing chamber, which is the aerosol flow V_{Ae} from the monodisperse outlet of the DMA. This is the only input flow entering the mixing chamber that is not actively controlled by an MFC as small particles could be deposited and therefore get lost inside it. Instead, this flow is passively controlled by a critical orifice, which has the dual advantage that it keeps the input flow of the monodisperse aerosol constant at a fixed value without any active control and without any significant

particle losses. The flow rate through the critical orifice is constant as long as the pressure drop across it is enough to maintain critical operation. The pressure dependent range for the desired nominal aerosol flow of 1 L/min was verified by an external mass flowmeter (MFM, Model 4140, TSI Inc.) and is given in Tab. 7 and Fig. 23. Based on these flow measurements it was decided to not use any results above 800 hPa for the performance calculations.

Tab. 7: Flow rates through the critical orifice as function of operational pressure (at 30% RH).

Pressure [hPa]	Flow rate [L/min]
1,013	0.20 ± 0.01
900	0.66 ± 0.01
800	0.89 ± 0.02
700	0.97 ± 0.02
500	1.08 ± 0.03
400	1.12 ± 0.03
200	1.14 ± 0.03

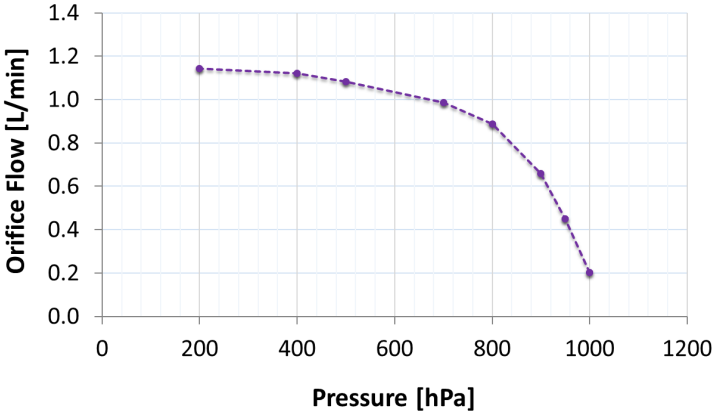

Fig. 23: Mass flow rate through critical orifice as function of the operational pressure as measured by an external mass flowmeter (MFM, Model 4140, TSI Inc.).

The reason is that at these higher pressures the critical orifice did not operate at or close enough to critical conditions. Although even a difference of 10 to 15% in the aerosol flow rate might seem large at first, it actually only has a minor effect on the mean electrical mobility of a particle and hence the size classification in a cylindrical

DMA. The main impact would be on the particle number concentration measured, which is not that important when both the CPC under calibration and the reference instrument measure it side by side.

In order to guarantee a stable operation of the pressure and RH control system, the aforementioned three input flows V_p, V_m und V_{Ae} must be kept in balance with the output flow V_{Out} at each pressure level. The output flow is dependent on the number of instruments sampling calibration aerosol from the main line as well as the excess flow V_E that is controlled by another MFC. The purpose of the excess flow is to ensure a minimum flow rate through the system that is needed to achieve the nominal pressure level especially at very low pressures but also to compensate for changes in the aerosol flow V_{Ae}, which is dependent on the pressure inside the mixing chamber. All instruments sampling from the main line are using built-in critical orifices or MFCs and their own connection to external vacuum. The pump providing the vacuum is operated so that it produces a pressure that is much lower than the one inside the mixing chamber to ensure proper operation of the critical orifices of the instruments.

5.1.2 Pressure and RH control

In this experimental setup, pressure and relative humidity are controlled in a closed-loop system by custom-software programmed in LabView (National Instruments Corp., Austin, TX, USA). This proprietary software program developed at Forschungszentrum Jülich ensures that all nominal conditions are maintained over the course of each experiment and also that data are simultaneously collected from all sensors and instruments in real-time. The automated control, measurement, and rapid data acquisition system was developed at the Institute IEK-8 in Jülich and adapted for these experiments. The following section provides some design criteria of the closed-loop control system (Fischer, 2019).

At the heart of the control loop is a PID controller that is used to control the pressure in the experiment. It uses the actual pressure value and the setpoint for the desired pressure as input variables to determine the necessary flow difference as its control variable. Under steady state conditions, the flow set in the MFC is a function of temperature, pressure and the flowrate itself. The PID controller now only varies the flow difference to increase or decrease the pressure in the mixing chamber. The controller assumes that the conversion from voltage to volume flow V_P is approximately proportional with a simple delay. Since the tubes and tubing in the experiment effectively represent a buffer volume, the volume flow from the MFC to the mixing chamber leads to a further time delay. At nominal operational settings, the pressure thus depends on the integral of the volume flow V_P.

For the humidity control, the relative humidity set point serves as the output parameter in the control loop. The ratio of the two MFCs that effectively produce the mixing flow V_m is the input parameter for the humidity control of the system, which leads to a

proportional setting of the humid air flow V_f through the corresponding MFC with a brief time delay. This in turn adjusts the relative humidity of the entire input flow into the chamber proportionally and with a time delay due to the buffer volume of tubes and tubing. Since the mixing chamber itself also has a considerable volume, the humidity control of the input flow is lagging, which leads to a large time constant that has to be compensated. In order to make the control respond as fast as possible, a PID controller was chosen as it permits the compensation of different time constants.

Both, pressure and humidity control, include dead times due to the duration of a program iteration of the control program as well as the buffer volume of the tubing. In addition, they influence each other and the humidity control in particular is influenced by the pressure control. The pressure control also has transfer coefficients that are time-variant, e.g. one which includes the pressure itself. In summary, both systems are non-linear, time-variant and use control parameters that often reach their physical limits. For these reasons, the controller parameters were set heuristically in the control-loop and thereby a sufficiently rapid control was made possible. It is also important that the closed-loop system essentially controls the balance, so only the differences are adjusted which leads to a comparatively quick response to all changes made. This control of pressure and relative humidity as well as of the various flows was implemented in a modified version of our laboratory's custom LabView program.

5.2 Instrumentation

In the calibration experiments, two different types of aerosol generators were used. A constant output atomizer (home-made version of the Model 3076, TSI Inc.) produced the ammonium sulfate (AS) aerosol from an aqueous solution. The second aerosol source was a soot generator, which was chosen for the combustion aerosol measurements. After the freshly generated aerosol from either source was conditioned by either drying or cooling depending on the aerosol generator used, it then passed through a T-connection where excess air was vented before the aerosol entered the size classification section. In that part, the aerosol was first charge-conditioned using an Am-241 aerosol neutralizer. Monodisperse particles were then selected using a Vienna-type Differential Mobility Analyzer (Model M-DMA 55-U, Grimm). The DMA was connected to the low-pressure section of the experiment by the critical orifice that drew the monodisperse aerosol into the mixing chamber. An important difference to the prior work of Bundke et al. besides the use of different aerosol generators is the addition of relative humidity control for each pressure level as described in the previous chapter. At each low-pressure stage, the relative humidity was varied to stable values between 2% and 40% RH. All of the experiments were made at discrete pressure levels between 800 hPa and 200 hPa, but for an initial characterization of all three CPC models at 950 hPa. Downstream of the mixing chamber, a 25 mm-diameter main line with a total length of 800 mm permitted the connection of up to five instruments simultaneously. The main line after the mixing chamber also permits the addition of

further sampling ports to accommodate even more instruments, provided the concentration of the calibration aerosol and the flow rates are large enough. The five sampling ports were positioned 100 mm apart along the length of the main line, with one additional port at the end to bleed off all excess air through a mass flow controller. Each of the ports draws its sample from the centerline of the flow through a custom-made nozzle. The nozzles were designed to enable isokinetic, isoaxial aerosol sampling and can be exchanged depending on the flowrates used. During the experiments, flexible conductive sampling tubing of 250 mm length was connected to the outer end of the sampling ports to all instruments that drew sample flows of 0.6 L/min. The length of the tubing was adjusted proportionally for those instruments that drew higher flows of 1.0 L/min. Fig. 24 presents the basic schematic of this experimental setup.

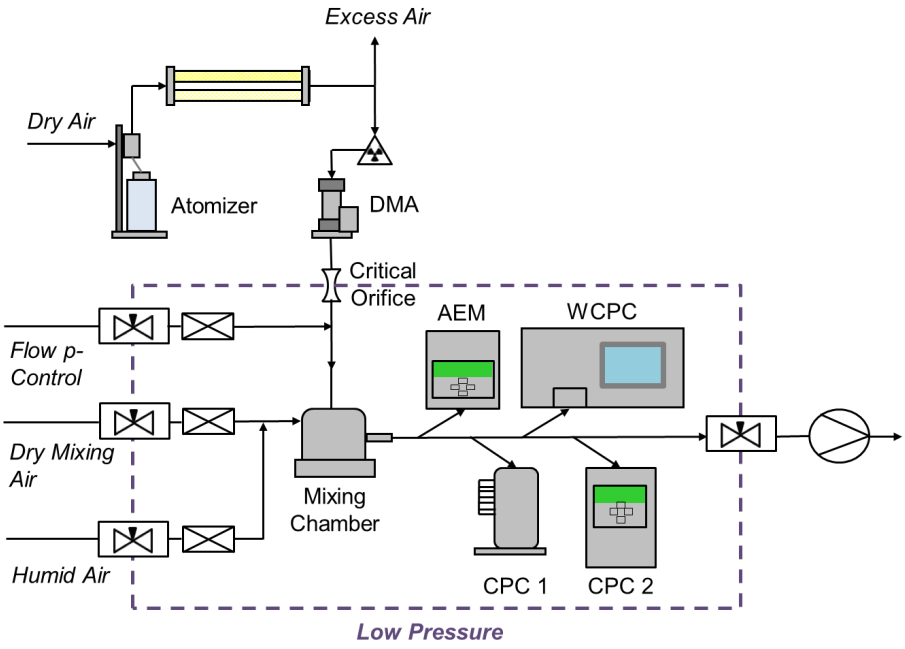

Fig. 24: Schematic of the experimental setup used for low-pressure calibration at defined humidity levels. In the above configuration, an atomizer is used as aerosol source.

5.2.1 Key characteristics of the CPCs

In most of the measurements two continuous-flow CPCs were operated side-by-side, which were the Sky-CPC 5.411 (Grimm) and the CPC 3772-CEN (TSI Inc.). Both instruments use butanol as their working fluid as such alcohol-based CPCs are the

ones that are by far the most common type operated at reduced pressure. Both models are of the full-flow design, so the entire aerosol flow that is sampled is subsequently passed through the measurement zone without any internal splitting of the flow. These CPCs are both comparable to the butanol CPC models used in the previous low-pressure studies, of which all but one model have been discontinued by their manufacturer since. The notable exception is the Sky-CPC 5.411 which is still in production. In this experiment it provides good comparability and consistency with the initial characterization of that same CPC model done by Bundke et al. (2015). This CPC is also part of the P2c aerosol package developed by our research group at Forschungszentrum Jülich for the IAGOS infrastructure. A brief overview of the nominal technical specifications of the two CPCs is given in Tab. 8.

Tab. 8: Overview of nominal key characteristic of the three CPC models intended for use in this work according to the manufacturers.

	Sky-CPC 5.411	**CPC 3772-CEN**	**WCPC 3783**
Working fluid	Butanol	Butanol	Water
Nominal detection limit (d_{50})	4 nm	7 ± 0.7 nm	7 nm
Maximum concentration	100,000 P/cm^3	50,000 P/cm^3	1,000,000 P/cm^3
Nominal flow rate	0.6 L/min	1 ± 0.05 L/min	0.6 ± 0.06 L/min
Response time (t_{10}-t_{90})	< 3 s	< 2 s	< 5 s
CPC temperatures (T_{sat}, T_{cond}, T_{opt})	36°C, 10°C, NA	39°C, 22°C, 40°C	20°C, 60°C, 60°C
Absolute pressure range	125 to 1,100 hPa	750 to 1,050 hPa	500 to 1,110 hPa

The CPC 5.411 is intended to be used for airborne applications and was therefore named “Sky-CPC” by its manufacturer. It has a nominal lower cut-off diameter of 4 nm, although it should be noted that in their prior study Bundke et al. (2015) decided to adjust their Sky-CPC to a 13 nm detection limit, so the influence of diffusion losses is reduced. The operational temperatures of this conventional cooling type CPC are maintained at T_{sat}= 38°C for its saturator and T_{con}= 10°C for its condenser. Its sample flow rate is kept at a constant 0.6 L/min by a critical orifice. The response time of the CPC 5.411 is specified as being less than 3 seconds for a 10% to 90% step change. Most importantly, the manufacturer guarantees operation at atmospheric pressures ranging from 125 to 1,100 hPa. It also is a relatively compact CPC that has been stripped to its core measurement engine as shown in Fig. 25.

Fig. 25: Picture of the two current CPC models used in the experiment: Sky-CPC 5.411 (Grimm) on the left and CPC 3772-CEN on the right (Photograph © TSI Inc.).

The Sky-CPC also reports a “C1/C0” value, which allows a general assessment of the quality of the CPC measurement. This value relates the light-scattering signal that is detected when particles pass through its laser beam to the growth of the butanol droplets. A calculated number concentration for the pulse height of the measured particles C1 is set into relation to the particle concentration for a given threshold value C0. If the ratio C1/C0 equals 1, C1 and C0 match and all particles grow into droplets of essentially the same size as expected under correct operation conditions. This is not the case for a ratio <1, typically because the assumed saturation conditions are not fully achieved. During the measurements the C1/C0 ratio was always read out with the raw data from the CPC and recorded in the respective data set.

The other butanol CPC in the experiment was the model 3772-CEN (TSI Inc.) that was introduced in mid-2016, which has not been characterized for its performance at reduced pressure previously. It is also a single-particle counting, continuous-flow instrument with a comparatively small footprint as can be seen in Fig. 25. In fact, the CPC 3772-CEN shares the same geometry with the Engine Exhaust CPC 3790 (EECPC, TSI Inc.) as well as with the CPC 3771 that Takegawa and Sakurai (2011) evaluated, which has not been commercially available since 2011. The CPC 3772-CEN is of particular interest to many users as it was developed for regulated measurements of the particle number in ambient air, which could lead to its use in cities located at high elevation as well as high-altitude research stations. It was specifically designed to meet the Technical Specification CEN/TS 16976:2016 that defines stringent performance characteristics for CPCs used to monitor atmospheric aerosol. The CPC 3772-CEN is specified with a lower size limit (d_{50}) of 7 nm based on a calibration with sintered silver particles produced by the evaporation/condensation method according to CEN/TS. The manufacturer offers a dedicated external

calibration by the World Calibration Center for Aerosol Physics (WCCAP) at the Leibniz Institute for Tropospheric Research (TROPOS) on request. The CPC 3772-CEN has a t_{10}-t_{90} response time of <2 seconds, which is helped by its comparatively high detected aerosol flow rate of 1.0 L/min. The aerosol flow is maintained using an internal critical orifice and an external vacuum source. Its internal temperatures of saturator and condenser are controlled to 39°C and 22°C, respectively, with the optics held at a constant temperature of 40°C. The CPC 3772-CEN has a built-in pulse height analyzer that triggers an error when the pulse amplitude decreases significantly below a minimum pulse height of 1 V. This automatically sets an error flag to indicate the presence of a measurement problem. Crucially for this work, the manufacturer only guarantees operation at an ambient pressure range from 750 to 1,050 hPa, so this CPC model is not actually intended or designed to work at very low pressure.

Finally, a third CPC was included in the initial phase of the experiments. This instrument was an environmental monitoring, water-based type (WCPC, Model 3783, TSI Inc.). The main objective for including a WCPC was to also test an instrument that uses a different working fluid. This second generation WCPC also has a lower detection limit of 7 nm, verified with DMA-classified sucrose. As explained in chapter 2.2.3, the WCPC 3783 uses more extreme operational temperatures, which are maintained at 20°C for the conditioner and at 60°C for both the growth tube and the optics. The second-generation design also relies on a more complex set-up, with water filling and draining lines as well as a corresponding fill valve and drain pump. Unfortunately, it turned out that I was not possible to perform any meaningful measurements with the WCPC 3783 at reduced pressure. While water has many advantages, the diffusivity of the water vapor in air is higher than the one of butanol vapor. Already slight changes to the ambient pressure resulted in water quickly flooding the instrument in several places. One specific issue was the water separator, from which water is pumped out by an ejector pump at standard condition. Its air outlet is connected to the external vacuum, but also to the transport flow and the auxiliary flow via several flow orifices. These constructive details contributed to the internal flooding and blocking of orifices when the WCPC was exposed to even the slightest changes from ambient pressure. A work-around that included disabling the WCPC 3783's low-pressure shutdown mode in the firmware and disconnecting cables that provide power to the solenoid valve that shuts-off once the pressure drops by about 70 or 80 hPa was tried. Further, the internal water separator was by-passed to avoid any free-flowing liquid ending up in undesirable places within the instrument when exposed to low-pressure. Unfortunately, this still did not enable any meaningful measurements once the inlet pressure dropped by more than 70 hPa.

Therefore, only corrected data for measurements done at 950 hPa are exemplarily reported here. As can be seen in Fig. 26, all three CPC models – 3772-CEN, WCPC 3783 and Sky-CPC 5.411 – behaved almost identical at near-standard pressure. The shape of the three counting efficiency curves, the maximum concentrations achieved at 30 nm and even the lower cut-off diameter were very similar.

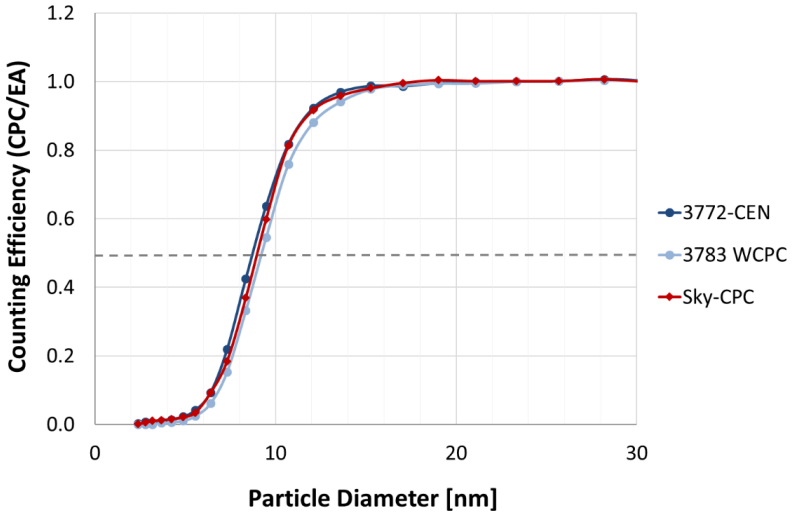

Fig. 26: Detection efficiency of the CPC 3772-CEN (dark blue), the water-based CPC 3783 (light blue) and the Sky-CPC 5.411 (red) for ammonium sulfate at 950 hPa.

It should be noted that these results from one specific set of measurements are only given as an example and that the agreement may vary depending on the exact measurement conditions. Just before the end of this work, I got involved with the low-pressure characterization of a new, third generation water-based CPC at Pacific Northwest National Laboratory in Richland, WA (USA). The Atmospheric Sciences & Global Change Division at PNNL has access to the Atmospheric Radiation Measurement (ARM) user facility for airborne measurements during intensive field campaigns. The ARM just acquired a new Bombardier Challenger 850 aircraft, which will be used to measure pollution plumes in Amazonas state in Brazil. PNNL plans to fit the aircraft with a versatile WCPC (Model 3789, TSI Inc.), which required a thorough characterization of its detection efficiency at different levels of low-pressure. They are also working on the development of a corresponding operation protocol. Initial performance data for that WCPC model were presented at the AAAR 2020 conference (Mei et al., 2020). It should be emphasized that I contributed to that characterization merely as a co-author and did not take part in any of the measurements myself, so it is only included here for further reference.

5.2.2 Technical modifications of the butanol CPCs

In general, a modification of the CPC is necessary in order to operate it successfully at reduced pressure. The exact details of the modification required will differ depending on the CPC model in question. Hardware modifications often concern the working fluid and its fill system but also components like internal filters that can

introduce a problematic pressure drop at high altitude or low pressure. Moreover, it is critical that the volumetric flow rate is always maintained while operating the CPC at reduced pressure, which is why internal pumps are often replaced by critical orifices and external vacuum. The Sky-CPC 5.411 is an exception to this as the manufacturer offers it as a device that is already optimized for low-pressure operation. Its special characteristics are that it is leak-tight, has a flow control independent of the ambient pressure and a working fluid management that complies with aviation safety rules. Along with that, the Sky-CPC 5.411 is specified to work over a range of absolute pressure from 125 to 1,100 hPa. In order for the instrument to function properly down to 125 hPa, the CPC must first be put into a service mode and receive a firmware command that enables its low-pressure operation.

The CPC 3772-CEN, on the other hand, is officially only specified by its manufacturer to work at an ambient pressure between 750 and 1,050 hPa. This pressure range is monitored by a built-in ambient pressure transducer, which has to be disabled and bypassed for low-pressure experiments. Under normal operation, this pressure measurement acts as a precaution as the air in the wick of the CPC can outgas which would cause the butanol to be displaced when the pressure on its inlet drops. With the wick above the aerosol inlet on the CPC 3772-CEN, any extra butanol could pool at the aerosol inlet and eventually get sucked up into the optical chamber, which would lead to flooding of the optics and cause false counts. Therefore, special care was always taken to lower respectively increase the pressure in the experiments only very slowly and gradually. An overview of these minor modifications is given in Tab. 9.

Tab. 9: Overview of modifications to the butanol CPCs.

Model	Modification
5.411 (Grimm)	• Firmware command for operation at reduced pressure (proprietary, needs to be obtained from manufacturer)
3772-CEN (TSI Inc.)	• Firmware command for operation at reduced pressure (proprietary, needs to be obtained from manufacturer) • Built-in ambient pressure transducer disabled and by-passed

5.2.3 Key characteristics of the Aerosol Electrometers

Furthermore, there were two aerosol electrometers in the experiment, the FCE Electrometer (Model 5.705, Grimm) and the Aerosol Electrometer 3068B (AEM, TSI Inc.). Both are Faraday cup instruments that are commonly used as reference for the particle number concentration in the calibration of CPCs. They consist of a Faraday cup containing a filter holder with a high efficiency particulate air (HEPA) filter, an

insulator, appropriately shielded housing and an electrometer circuit. The flow through the electrometer is generated by an external vacuum source, which is controlled either by internal means as shown in the schematic diagram in Fig. 27 or by an external mass flow controller.

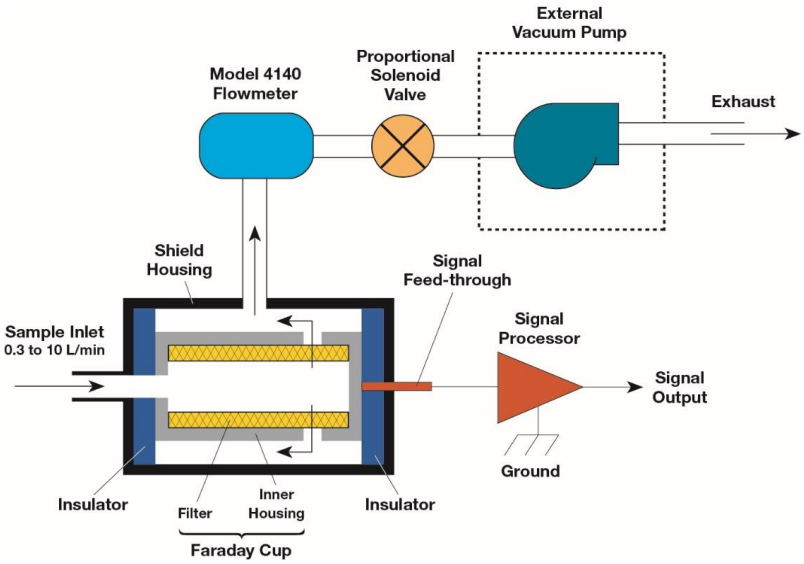

Fig. 27: Operating principle of aerosol electrometers (Schematic courtesy of TSI Incorporated, Model 3068B User's Manual).

When charged particles pass through the aerosol electrometer, they are collected on the conductive filter inside the Faraday Cup. The electrometer sensor that is connected to the filter detects that rate of charges. The signal processor subsequently delivers an electric current that is proportional to the charges collected. When the flowrate through the Faraday cup is accurately known and multiple-charge effects are properly corrected, an aerosol electrometer delivers very precise measurements of an aerosol's particle number concentration.

The FCE 5.705 is actually identical with the unit that Bundke et al. (2015) used for their low-pressure performance work on the Sky-CPC 5.411. One difference to other electrometers is an internal rinse flow that surrounds the insulator of the Faraday cup, which was introduced to minimize the effect of current leakage caused by contamination. In the experiment the rinse flow was controlled to 0.5 L/min by an external MFC. The AEM 3068B is identical to the model used by Takegawa and Sakurai (2011), although they stated that they had their unit calibrated separately to the primary standard aerosol electrometer of the National Institute of Advanced Industrial Science and Technology (AIST). For several measurements both

electrometers were included, one as the actual concentration reference and the other as an independent method to validate the results of it. Some of the salient technical specifications of these two aerosol electrometer models are given in Tab. 10.

Tab. 10: Overview of main specifications of aerosol electrometer models used in this study.

	FCE 5.705	**AEM 3068B**
Manufacturer	Grimm	TSI Inc.
Nominal cut-off [nm]	0.8	2
Nominal flow rate [L/min]	1.0	0.3 to 10
Sensitivity (RMS) [fA]	0.1 (0.35 RMS)	1 (±1)
Maximum range [fA]	4,000	12,500
Operational humidity range	0 to 95% RH	0 to 90% RH

5.2.4 Electrometer characterization

It is well known that aerosol electrometers are subject to an inherent noise of the current in their electronic system. The shot noise comes from unavoidable random fluctuations of the electric current when charged particles move inside the Faraday cup, which results in a background signal or offset current. This offset current fluctuates second by second but it can vary day by day particularly when the ambient temperature changes. Therefore, before any calibration can be carried out the aerosol electrometer's offset current has to be measured by sampling particle-free air. Once the zero offset has been determined it can be subtracted from the total current measured to calculate only the current caused by the charged particles.

The zero offsets of the two electrometers, the AEM 3068B and the FCE 5.705, were measured while sampling HEPA-filtered air in 3 min intervals with 1 s averages. The measurements were then repeated also at four levels of low-pressure and for a defined relative humidity as given for the FCE 5.705 electrometer in Tab. 11.

Tab. 11: Averages and standard deviations of the electrometer offset currents of the FCE 5.705 for a relative humidity of 20% at four low-pressure levels.

	200 hPa	**400 hPa**	**700 hPa**	**900 hPa**
RH [%]	20.2	20.0	20.0	19.9
AVG [fA]	131.3	142.6	128.8	105.2
STD [fA]	60.7	67.3	44.6	45.0

These measurements were done in an air-conditioned laboratory to minimize any contribution due to temperature fluctuation. Before starting the measurements, several minutes had to pass for the current readings to reach steady values, to ensure that any remaining charged particles were purged from the instruments. As can be seen in the values shown as function of measurement time in Fig. 28, both of the electrometer models have proven to be quite stable. The four intervals in that graph correspond to 35%, 20%, 5% and 3% RH. There is no apparent drift in the offset and no notable dependence on relative humidity for the levels tested. The apparently higher scatter of the FCE 5.705 electrometer is only caused by its higher sensitivity and the more rapid 200 ms response time. Also, the AEM 3068B has a running average time option, which was set to 5 s during all of the offset measurements.

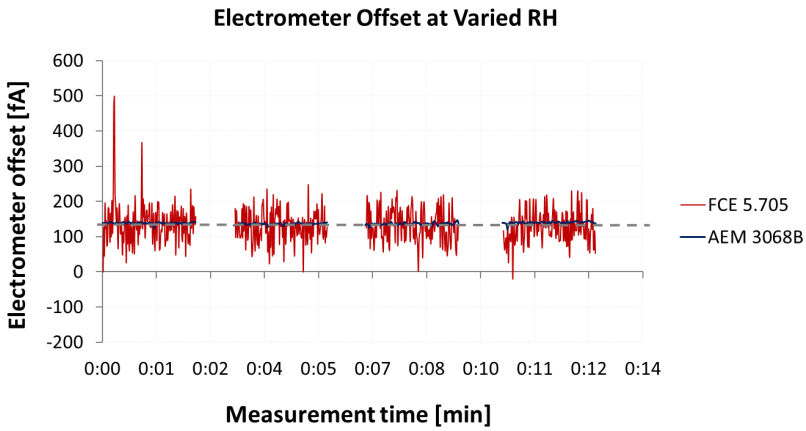

Fig. 28: Electrometer offset current for the FCE 5.705 and AEM 3068B electrometers over 3-minute intervals at varied RH. The dotted line represents the average noise value.

Since both aerosol electrometers agreed well with each other, it was decided to continue with the FCE 5.705 electrometer that was previously used by Bundke et al. (2015) as the primary concentration reference. This allowed a direct comparison to the data that they obtained with a largely similar experimental setup. Based on the offset measurement results, the corresponding averages were used as electrometer zero offset values for the calibration, which always resulted in offset values being in a range between 100 and 200 fA.

5.3 Choice of calibration aerosols

Over the years various aerosols have been used for the calibration of CPCs, both at ambient and also reduced pressure conditions. These include but are not limited to sodium chloride (NaCl), ammonium sulfate (AS, $(NH_4)_2SO_4$), sucrose ($C_{12}H_{22}O_{11}$),

tungsten oxide (WO_x), silver (Ag), combustion soot and oil droplets from e.g. di(2-ethylhexyl) sebacate (DEHS) or poly-alpha-olefin (PAO, also known as Emery oil). Some of these particles are spherical, some are cubic or crystalline, and others are aggregates. Although differences in the aerosol material are not likely to account for a large difference in the total concentration performance of butanol-based CPCs, they can have a notable influence on their lower detection limit. There were several earlier studies that have investigated the activation response in butanol-based CPC's based on the particle composition (Sem 2002, Kulmala et al., 2007, Giechaskiel et al., 2011b), although none of them did so at reduced pressure. In this study one goal was to calibrate the CPCs with two well-defined calibration aerosols, one being representative of atmospheric background and a combustion aerosol to represent urban aerosol dominated by traffic emissions. Crucially for this work, the calibration aerosols had to be produced stably down to the small nanometer size range. In addition, concentrations were also required to be high enough for simultaneous detection by the different CPCs under calibration and at least one aerosol electrometer used as concentration reference.

5.3.1 Calibration aerosol for atmospheric background

Ammonium sulfate (AS) was chosen as proxy for an atmospheric background aerosol in this work. It is a hygroscopic salt, so it takes up water from the relative humidity of the ambient air. Under high RH conditions it could thus be expected that the size distribution of an AS aerosol shows more or less pronounced shifts to larger particle sizes when compared to completely dry conditions. An additional benefit of using ammonium sulfate is that it allows a direct comparison to the work done by Bundke et al. (2015) with the same particle material. From a practical perspective, ammonium sulfate is a white solid that is extremely soluble in water due to its ionic nature. Therefore, a calibration aerosol can be easily generated by atomizing ammonium sulfate dissolved in distilled water. It is known to form almost spherical particles when atomized and to activate easily inside a CPC. The AS calibration aerosol was generated in a home-made variant of the constant output atomizer. The Ammonium sulfate aerosol then passed through a self-built diffusion drier of approximately 350 mm length that consists of two concentric cylinders made of wire mesh. The annular space between them is filled with silica gel and the aerosol passes undisturbed through the inner cylinder. An initial experiment was done to determine what amount of AS solid powder should be dissolved in ultrapure water (high-performance liquid chromatography respectively HPLC grade water), so suitable aerosol concentrations in the small nanometer size range are achieved.

The ammonium sulfate aerosol was generated by putting a defined mass of AS powder into distilled water and by aerosolizing it in the atomizer aerosol generator. The generator was a device built at the aerosol laboratory of IEK-8 in Jülich, which is essentially identical to a constant output atomizer (COA, Model 3076, TSI Inc.). In the

atomizer head, compressed air is forced through an orifice, resulting in a high-velocity jet. This jet uses the Bernoulli effect to draw up the liquid solution through a vertical suction tube from the atomizer's reservoir bottle, which is then atomized. The aerosol leaves the atomizer through its aerosol outlet at the top as is illustrated in Fig. 29. This aerosol consists of water droplets containing small amounts of ammonium sulfate, which are subsequently dried in a diffusion drier to remove the water content so that only solid ammonium sulfate particles remain as the calibration aerosol.

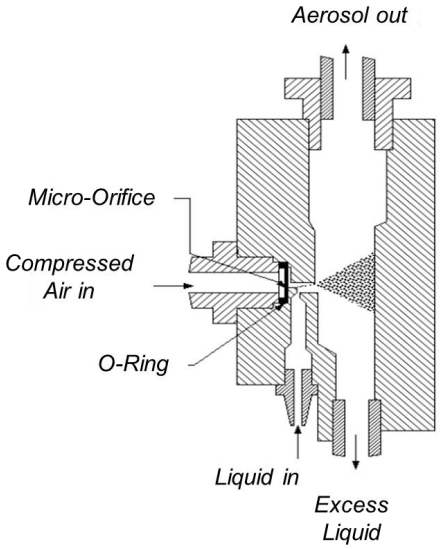

Fig. 29: Schematic of the atomizer head (TSI Inc., Model 3076 Manual).

Note that the inner wall opposite the orifice in the COA serves as an impactor that removes undesirably large droplets and drains them back into the atomizer bottle as excess liquid solution. The large droplets that are drained back contain a greater amount of dissolved material, which can cause the atomizer solution in the reservoir to become more concentrated when the atomizer is operated in this recirculation mode. Depending on the initial concentration, the result can be a notable increase in the diameter of the particles already over a period of several minutes. One approach to address this especially when using volatile solvents is to operate the atomizer in a non-recirculating mode. In this mode of operation, the excess liquid drains off into a separate atomizer bottle that collects the waste solution. Both atomizer bottles then also need to be connected by another line that equalizes the pressure between them.

The primary droplets produced by the atomizer are dried to form a secondary aerosol from the dissolved particles. This atomizer design produces a polydisperse droplet aerosol with a geometric standard deviation σ_g of 1.6 to 2.0. The final calibration

aerosol generated by the atomizer depends on the amount of dissolved AS material contained in the initial water droplets. Accordingly, an optimum particle size range exists for each concentration and the particle size distribution can be varied over a limited range by putting more or less AS powder into solution. The more material is contained in a single droplet, the larger the median diameter of the particle that forms from the dissolved material. The resulting particle diameter can be theoretically expressed by the following equation (Hinds, 1999):

$$d_p = d_d * \sqrt[3]{F_v} \tag{5.1}$$

where d_p is the particle diameter,

d_d the initial droplet diameter, and

F_v the volume fraction of the dissolved solid material.

Unfortunately, this formula seems to be insufficient to fully describe the relationship between the dissolved material and the resulting mean particle size in reality. Chen and Chein (2006) reported discrepancies between their experimental and theoretical results that grew larger when concentrations of the dissolved solid material decreased.

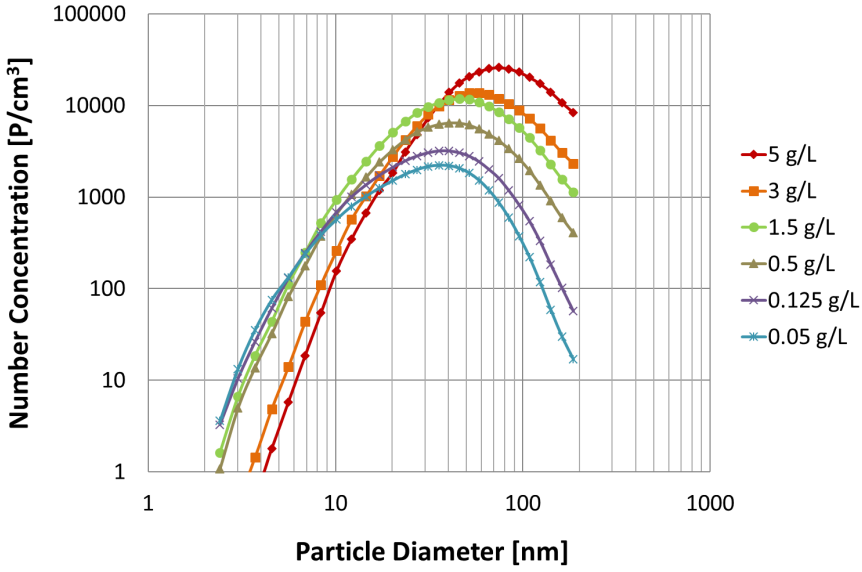

Fig. 30: SMPS size distributions for a range of AS concentrations in distilled water.

Their conclusion was that this observed effect was due to an accumulation of impurities from the solvent on the resulting solid particles, even when using laboratory-grade purified water. So, rather than relying on the formula, it has been experimentally determined what concentration of ammonium sulfate to put into solution with the help of a Scanning Mobility Particle Sizer (SMPS). The relationship between the AS concentration dissolved in one liter of distilled water and the resulting particle size distribution from these measurements can be seen in Fig. 30.

Building on prior measurements, six different solutions ranging from 0.05 to 5 g AS per liter of distilled water were tested to achieve a size range that works well for these experiments. The median diameter of the resulting aerosol, its geometric standard deviation and total concentration for these measurements are given in Tab. 12.

Tab. 12: Key parameters of the aerosol produced by atomizing a range of AS concentrations.

	5.0 g/L	**3.0 g/L**	**1.5 g/L**	**0.5 g/L**	**0.125 g/L**	**0.05 g/L**
Median [nm]	31.2	23.5	17.2	15.7	12.2	10.3
GSD	1.66	1.72	1.82	1.82	1.86	1.86
Total conc. [P/cm^3]	2.7 x 10^5	1.5 x 10^5	1.4 x 10^5	7.6 x 10^4	3.8 x 10^4	2.5 x 10^4

The calibration of CPCs requires a sufficient concentration of the aerosol also in the small nanometer size range near the lower cut-off of the instrument. For that reason, the solution that produced the highest number of particles between 5 and 20 nm was selected. According to the results from these preliminary measurements, it is the case for a concentration of 1.5 g AS per liter of distilled water. While that concentration is not the highest at 5 nm but very comparable to the other solutions, it is 37% higher than the next highest solution at 10 nm and even 54% higher at 20 nm in the above measurements. In consequence, 1.5 g of ammonium sulfate per liter of distilled water was used for all of the calibration experiments representing ambient aerosol.

5.3.2 Calibration aerosol for urban air

In urban areas and especially in locations close to major roads, an abundance of particles can be found that were released as emission from diesel vehicles but also other by-products from the incomplete combustion of fossil fuels. It is difficult to reproduce real-life traffic emissions in the laboratory, other than by putting an actual vehicle on a chassis dynamometer in an automotive emission laboratory as done during a vehicle's type-approval test. Consequently, it was decided to use a soot aerosol generated by a laboratory combustion burner as proxy for the solid particles from combustion processes found in urban environments. Compared to the experimental setup for the AS calibration aerosol explained earlier, the soot generator

replaced the atomizer aerosol generator and the subsequent diffusion drier in the experimental setup. All other components and dimensions were kept the same as displayed in Fig. 31.

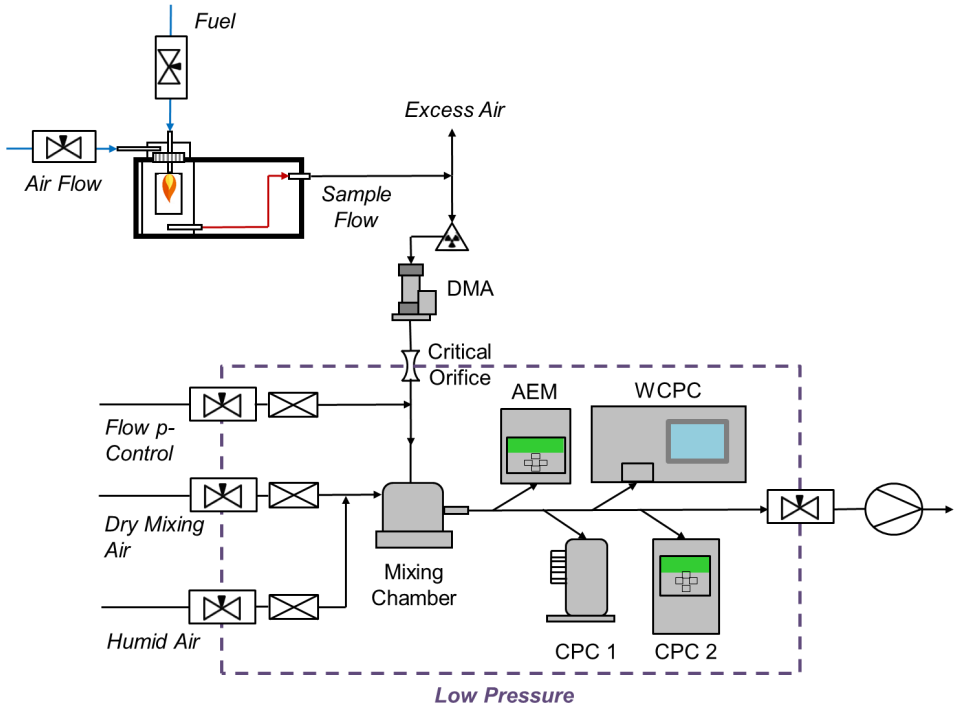

Fig. 31: Experimental setup using the soot generator as aerosol source.

Flame burners are said to be a suitable source of solid soot particles for calibrating measurement devices. In fact, the PMP group recommended soot particles generated by the CAST method for the calibration of CPC's used in emissions tests required for vehicles to obtain type approval, even though other particle materials were not excluded provided it has been shown that they deliver comparable results (Giechaskiel et al., 2009). Originally this caused some discrepancies as the calibration requirement at the 23 nm cut-off diameter required for vehicle emissions testing was not met when re-calibrated with CAST particles, while it was achieved with the original manufacturer's calibration based on Emery oil and also when subsequently checked with the same oil (Giechaskiel et al., 2011a). In the same year, Takegawa and Sakurai (2011) were the first to report on the use of soot particles for the calibration of a CPC

at reduced pressure. Their soot aerosol was also produced by a CAST burner but the experiment was limited to particle sizes larger than 50 nm.

In this work a novel inverted burner design was chosen instead of the more established CAST device. This burner can produce high concentrations of soot particles with a fractal-like structure independent of fuel composition and flow rate (Kazemimanesh et al., 2019). Weingartner et al. (1995) have shown that freshly generated soot is hydrophobic and does not activate or grow easily, which only changes once water-soluble compounds typically of an organic nature condense on its surface. The downward-flowing diffusion flame method promises a more stable, fairly constant soot production and ideally also a larger fraction of particles smaller than 50 nm. An additional aspect of this work was that this new miniaturized inverted flame burner first had to be characterized for its suitability for calibrating the counting efficiency of a CPC and its lower cut-off size in the small nanometer range. These results were published in Bischof et al. (2019) and are explained in more detail in the following chapter.

5.3.3 Particle size characterization of the soot generator

As the laboratory source of the soot calibration aerosol a Miniature Inverted Soot Generator (Argonaut Scientific Corp., Edmonton, AB, Canada) was chosen. This more recently introduced device is a soot generator that promises to produce a larger fraction of nanoparticles than other commercially-available burners such as the CAST generator mentioned in chapters 2.4.3 and 3.4. This specific type of soot generator uses a downward-flowing diffusion flame inside the burner as can be seen in Fig. 32, which promises an increased stability of the flame according to Stipe et al. (2005).

Fig. 32: The Miniature Inverted Soot Generator (on the right), and the image of an open-tip propane flame from the experiments on the left.

The underlying fundamental reason is that the force of the buoyant hot products from the combustion is directed upwards, so a more uniform downward pointing flow is achieved inside the generator's co-flow air tube. In the inverted design this steadies the flame and results in a more constant soot production, which directly impacts the stability of the size distribution and the number concentration of the resulting soot calibration aerosol. The aerosol laboratory at IEK-8 in Jülich had purchased it just prior to the start of these experiments and hence it deserved an in-depth characterization. All details of this study have been published in Bischof et al. (2019).

In more detail, the Miniature Inverted Soot Generator uses two co-annular tubes that provide the fuel and air flows as presented in Fig. 33. These flows enter the generator at its top section after passing through separate mass flow controllers (MC-series, Alicat Scientific Inc., Tucson, AZ, USA) that we purchased separately and added to our soot generation setup. In order to start up the generator, one has to open its top cap to light the flame manually. After closing it, the diffusion flame burns inside the quartz tube in a downward direction. The co-flow air provided delivers the oxygen required for the combustion process but it also achieves an early dilution of the soot aerosol escaping the flame and hereby limits successive coagulation.

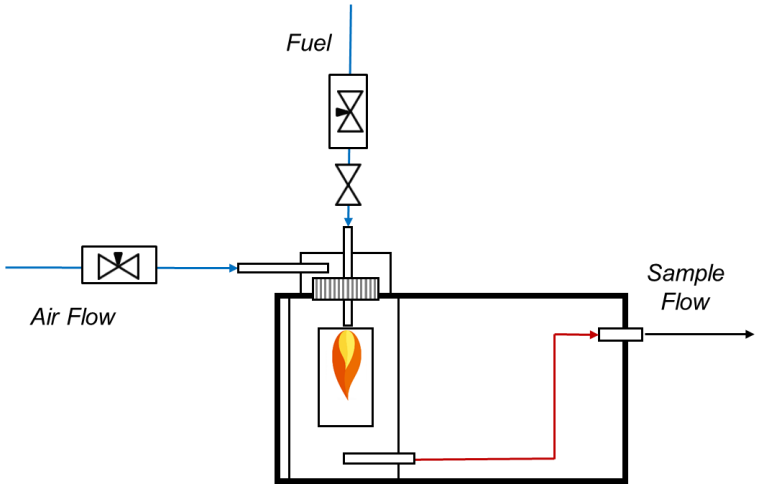

Fig. 33: Basic operational principle of the Miniaturized Inverted Flame Burner.

After leaving the co-flow air tube, the soot aerosol first passes through a cooling coil before exiting the generator through its sample flow connector. The soot generator was operated with propane as fuel, as it is easily available and known to burn efficiently. At first, warm-up experiments were conducted to determine when the soot

generator reaches stable output as expressed by the total particle number concentration, which is reported in detail in the corresponding publication.

Next, the generator's output was characterized for a dozen chosen test conditions with different air flow and fuel flow rate settings. These operational settings were selected so they are in line with what was previously identified as the open-tip flame (sooting) regime in the paper published by Moallemi et al. (2018); see Fig. 34.

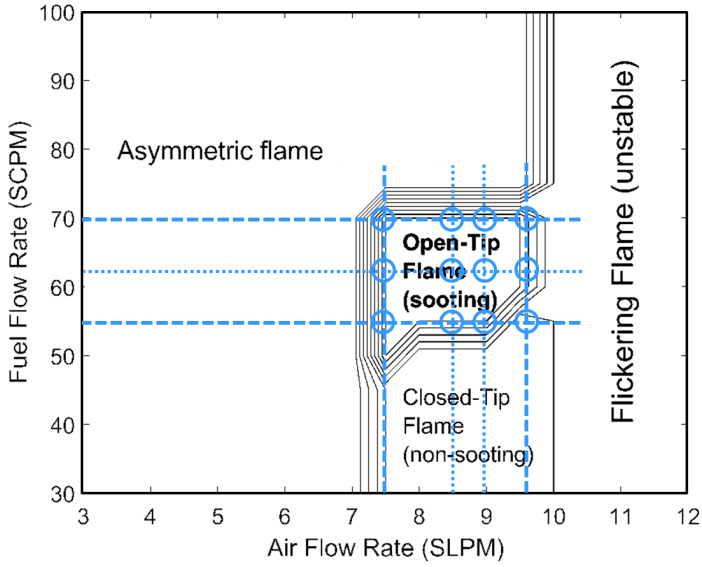

Fig. 34: Regimes of the soot generator reproduced from Moallemi et al. (2018), with the dozen test conditions used in the preparatory characterization superimposed.

The experiments were started with the soot generator operated at the highest airflow rate and the highest propane flow rate shown in Fig. 34. After that measurements continued by reducing the fuel flow to the next value of that matrix and finally to the lowest one. Once completed, the airflow rate was also lowered and measurements for the same three propane flow rates were conducted. This process was duplicated twice until the lowest airflow rate and the lowest fuel flow rate was reached.

The particle size distributions of the soot aerosol were measured for each of the dozen selected test conditions with particle size spectrometers. The CPCs were used to monitor the particle number concentration for each of the DMA-classified sizes. These measurements were complemented with an optical particle counter (Sky-OPC, Model 1.129, Grimm) to also obtain some additional information on the presence of large particles in the 250 to 2,250 nm range. Since an OPC measures all of its size channels simultaneously, these measurements were done by bypassing the DMA. For simplicity

the particle size distributions based on the electrical mobility diameter and those with a light-scattering equivalent diameter are displayed side-by-side, with gaps left to separate these two different methods. It is important to stress that the OPC was not custom-calibrated for soot aerosol and that its results were not fitted to the DMA-CPC data either. Obviously, an optical particle counter can be expected to respond quite differently to soot particles than to the polystyrene latex (PSL) reference particles that are typically used for its factory calibration. Yet as a minimum, the supplementary OPC data can provide indicative information if there is a large number of coarse particles outside the range of interest. The respective particle size distributions for each of the dozen test conditions are presented in Fig. 35 (a) – (d). The graphs highlight that the modal values of the size distribution are clearly dominated by the SMPS data, with what appears to be only a comparatively small fraction of particles larger than 250 nm.

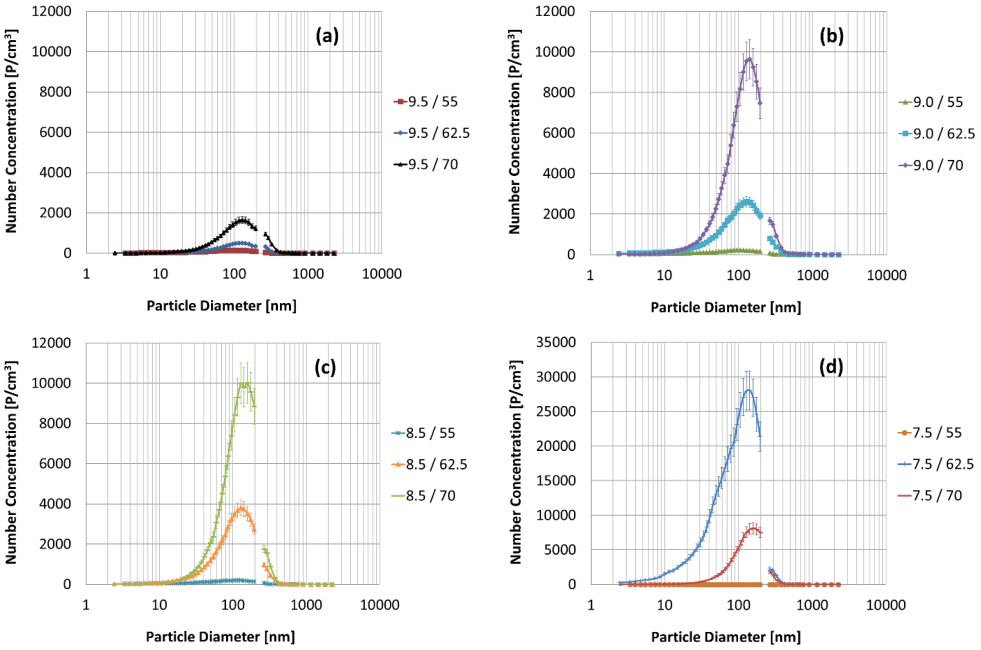

Fig. 35: Particle size distributions of the soot generator as measured by the combination of two instruments. The gaps in the graphs are to distinguish SMPS data (up to 200 nm) from OPC results (starting at 250 nm). The four graphs each represent a fixed air flow rate ranging from (a) 9.5 SLPM, (b) 9.0 SLPM, (c) 8.5 SLPM to (d) 7.5 SLPM and the same three fuel flow rates (55, 62.5 and 70 SCPM), which are color-coded.

The graphs in Fig. 35 also show that the Argonaut soot generator produces mono-modal particle size distributions with a predominant mode between 100 and 150 nm, which varies depending on the flow rates. At their peak values, the corresponding

number concentrations exhibit differences by up to two orders of magnitude. Note that the graph in Fig. 35 (d) uses a different concentration scale as one of the fuel flow rates results in a much higher output of close to 28,000 P/cm^3. Compared to that the operation condition with 7.5 SLPM (standard liter per minute) air flow and 55 SCPM (standard cubic centimeter per minute) fuel flow produces almost no particles, irrespective of their diameter. The conclusion is that at this setting with the lowest fuel flow and air flow rates, the flame burner is operating in its closed tip-flame regime that results in essentially no soot being formed. Tab. 13 provides an overview of the key physical properties of the aerosol produced with the dozen operational settings used in these experiments.

Tab. 13: Select aerosol properties for the stated operating conditions of the soot generator.

Air flow rate [SLPM]	Fuel flow rate [SCPM]	Modal diameter [nm]	Total number concentration CPC [P/cm^3]	Total number concentration OPC [P/cm^3]
9.5	70.0	128.1	2.1×10^4	3.3×10^3
9.5	62.5	128.1	6.4×10^3	8.8×10^2
9.5	55.0	95.2	2.8×10^3	1.5×10^2
9.0	70.0	141.9	1.1×10^5	1.0×10^4
9.0	62.5	128.1	3.5×10^4	3.4×10^3
9.0	55.0	104.9	4.2×10^3	2.4×10^2
8.5	70.0	157.5	1.1×10^5	1.1×10^4
8.5	62.5	128.1	4.7×10^4	4.4×10^3
8.5	55.0	104.9	3.8×10^3	2.3×10^2
7.5	70.0	157.5	7.8×10^4	1.0×10^4
7.5	62.5	141.9	4.0×10^5	2.2×10^4
7.5	55.0	157.5	2.3×10^1	2.0×10^0

Some of the distributions in Fig. 35 exhibit a slight shoulder to the left of their modes that is more or less pronounced, which indicates that there are operating conditions of the soot generator that result in more particles in the small nanometer size range. As explained in chapter 2.4.1 and shown in Fig. 7, the detection efficiency of a CPC starts to drop at a certain particle size below 20 nm, which is why greater scrutiny was given to the soot generator's output for nanoparticles between 3 and 20 nm in diameter. The corresponding analysis in Fig. 36 highlights that there is one operational setting that produces clearly the highest concentrations in this smaller size range. When the soot generator is operated with 7.5 SLPM air flow and 62.5 SCPM propane flow it achieved

approximately one order of magnitude higher concentrations across that range. This proved to be the most promising operating condition in order to produce adequate particle number concentrations below 20 nm. Although concentrations in the low to mid thousand particles of the calibration aerosol at these sizes would be preferable, the lowest number concentration of approximately 400 P/cm^3 at a particle size of 3 nm is just sufficient enough. It is approximately a factor of three higher than the average zero offset values determined based on the noise level of the reference electrometer.

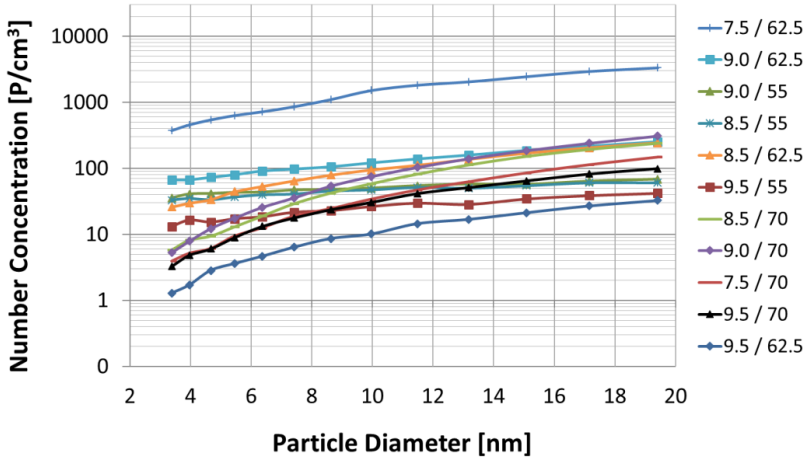

Fig. 36: Output concentrations in the sub-20 nm range for the stated operating conditions of the soot generator.

Since these are by far the lowest concentrations in the experiments, a simple approximation of the diffusional loss to the walls for the tube length between the DMA and the CPCs was made. Gormley and Kennedy (1949) first derived an empirical equation for particle loss due to Brownian diffusion in a straight cylindrical tube, for which they assumed a fully developed laminar flow. A dimensionless deposition parameter β is used to describe the diffusional particle loss,

$$\beta = \frac{\pi * D * L}{q} \qquad (5.2)$$

where D is the diffusion coefficient, L the length of the cylindrical tube and q the volumetric flow rate through it. According to Hinds (1999), the diffusion coefficient is expressed as follows:

$$D = \frac{k * T * C_c}{3\pi * \mu * d_p} \tag{5.3}$$

where, k is the Boltzmann constant, T the absolute temperature, C_c the Cunningham slip correction, μ the viscosity of air, and d_p the particle diameter.

For $\beta \geq 0.0312$, the penetration of particles P through the tube can then be determined by the following equation (Gormley & Kennedy, 1949):

$$P = 0.8191\, exp(-3.66\,\beta) + 0.0975\, exp(-22.3\,\beta) + 0.0325\, exp(-56.7\,\beta) \tag{5.4}$$

For our experimental setup this approximation resulted in a penetration efficiency of 94% for particles that are 20 nm in diameter. Contrarily, for the smallest particles in the experiments with a diameter of 2.4 nm it was only 33%. The relative measurement with the CPCs under calibration and the reference electrometer side-by-side and identical or a flow-rate adjusted length of the sampling tubing ensures that diffusion loss has essentially no effect on the performance efficiency measurement. However, the lower concentrations caused by diffusional loss do have an additional, adverse impact on the already poor counting statistic for the smallest particle sizes.

5.4 Boundary conditions and corrections for the data analysis

The measurement strategy for the experimental work of this thesis produced high dimensional datasets, with 68 instrument parameters and measurement values recorded over at least 1,200 seconds per experiment. This large number of data was chosen to minimize variance and bias, but it added much complexity. In addition to that, the number of ultimately usable data was limited by experimental issues, problems of the measurement devices and user errors. Common instrument problems included flooding due to pressure changes happening too quickly, CPCs running out of butanol, incorrect flow rates and communication problems between the instruments and the data acquisition system. These errors were often only detected when the data were analyzed, so the data sets had to be corrected accordingly. In order to analyze several hundreds of these large data sets, a custom spreadsheet with boundary conditions that could be selected based on the type of data analysis was used.

For the analysis the first 10 seconds of each measurement were discarded to account for achieving stable conditions after changing from the previous voltage step. Then average values for the 20 seconds that are considered to be stable conditions were

calculated, using the pre-defined constraints. This enabled the identification of gaps in the experimental data and excluding outliers from these large, convoluted data sets. Outliers occurred in the shape of sudden and highly improbable spikes, e.g. when the concentrations reported by the Sky-CPC went up by a factor of 100 from one second to another only to drop down again the next second or when a CPC reported zero values mid-measurement. Some outliers were clearly caused by data transmission errors, for instance when voltage steps were missed, one of the DMA's control parameters suddenly shifted for no reason, or no data were reported by one of the CPCs. In addition, data were also excluded when the Sky-CPC reported values smaller than 0.95 for its internal C1/C0 performance criterion or when the 3772-CEN CPC set an error flag as explained in chapter 5.2.1. Lastly, boundary conditions for the counting efficiency calculation were defined as:

- Counting efficiency ratio: >0.001 and <=1.15
- Raw electrometer value less offset: >200 fA,

with the electrometer zero offset value representing the upper limit of the range determined during the electrometer characterization presented in chapter 5.2.4.

5.4.1 Coincidence correction

Coincidence errors occur in all particle counters when they are used for measurements at high concentrations. During a coincidence event, two or more particles simultaneously pass through the viewing volume. If the particles are close enough to each other, they become optically indistinguishable from one another and are erroneously detected as one. For CPC measurements, a coincidence-corrected number concentration can be calculated by this equation (Picard et al., 2019):

$$N_a = N_i \exp(N_\mathrm{a} * q_\mathrm{ae} * \tau_\mathrm{p}) \qquad (5.5)$$

where N_a is the actual concentration (P/cm^3), N_i the indicated concentration (P/cm^3), q_{ae} the aerosol flow rate of the CPC, and τ_p the nominal effective time during which a particle remains in the viewing volume. The value for N_a in the exponent is typically approximated by the use of N_i. In case of the CPC 3772-CEN the aerosol flow rate q_{ae} is 16.67 cm^3/s and the nominal effective time τ_p is 0.35 µs, which results in a calculated coincidence of 6.4% at 10,000 P/cm^3. It should be said that in this work coincidence was calculated and applied to the CPC data only for completeness. The number concentrations of the size-classified aerosol leaving the DMA were typically well below levels when coincidence occurs. This correction therefore only had a negligible effect during the CPC calibration experiments.

5.4.2 Multiple charge correction

As explained in chapter 2.4.3, the size-classified aerosol leaving a Differential Mobility Analyzer (DMA) is not strictly monodisperse but only of a mono-mobility caused by the presence of a size-dependent fraction of multiple charges. Therefore, the error in the number concentration of a reference electrometer caused by this effect must be corrected. In this work, the multiple charge correction method first introduced by Bundke et al. (2015) was applied. They demonstrated that an appropriate multiple-charge correction factor $\xi(d_P)$ can be determined when taking the actual size distribution of the aerosol present into account. The effect of this particle size dependent correction can be seen when comparing it to the simplified first-order approximation that does not consider the size distribution. As can be seen in Fig. 37, the curve of the first-order approximation differs considerably from the curve of the calculated correction factor $\xi(d_P)$. While even the first-order approximation might be acceptable in principle, at least if no measured size distribution is available at all, a higher accuracy can be achieved when the particle size distribution is considered.

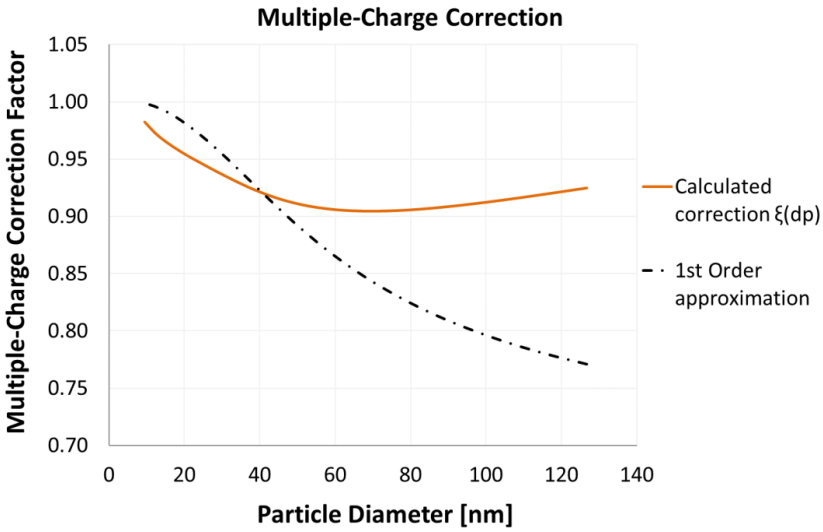

Fig. 37: Visualization of the multiple-charge correction factor $\xi(d_P)$ (solid orange line) and a simplified first-order approximation (dashed black line), data from this work.

The paper by Bundke et al. (2015) provides the theoretical background and formulas for their multiple charge correction method, which was practically implemented as follows. At first, a sequential measurement for all particle sizes chosen for the calibration measurements is performed. The average concentration values for the reference electrometer and CPC measurements can then be calculated for selected residence times per voltage step and an acceptable concentration minimum of the

electrometer. Since these sizes cover the lower end of the size distribution very well but not all of it closer to its upper end, a log-normal fit to the measured size distribution is calculated to extend it to larger particle sizes. This is done by applying iterative steps to find the best solution based on the input values, the desired solution, and some predefined constraints. As each iteration that attempts to get closer to the optimum fit takes time to compute, the entire calculation takes around 5 min for each data set. Although the resulting fit is an assumption, certainly the size distributions generated by the constant output atomizer aerosol generator follow a log-normal distribution. Subsequently, the diameters of doubly charged particles d_p (n= -2) that have the same electrical mobility as the singly charged particles at the original discrete DMA voltage steps are determined. Using the widely accepted approximation of the bipolar charge distribution according to Wiedensohler (1988), the normalized charge distribution of particles carrying -1 and -2 charges, η (-1) and η (-2), can then be calculated. A successive fit of the size distribution for the doubly-charged particles then allows the determination of their concentration at the original particle sizes. The ratio between singly and doubly charged particles permits the calculation of the correction factor $\xi(d_p)$ to adjust the initial electrometer concentration N_{AEM} for the contribution of doubly charged particles. After that the electrometer concentration N_{ref} at each size can be calculated by using this equation:

$$N_{ref} = \xi(d_p) * N_{AEM} \tag{5.6}$$

This multiple charge correction method works very well for a near lognormal aerosol size distribution as it is typically produced by an atomizer (He et al., 2015). It is easy to apply to the resulting log-normal size distributions with a mode around 50 nm and sufficient concentrations even below 10 nm. It is less appropriate for a soot aerosol with a mode well above 100 nm and thus a substantial contribution of particles that statistically carry more multiple charges. Yet Mamakos (2016) showed that for sub-50 nm soot particles generated by a combustion aerosol standard burner (miniCAST, Jing Ltd, Zollikofen, Switzerland) the ratio of doubly to singly charged fractions as a function of their mobility diameter was within ±10%. This is within the limit for acceptable multiple charge corrections according to ISO 27891 (2015), the international standard for determining the detection efficiency of CPCs. Especially in the sub-20 nm size range of interest in this work the difference in multiple charged particles is therefore also considered minor.

5.4.3 Data analysis procedure

The data analysis was always started by converting the raw measurement values to corrected data. The raw number concentrations from a CPC only has to be corrected

for the concentration-dependent counting coincidence in its optics. A flow correction was not deemed necessary as both of the CPC models use critical orifices. The raw data from the electrometer reference instruments underwent more corrections. Offset and flow corrections for low pressure were made before the multiple charge correction was applied to the electrometer data (EA):

1) At first, the EA offset value previously determined for the present conditions was subtracted from the EA raw data for each of the particle sizes.
2) Then the multiple-charge correction factor $\xi(d_P)$ was calculated and applied to the EA data.
3) Ultimately, corrections to the electrometer flow rates were made to account for the corresponding conditions of reduced pressure.

It is important to point out that the corrections for some measurement conditions for particle sizes below 10 nm have to be made at very low electrometer currents, due to the low concentrations of DMA-classified particles. This required a diligent inspection of each data set to identify outliers that would skew the counting efficiency results. The flowchart in Fig. 38 provides an overview of the data analysis procedure and the corrections made to determine the CPC counting efficiency.

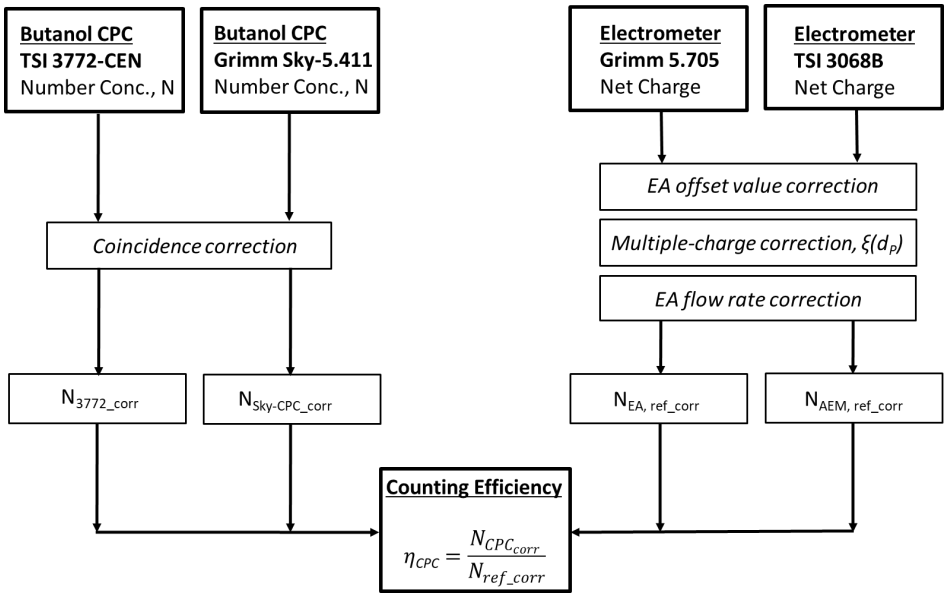

Fig. 38: Flowchart of the data analysis process for all particle concentration instruments.

Ultimately, the counting efficiency η_{CPC} for each valid measurement point was calculated as shown in the following equation:

$$\eta_{CPC} = \frac{N_{CPC\_corr}}{N_{ref\_corr}} \tag{5.7}$$

where N_{CPC_corr} is the corrected CPC concentration and N_{ref_corr} the corrected EA reference concentration.

6. Experimental results for the CPC performance at low pressure

In this chapter, several sets of experimental data are presented to highlight the impact of reduced pressure on the detection efficiency of the CPC models characterized in this work. Initial experiments show the total concentration progression when the CPCs are challenged with selected monodisperse sizes at different levels of low pressure. Subsequently, detailed counting efficiency results are reported in relation to the two particle materials used for the low-pressure calibrations. Finally, the effect that small to moderate amounts of relative humidity can have on the detection efficiency of CPCs near their cut-off diameter is investigated.

6.1 CPC response to selected monodisperse sizes

The first set of experiments conducted were CPC inter-comparison measurements at low pressure. Although these measurements do not have the same significance as a calibration, they can reveal how the total number concentration varies when CPCs are challenged by monodisperse particle sizes at different levels of low pressure. For each pressure level, a series of total concentration measurements was conducted over 90 seconds per DMA size-selected monodisperse size, while the relative humidity was kept at a constant 30% RH. The seven levels of reduced pressure were 800, 700, 600, 500, 400, 300, and 200 hPa. The first step of 900 hPa pressure has always been excluded as the critical orifice could not be operated at critical conditions with the experimental setup. The initial 60 s of measurement for each pressure level was discarded as stabilization period and only data of the remaining 30 s were used for the analysis. This process was then repeated to obtain three measurements total for the same conditions. The data are plotted as one measurement series for the seven pressure levels to emphasize the stability of the number concentration during the measurement, omitting the pressure changes and corresponding stabilization phases. The corresponding graphs in Fig. 39 and Fig. 40 each show two series of total concentrations that were simultaneously measured by the CPC 3772-CEN and the Sky-CPC 5.411 per particle size.

6.1.1 Concentration as a function of pressure

The first series of the total concentration measurements shown here is for ammonium sulfate (AS) particles of 100 nm in diameter, a size that is at or near the modal value of the size distribution of this atomized aerosol. As the mode is the size with the highest particle numbers, this experiment should clearly be expected to deliver the best counting statistics. As can be seen in Fig. 39, the initial concentration at a DMA-classified, monodisperse particle size of 100 nm was about 15,000 P/cm^3 within a range of ±6% for both of the CPCs.

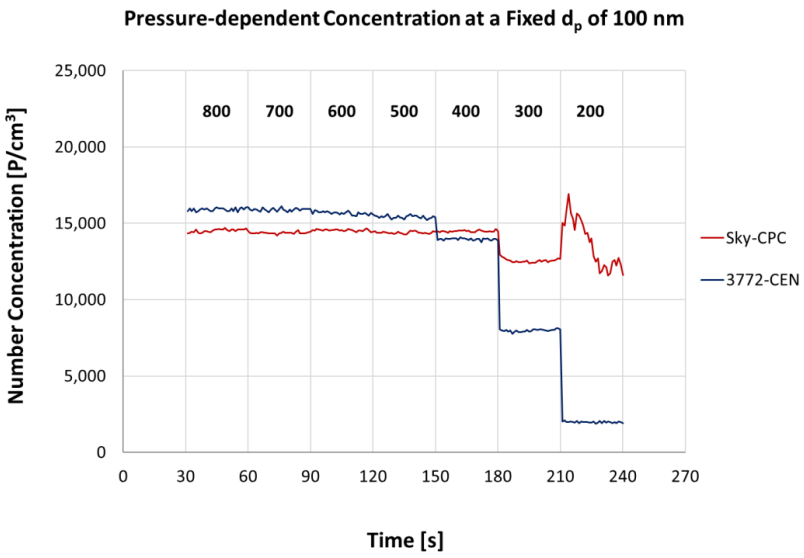

Fig. 39: Total concentration for two CPCs as function of pressure for 100 nm AS-particles. The blue line represents the CPC 3772-CEN and the red the Sky-CPC 5.411.

Although the measurement data show a slight shift in concentration, both models reported comparable concentrations at stable levels. For the measurements of the same CPC model, results were even within ±2% deviation for the different pressure levels down to 500 hPa. At 400 hPa, the Sky-CPC 5.411 kept reporting a concentration very much of the same order, while the CPC 3772-CEN shows an initial drop in particle number by about 10%. When reducing the pressure further to 300 hPa, both CPCs report a lower concentration than at higher ambient pressures. The CPC 3772-CEN drops by almost 45%, making the data useless at this pressure level and any pressure below. The Sky-CPC 5.411 also starts showing a drop of about 15%, which still allows applying a reasonable correction factor. When reducing the pressure further, the Sky-CPC 5.411 reports a total concentration that is about 10% higher over the 30 sec measurement intervals on average, so seemingly getting back to a stable level and similar to what it reported at higher ambient pressure. However, when looking at the data with a high time resolution of one measurement per second, it is obvious that the concentration is not completely stable. It actually fluctuates by up to ±20% between its lowest and its highest value during that 30-second measurement period.

Subsequently, experiments for a further three monodisperse sizes, which were 50, 20 and 15 nm, were conducted. The low-pressure response of the same CPC models for particles of 20 nm is shown in Fig. 40 below, which is frequently the smallest size at which an almost complete activation results in a 95% counting efficiency. Below that

diameter the slope of the counting efficiency curve becomes an increasingly important factor, which is not of interest for this set of measurements but something that was investigated in greater detail in the subsequent experiments reported in this chapter.

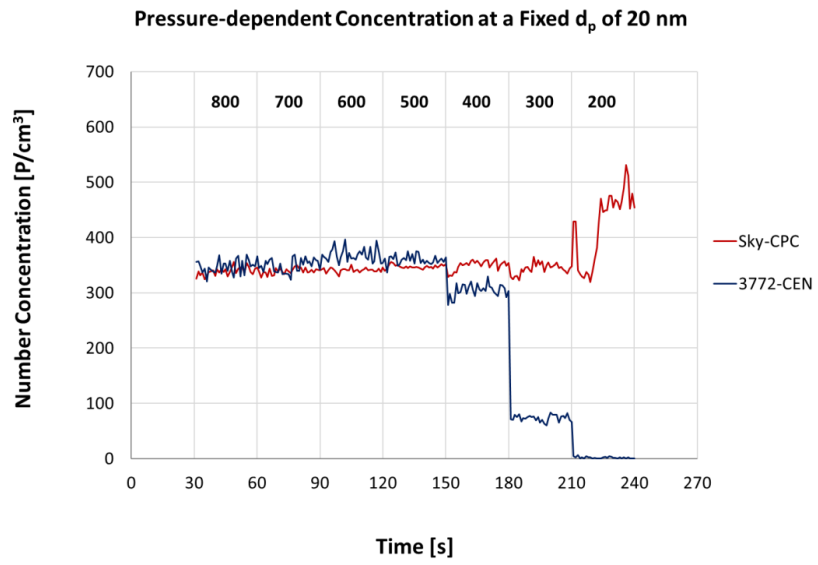

Fig. 40: Total concentration for the two CPC as function of pressure for 20 nm AS-particles. The blue line represents the CPC 3772-CEN and the red the Sky-CPC 5.411.

The first thing that can be seen from this measurement is that the total concentration is a factor of more than 40 lower than at the 100 nm size representative of the mode of the distribution, so counting statistics are much poorer in consequence. This is not due to the CPC performance but a result of the underlying polydisperse size distribution having a respective lower percentage of 20 nm than of 100 nm particles. Apart from that, a very similar pattern to the one seen at 100 nm can be observed. Down to a pressure level of 500 hPa both CPC models agree again very well, and vary less than 2% per instrument at each of the different levels of reduced pressure. At 400 hPa, the concentration measured by the CPC 3772-CEN once again drops notably. For the 20 nm particles it falls by about 15%. As previously, the concentration reported by the Sky-CPC 5.411 remains on average the same also at this pressure level. When reducing the pressure by another increment of 100 hPa to a level of 300 hPa, the data reported by the CPC 3772-CEN become again meaningless while the total concentration reported by the CPC 5.411 stays roughly the same. When going to the lowest pressure of 200 hPa tested, the total concentration of the Sky-CPC 5.411 is more than 20% higher than the average results at all other pressures. Yet, the 1-

second data again reveal that the measurement is not fully stable at 200 hPa and actually sways by about 50% between its lowest and its highest data point.

6.1.2 Key results of monodisperse experiments

At low pressure values between 800 and 500 hPa, the total concentrations reported by the two butanol CPCs display a very similar progression. There are only small, acceptable differences between the two models for the four monodisperse sizes tested. This changes when a certain threshold pressure is reached, which is at a different level for each of the CPCs. The response of both CPC models to monodisperse particles with diameters of 100, 50, 20 and 15 nm at the seven discrete pressure levels is shown in Fig. 41, with each data point averaged over 30-seconds.

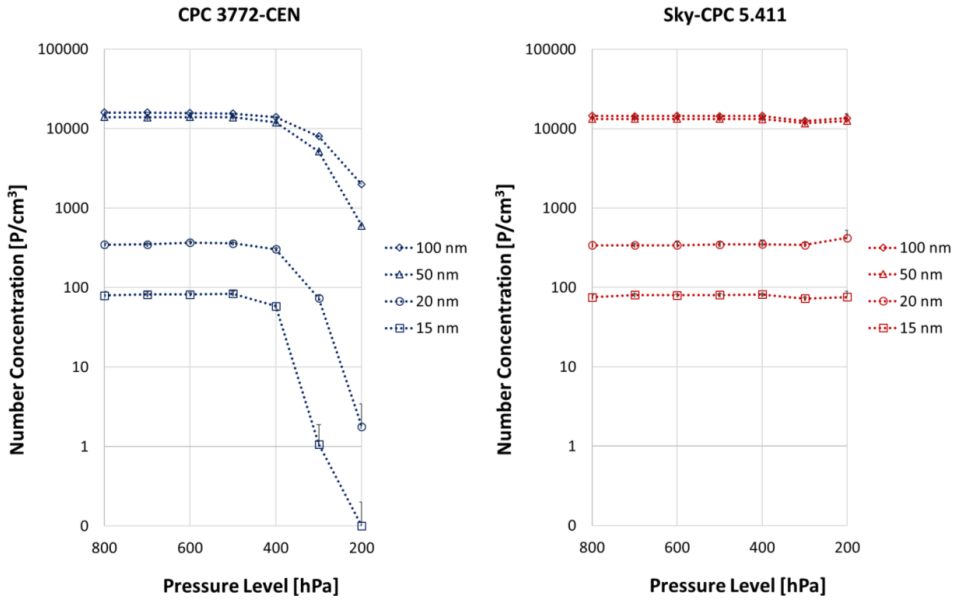

Fig. 41: Total concentration as function of pressure at 4 monodisperse particle sizes for CPC 3772-CEN (left, in blue) and Sky-CPC 5.411 (right, in red).

The CPC 3772-CEN performed as expected at these four sizes even well below its minimum operating pressure of 750 hPa. It measured concentrations in line with the higher pressures down to 500 hPa and still reported useable data down to 400 hPa, when appropriate corrections are made. The Sky-CPC 5.411, which the manufacturer specifies to work down to 125 hPa, even delivered meaningful concentrations at 300 hPa and still reported useful data at 200 hPa. Upon closer examination with higher

time resolution, the concentration at the lowest pressure revealed notable fluctuations. These data should therefore be used with some caution and ideally be averaged over a certain period, such as the 30-s average applied to the data presented in Fig. 41.

The final analysis of the experimental response to the total particle number for these monodisperse sizes is an instrument-to-instrument comparison by looking at the ratio of the two CPCs in one and the same plot. Although the true values will remain unknown as long as no independent concentration reference is used, it does provide a practical indication until which pressure level there is sufficient agreement between the CPCs when the common ±10% accuracy criterion is considered. In the comparison in Fig. 42 it is obvious that both CPCs agree very well with a ratio close to 1 down to 500 hPa of atmospheric pressure. It is only at a point between 500 and 400 hPa that the ratio of the measured concentrations begins to drop off notably.

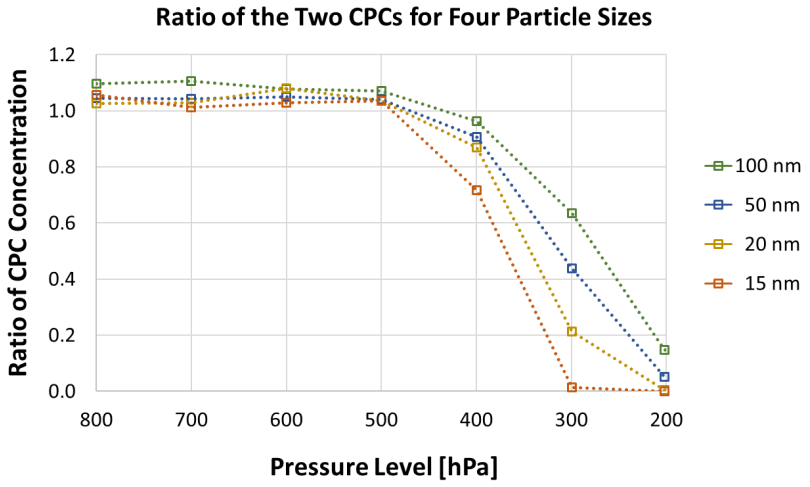

Fig. 42: Ratio of the total concentration of the CPC 3772-CEN to the Sky-CPC 5.411 as a function of pressure, for four particle sizes averaged over 30 seconds.

The performance of these two CPCs at 400 hPa remains at least comparable with acceptable corrections still possible. This graph also reveals that at 400 hPa the required correction to the total concentration reported by the CPC 3772-CEN for the given test aerosol is on the order of 10% or less, but that it has a size dependence that increases the smaller the particles get. The most likely reason for this observation is that the counting efficiency curve of the CPC 3772-CEN starts to change more prominently at this pressure, which is investigated in great detail in chapter 6. The correlation in Fig. 42 also highlights that any notion of correcting the CPC 3772-CEN's

data at 300 hPa based on its results for 100 nm particles is to be discarded. The difference to the data of the Sky-CPC increases to more than 50% already at a size of 50 nm and is well below 95% at 15 nm.

6.2 CPC counting efficiencies for ammonium sulfate (AS)

The counting efficiency characterizations constitute the most comprehensive part of the experimental work done in this thesis. All measurements were performed with the CPC 3772-CEN and the Sky-CPC 5.411, as well as the reference electrometer, in parallel. The measurements were made at 100 hPa increments of reduced pressure between 200 hPa and a maximum of 900 hPa. The DMA was always operated in a sequential mode using a total of 39 voltages starting at 3,300 V and stepping down to 10 V, which resulted inversely in a particle size range from 2.4 to 138 nm. This range is appropriate for investigating the impact of reduced pressure on particle activation inside a CPC. At each step, the voltage and the corresponding particle size were kept constant for 30 seconds to obtain several values of the particle concentration.

6.2.1 Counting efficiency of the Sky-CPC 5.411 for AS

Counting efficiencies for ammonium sulfate (AS) were experimentally determined at equidistant pressure levels down to 200 hPa. Results at 900 hPa were excluded as the lower flowrate through the critical orifice in the experiment at that pressure resulted in a too low monodisperse output from the DMA and hence an incorrect particle size.

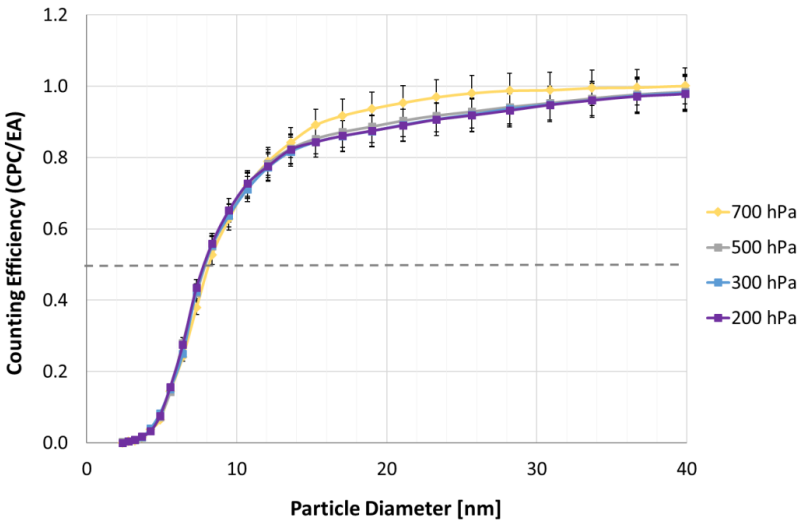

Fig. 43: Measured counting efficiency curves of the Sky-CPC 5.411 for ammonium sulfate at reduced pressures from 700 to 200 hPa.

The curves in Fig. 43 represent the experimentally determined counting efficiencies of the Sky-CPC 5.411 and divulge its lower-size detection limit (d_{50}) at the discrete pressure levels. Error bars are added for the ordinate to indicate the experimental standard deviation. It appears as if the efficiency curves of the Sky-CPC are almost on top of each other. In addition, the lower cut-off diameters appear to be very similar, with a d_{50} that varies only between 7.2 and 8.1 nm. The largest of these cut-offs is the one for the highest pressure. Further, there is a notable decrease in the asymptotic maximum counting efficiency between 10 and 40 nm when the pressure is reduced to 500 hPa and below. All of these characteristics follow the same trends reported by Bundke et al. (2015), although they are less pronounced. They agree well with the measurements of the total concentration at low pressure as summarized in Fig. 41.

6.2.2 Counting efficiency of the CPC 3772-CEN for AS

Results for the simultaneously measured efficiency of the CPC 3772-CEN for the same ammonium sulfate aerosol are shown in Fig. 44 and Fig. 45. These data are broken out into two graphs based on the behavior that was observed during the previous total concentration measurements. The first graph shows two efficiency curves for the ambient pressure reduced down to 700 hPa and 500 hPa.

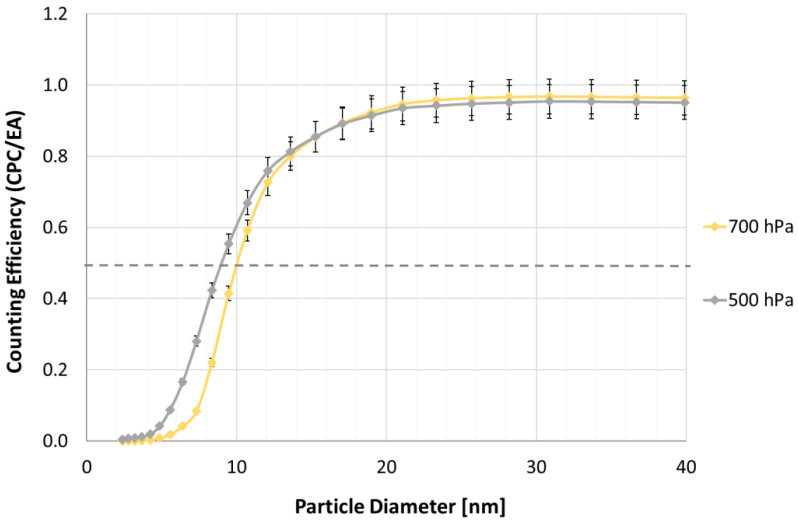

Fig. 44: Measured counting efficiency curves of the CPC 3772-CEN for ammonium sulfate at reduced pressures of 700 hPa and 500 hPa.

In this graph it can be seen that apart from a slight drop in the maximum efficiency, the CPC 3772-CEN seems to respond stably down to 700 hPa, which is just below its specified lower operating pressure. The impact gets more pronounced once the pressure is reduced further. There is a shift in the d_{50} cut-off diameter of about 1 nm

at 500 hPa and the asymptotic maximum counting efficiency decreases to below 95% at its peak value.

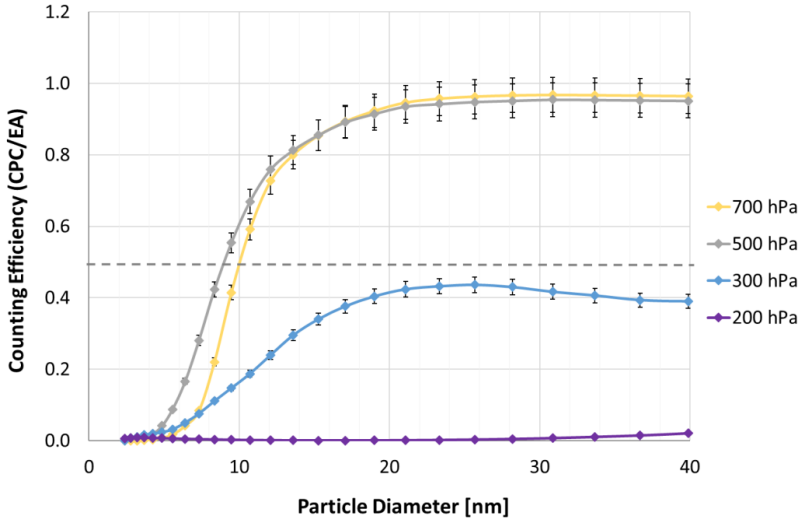

Fig. 45: Measured counting efficiency curves of the CPC 3772-CEN for ammonium sulfate at reduced pressures between 700 hPa and 200 hPa.

As can be seen in Fig. 45, the impact on the counting efficiency curve is severe when the pressure is reduced further to 300 hPa, with a maximum efficiency well below 50%. When further decreasing the pressure to 200 hPa it leads to an almost flat, completely suppressed progression that lacks the characteristic size dependency of a typical CPC efficiency curve. A possible explanation is that a notable amount of butanol vapor starts to leak at that pressure. With less butanol vapor available, only some particles will be activated until a point is reached where activation ceases almost completely. These results agree with the total number concentration measurements, where it was also observed that measurements with the CPC 3772-CEN at 300 hPa and below are no longer meaningful.

6.2.3 Linearity of the two CPC models for AS

As explained in chapter 2.4.2 and as shown in our earlier CPC calibration study (Liu et al., 2005), CPCs have a very linear measurement response with regards to their total number concentration measured at standard pressure. This is also expected at reduced pressure as long as the total CPC counting efficiency is close to 100%. In this work, the linearity behavior of the two CPCs for the ammonium sulfate aerosol was determined by plotting their measured number concentrations versus the corrected electrometer concentrations for the entire data set as explained in chapter 2.4.2. In

Fig. 46, the CPC data were analyzed for experiments performed at 700 hPa and 400 hPa, so low-pressure experiments that have delivered useful data for both CPCs.

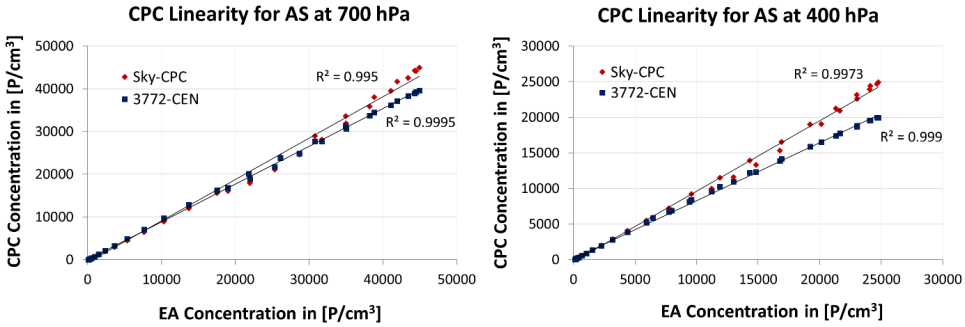

Fig. 46: Concentration linearity response of the CPC 3772-CEN and the Sky-CPC 5.411 for AS at pressures of 700 hPa (left) and 400 hPa (right).

The linear regression analysis performed for these data verified that the response of the CPCs is linear compared to the reference aerosol electrometer for the present conditions. The correlation coefficients (R^2 values) were larger than 0.995 for both CPC models at these pressures. The concentration linearity of the Sky-CPC 5.411 was 0.97 at 700 hPa and almost unchanged with a value of 0.99 at 400 hPa, while the slope of the CPC 3772-CEN decreased from 0.88 at 700 hPa to 0.82 at 400 hPa.

6.3 CPC counting efficiencies for flame soot particles

There has been much interest in using soot for CPC calibrations especially related to their usage by the automotive industry. For this purpose, the Miniature Inverted Soot Generator was extensively characterized as reported in chapter 5.3.3, such that the counting efficiency experiments could be repeated with freshly generated combustion particles. All of the subsequently shown flame soot measurements were done with settings of 7.5 SLPM air flow and 62.5 SCPM propane flow for the soot generator.

The CPC counting efficiency experiments with flame soot proved to be much more difficult to perform due to the necessary warm-up period, much lower concentrations of the classified particles, the influence of charge on the flame-generated particles, large amounts of water vapor that exit the burner and a stickiness of the flame soot agglomerates. In particular the importance of particle charging was not evident while performing the experiments and only came to light while analyzing the large data sets. Several measurements had to be discarded as concentrations of particle sizes below 20 nm measured by both CPCs were up to 50% higher than the corrected concentration from the reference aerosol electrometer. One hypothesis for the cause

of this are more pronounced multiple charge effects on the fractal-shaped particles that are concentration dependent. Therefore, the brief residence time in the aerosol neutralizer might not have been sufficient to achieve charge equilibrium at higher concentrations. It is particularly important to take proper charge conditioning into account when going to larger particle sizes. This was less of an issue in these experiments as the focus of this work was only on the counting efficiencies for particles of up to 40 nm in diameter, which under normal pressure conditions is a size at which 100% efficiency is easily achieved.

All curves in this chapter are spline graphs that are plotted through each data point. This is in contrast to the more common fit of the counting efficiency curves using an exponential function as introduced by Banse et al. (2001). The choice for this presentation comes with the drawback that one might consider it to imply a functional relationship that does not exist. Nonetheless, it was done deliberately in this work to emphasize the much larger fluctuations of the flame burner as aerosol source, which are in strong contrast to the almost completely smooth graphs for ammonium sulfate.

6.3.1 Counting efficiency of the Sky-CPC 5.411 for flame soot

The curves for the detection efficiency of the Sky-CPC at ambient pressures ranging from 800 hPa down to 200 hPa are presented in Fig. 47. It can be clearly seen that the data points for sizes above 10 nm have a larger scatter and the curves appear less smooth when flame soot is used as particle material in the experimental setup.

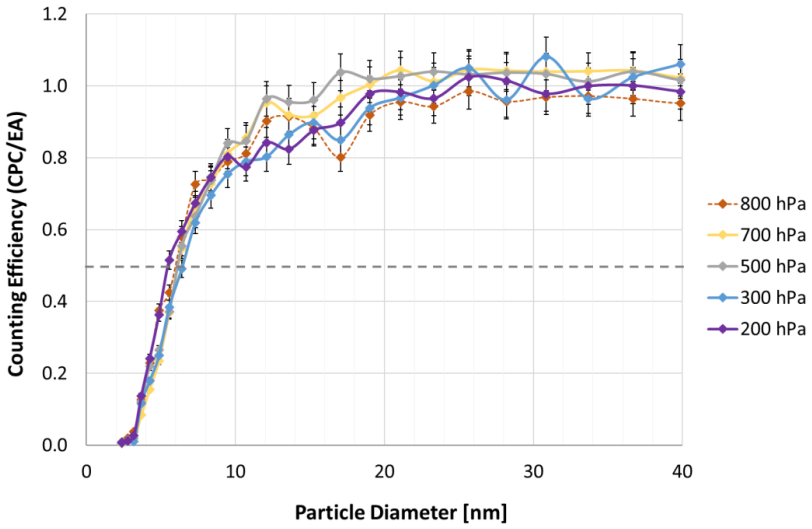

Fig. 47: Measured counting efficiency curves of the Sky-CPC 5.411 for flame soot at low pressure increments from 800 hPa to 200 hPa.

The curves agree reasonably well with one another in the steep slope of the curves but differ on the order of ±10% with increasing particle size. The cut-off diameter shows the smallest size of 5.5 nm for 200 hPa, although the difference to curves at other pressure levels is within the experimental uncertainty. It is evident, however, that the cut-off diameter is about 1.7 nm lower for soot compared to the one determined when ammonium sulfate was used as particle material for the calibration.

6.3.2 Counting efficiency of the CPC 3772-CEN for flame soot

The experimentally determined size dependent detection efficiency of the CPC 3772-CEN for flame soot at reduced pressures is illustrated by the graphs in Fig. 48. In general, the curves at 800 down to 500 hPa are largely similar, with a cut-off diameter around 6.3 nm. Clear differences can once again be seen once the ambient pressure is reduced further. The efficiency curve at 300 hPa is already very obviously different and is characterized by a much larger cut-off size and a lower asymptotic detection efficiency progression, while the one at 200 hPa hardly reaches a maximum efficiency of 50% at the largest particle size in that graph and thus shows no d_{50} cut-off diameter. The steepness of the slopes also drastically decreases at 300 hPa and much more so at 200 hPa, although it does not break down completely as for the ammonium sulfate calibration of that CPC.

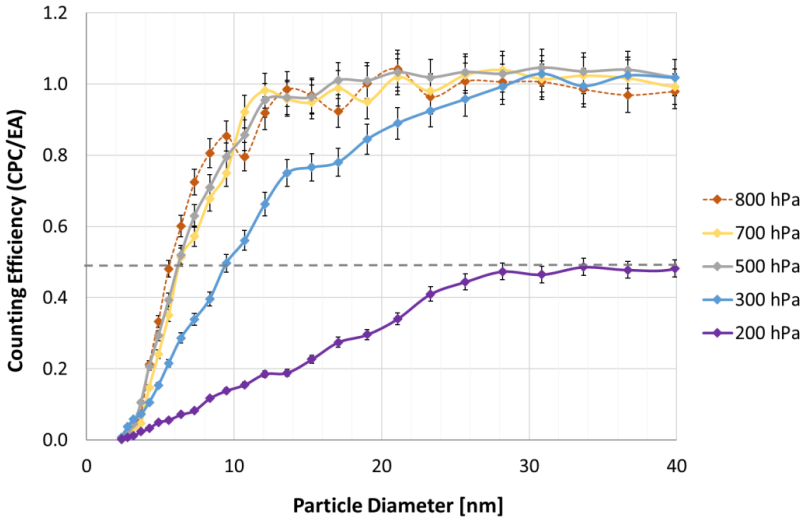

Fig. 48: Measured counting efficiency curves of the CPC 3772-CEN for flame soot at low pressure increments from 800 hPa to 200 hPa.

6.3.3 Linearity of the two CPC models for flame soot

The analysis of the instrument linearity was also repeated for the soot data. For pressures down to 500 hPa, the response of the CPCs was again highly linear compared to the aerosol electrometer also during the flame soot experiments, with R-squared values for the coefficient of determination greater than 0.99. The results for the linearity of the response are shown exemplarily in Fig. 49 for measurements performed at ambient pressures of 700 hPa and 500 hPa. When comparing these graphs to the same analysis done for ammonium sulfate it is important to notice that the number concentrations for soot did not exceed 10,000 P/cm^3, so it was about a factor of 4 lower. The linear regression for concentrations measured by the two CPCs vs. the reference electrometer resulted in a slope of larger than 0.993 for both CPCs at 700 hPa and even above 0.996 at 500 hPa.

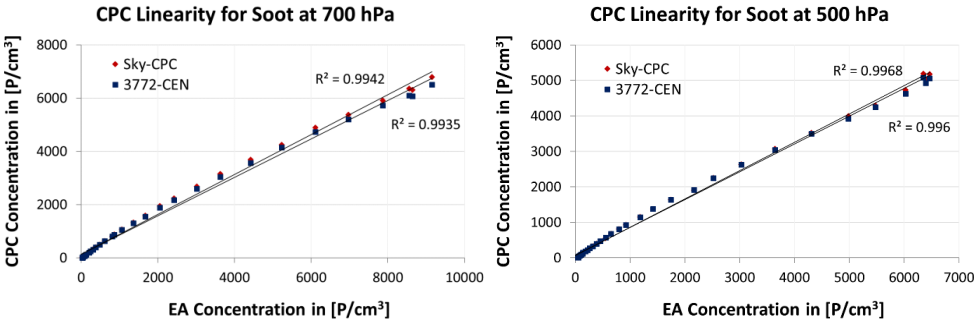

Fig. 49: Concentration linearity response of the CPC 3772-CEN and the Sky-CPC 5.411 for flame soot at pressures of 700 hPa (left) and 500 hPa (right).

The graphs also reveal that data points at concentrations of just a few hundred P/cm^3 drop below their trend line at both pressure levels, which is due to the larger role that RMS noise plays at these low particle number concentrations. For the soot data, there is also a larger difference in the slopes of the linearity curves, which was between 0.75 and 0.80 for the Sky-CPC and between 0.72 and 0.78 for the CPC 3772-CEN.

6.3.4 Impact of the particle material

In aerosol research, the term particle material is commonly used to summarize a particle's properties including its chemical composition and morphology. The particle material affects how a particle interacts with its immediate environment and crucially also how it impacts our climate. It also plays a role in how aerosols can be measured, e.g. due to differences in optical properties or interactions with the working fluid in the case of a CPC. This chapter presents a direct comparison of the detection efficiency experiments performed with ammonium sulfate to the ones with flame soot particles.

Data in this chapter are reported for the size range of 2.4 to 30 nm, as any effects are the most pronounced near the lower detection limit. Several things can be observed. The first and rather trivial observation is that the efficiency curves for soot appear more jagged, with notable turns between points even close to the CPC's maximum efficiency. However, this effect should not be attributed to material dependence but is caused by the aforementioned larger fluctuation of the flame burner compared to the constant output atomizer. At diameters below 10 nm the counting statistics is also much poorer due to the significantly lower concentrations of the monodisperse aerosol classified by the DMA. The example for the experiments made at 500 hPa shows a concentration that is 4.5-times higher for ammonium sulfate than for soot measurements at that size.

More importantly, both CPCs respond to the change in particle material with a modest change in their performance at reduced pressure. This impacted all characteristic parameters of their detection efficiency. The slope of the curves is slightly steeper for the soot particles as can be seen in Fig. 50 and Fig. 51. Also, their smallest size detection limits shifted by about 2 nm to 3 nm to smaller diameters the lower the pressure, at least until the threshold pressure at which the performance of the CPC 3772-CEN breaks down. In addition, the maximum asymptotic detection efficiency is higher for the soot measurements.

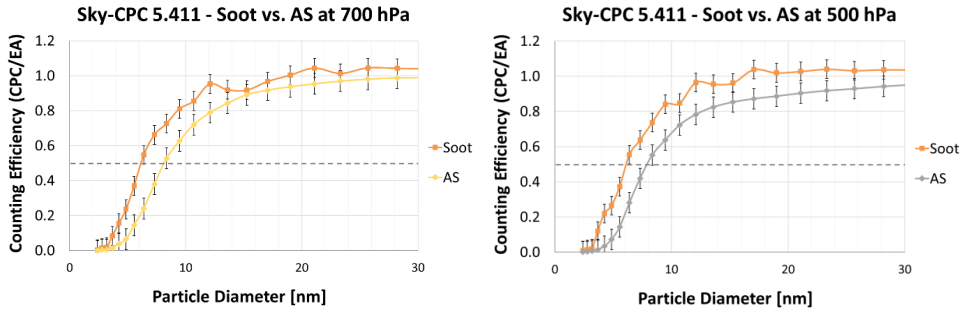

Fig. 50: Material dependent counting efficiency of the Sky-CPC 5.411 at 700 hPa (left) and 500 hPa (right) for ammonium sulfate and soot (orange curves).

Already during the experiments, it was observed that the flame soot aerosol contained much water vapor, even to the degree that it became necessary to install a droplet separator. The fresh soot aerosol generated by the inverted burner method was therefore not hydrophobic at all. However, the wettability with water alone should be a minor factor at best. A much more important aspect is its complex microstructure, as soot consists of chain agglomerates with a strong curvature of the graphene layers. This irregular morphology and the complex structure are the most likely reasons why soot activates more readily in a CPC. This is supported by Kulmala et al. (2007) who

stated that it is predominately the soot's distinctive surface properties and especially the contact angle that decide at what size insoluble particles get activated. In addition, soot particles can also carry functional groups with active surfaces that make it polar.

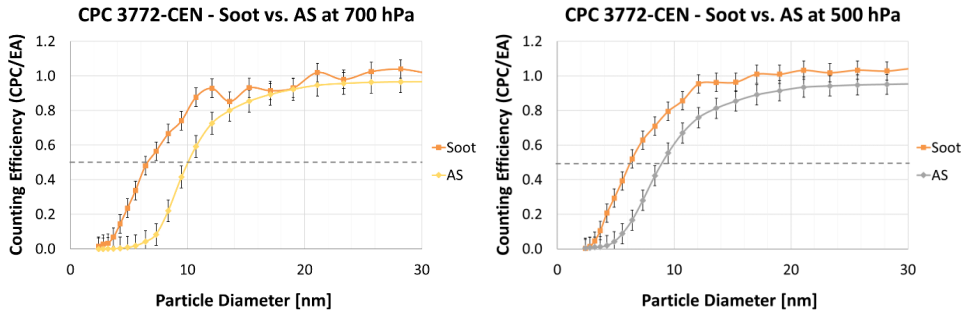

Fig. 51: Material dependent counting efficiency of the CPC 3772-CEN at 700 hPa (left) and 500 hPa (right) for ammonium sulfate and soot (orange curves).

Another notable observation is the collapse of the detection efficiency of the CPC 3772-CEN at very low-pressure levels below 400 hPa. This break-down was not as drastic in the case of the soot particles as can be seen in Fig. 48. However, rather than attributing this to the particle material it seems more likely that the lower concentration of particles in case of the flame soot was the reason for this. As explained by the Schlarb effect in chapter 3.1, the presence of fewer particles would mean that they have a higher probability of attracting the saturated butanol vapor at very low pressure and thus get somewhat better activated than a significantly larger number of particles.

6.4 Humidity dependence of the counting efficiency

In earlier work performed at standard conditions, Sem (2002) reported that the lower cut-off diameter of a predecessor model of the 3772-CEN CPC could change slightly when the relative humidity was increased from very dry conditions of 0% RH to a value of up to 50%. For an increase of up to 25% RH, the minimum detectable particle diameter of the model 3010 CPC that he tested also increased, yet it dropped again once humidity was further increased to values above 25% RH. According to Sem, this effect was clearly notable for hydrophilic NaCl salt particles but much smaller for hydrophobic silver particles. The Ag particles were generated by the Scheibel-Porstendörfer aerosol generation method (Scheibel & Porstendörfer, 1983), in which a tube furnace is operated at temperatures as high as 1,200°C. With this in mind it was decided to also investigate a possible impact of humidity on the CPC performance at low pressure as third parameter in this work. The working hypothesis was that micro-scale effects might lead to an improved wettability of the particle surface during the

initial activation of the smallest nanoparticles in a CPC, especially when the particle material is not hydrophilic to begin with. While thermodynamic relations are capable of describing how the majority of particles activate, the aim was to investigate if micro-scale phenomena can have an impact on the lower cut-off and the counting efficiency curve of a CPC specifically at sizes of 10 nm and below. A conjecture is that even nanometer-sized particles of non-soluble material might activate more readily when enough water molecules are present in the air that can attach onto their surface.

The relative humidity of the aerosols generated by both the atomization and the flame burner method was therefore varied between almost completely and moderately dry, so that their physical size does not change significantly due to the RH alone and any shift in the detection efficiency has to be caused by the activation inside the CPC. Both CPC models were tested at relative humidities between 1% and 40%, with the maximum value being a constraint of the experimental setup due to the primary focus on a high stability at reduced pressure.

6.4.1 Effect of humidity on the counting efficiency of the Sky-CPC 5.411

In order to assess the impact of relative humidity on the CPC performance, measurements were conducted at fixed levels of low pressure and up to five different humidity levels for both of the particle materials of choice at each pressure.

In the case of ammonium sulfate, 2% of RH and even slightly below were achieved as the lowest value, and a maximum RH level of 34% and slightly above. As can be seen in Fig. 52, there was no statistically significant effect of these levels of relative humidity on the counting efficiency of the Sky-CPC for the ammonium sulfate salt aerosol. During the measurements at the 200 hPa level, the pressure and humidity control of the experimental set up reached its limits. It is for this experimental constraint that at 200 hPa, only a maximum relative humidity of 22% instead of the desired 35% or 40% RH could be achieved.

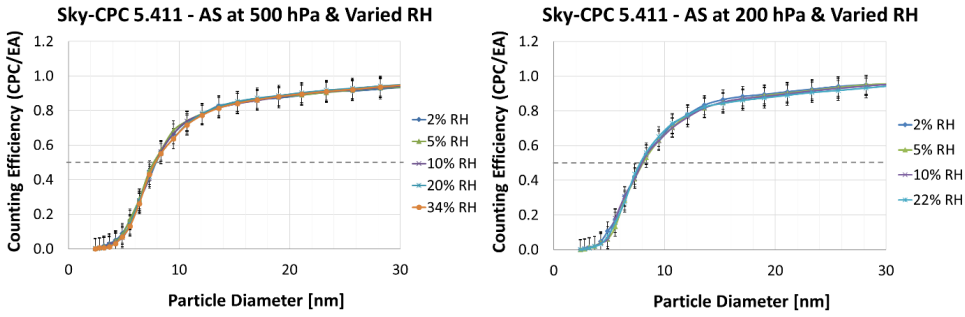

Fig. 52: Humidity dependent counting efficiency of the Sky-CPC 5.411 for ammonium sulfate at 500 hPa (left) and 200 hPa (right).

These RH experiments were then repeated also for the flame material aerosol. As explained in chapter 6.3.4, the flame burner generated soot with a large amount of water vapor. This also meant that RH values below 6% could not be achieved as there was not enough dry mixing air available to compensate for this very humid aerosol flow. An additional limitation was again the humidification of the flow at the lowest pressure of 200 hPa, which reached its practical limits at 25% RH.

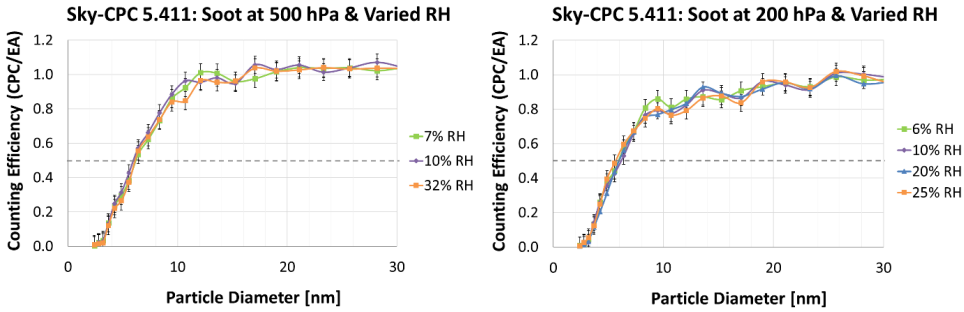

Fig. 53: Humidity dependent counting efficiency of the Sky-CPC 5.411 for flame soot at 500 hPa (left) and 200 hPa (right).

Results for pressure levels of 500 hPa and 200 hPa are shown in Fig. 53. As can be seen, there is no apparent humidity dependency of the counting efficiency of the Sky-CPC for flame soot under these two pressure conditions. In fact, the only notable difference between the two pressure levels is in the asymptotic detection efficiency, which is the same effect observed for flame soot in Fig. 47 when going down to 200 hPa. The soot data show that 100% detection efficiency is only achieved at a particle size of around 20 nm at 200 hPa, compared to about 12 nm at 500 hPa. Once again, this effect has to be attributed to the impact of the reduced pressure on a lower concentration aerosol rather than any real effect of relative humidity.

6.4.2 Effect of humidity on the counting efficiency of the CPC 3772-CEN

The impact of low to moderate levels of relative humidity on the performance of the CPC 3772-CEN was simultaneously investigated. This model CPC was tested in parallel to the Sky-CPC reported in the section above, using the same experimental conditions with identical levels of reduced pressure and humidity levels for both particle materials. The main difference is in their performance at 200 hPa, which as reported before did not deliver any useful data in case of the CPC 3772-CEN. Therefore, the more meaningful RH-dependent data for 700 hPa are shown instead. The graphs for these two levels of reduced pressure as a function of RH are presented

in Fig. 54. Unfortunately, in the experiment at 700 hPa, the humidity control malfunctioned at 25% RH, which was not detected until the data analysis. It is for this reason that data for only three discrete levels of relative humidity were recorded.

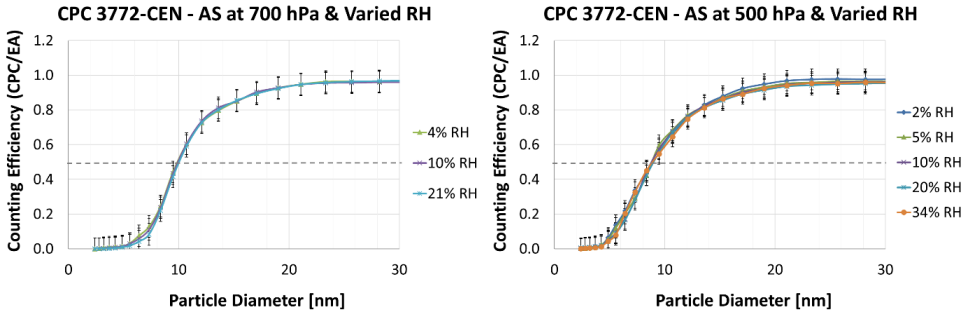

Fig. 54: Humidity dependent counting efficiency of the CPC 3772-CEN for ammonium sulfate particles at 700 hPa (left) and 500 hPa (right).

Very much like in the measurement data for the Sky-CPC reported in the previous chapter, no statistically significant effect of these moderate levels of relative humidity on the performance of the CPC 3772-CEN for ammonium sulfate particles could be observed. The counting efficiency curves are almost on top of each other and neither the slope nor the asymptotic efficiency show any notable variations.

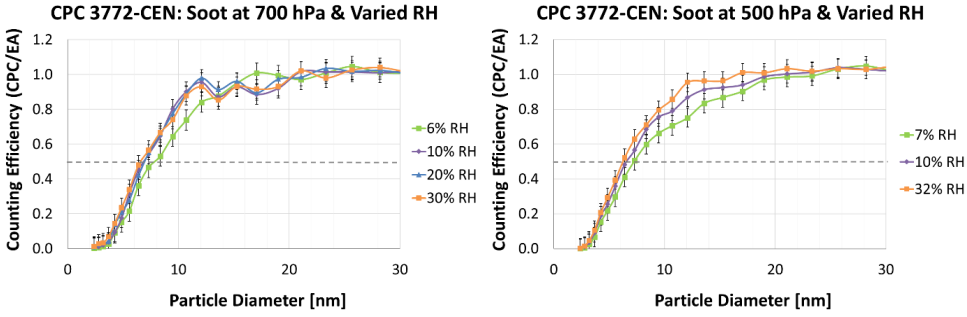

Fig. 55: Humidity dependent counting efficiency of the CPC 3772-CEN for flame soot at 700 hPa (left) and 500 hPa (right).

The model 3772-CEN was also included in the measurements with varied RH for the flame soot aerosol. Based on Fig. 55 one could speculate that there is a minor influence of low levels of RH on the counting efficiency of that CPC for soot particles at 500 hPa. The graphs reveal a difference of roughly 1 nm between the cut-off

diameter for the lowest RH level of 7% and the highest level of 32%. As the error bars indicate, this difference is still within the experimental uncertainty at least for the d_{50} value of this CPC, especially as the data reported are for a very low number concentration of the calibration aerosol.

More importantly, however, is that the asymptotic efficiency at 500 hPa of reduced pressure stays lower up to a particle size of about 17 nm. This effect could result in a small difference in the total number concentration if a soot aerosol is measured that is dominated by particles in the nucleation mode. When considering the graph for 700 hPa, this effect is less pronounced but still notable also at that pressure level. A method to estimate the impact of a corresponding slight change in the CPC's measurement performance is explained in the next chapter.

6.5 Impact on total PN concentration and basic estimates

In this chapter, a final analysis is presented that puts the experimentally determined counting efficiency curves and the measured total concentration in relation to the particle size distribution of the aerosol measured. This analysis is a practicable approach that allows estimating the impact of reduced pressure on the total particle number (PN) concentration reported by a CPC due to the effect that the pressure has on its counting efficiency. It was again Dr. Ryan Han who introduced me to this concept, albeit not in the context of this work. All calculations in this chapter were done by me and all of the data are my own, unless stated otherwise. Even though this analysis is only shown for one particular CPC, it can easily be applied to any model CPC. The reason that results for the CPC 3772-CEN are presented here is that it was used throughout this work and is the only model where access to all constructive details and operational parameters was possible. As importantly, this assessment also requires either knowledge of the actual particle size distribution or the use of one that is typical for the measurement conditions and that can be inferred to be representative of it. This approach is illustrated for two scenarios.

The first scenario is an analysis of the ammonium sulfate (AS) aerosol that was used to exemplify atmospheric aerosol throughout this thesis. With it being a laboratory-generated aerosol from experiments made during this work, a very large set of particle size distributions was available from the SMPS measurements. These size distribution data are from the preparatory work when an appropriate solution of AS per liter of distilled water was determined as well as from experiments made to characterize the counting efficiency curves in the previous chapters. The graphs in Fig. 56 show the aerosol's particle size distribution normalized to its modal value and two curves for the CPC's efficiency at different pressures. The count median diameter of the size distribution is at 47 nm. The curve for 1,013 hPa represents standard conditions and is a nominal curve. These data were recorded for an identical model CPC 3772-CEN at the World Calibration Center for Aerosol Physics (WCCAP) at TROPOS in Leipzig.

This counting efficiency curve is presented here as users of this particular model CPC can either obtain such an accredited calibration from the instrument manufacturer at the time of purchase or request it from TROPOS at a later time. Furthermore, efficiency data from the characterization at 700 hPa are shown as it represents a regular use of this specific model CPC in ambient monitoring, where very similar levels of reduced pressure can be found at mountain top research stations. A typical example is the Sonnblick (SNB) monitoring station of the Global Atmosphere Watch (GAW) program on the northern side of the Alps at an altitude of 3,100 m asl, which corresponds to 692 hPa. As can be seen in the plot, both counting efficiency curves reach more than 99% of their respective maximum efficiency well before the mode of the particle size distribution. Even though there is a notable difference between the two curves for the two pressure levels, already a visual analysis reveals that this difference in ambient pressure has little to no impact on the total number of particles measured by the CPC for the aerosol in this specific scenario.

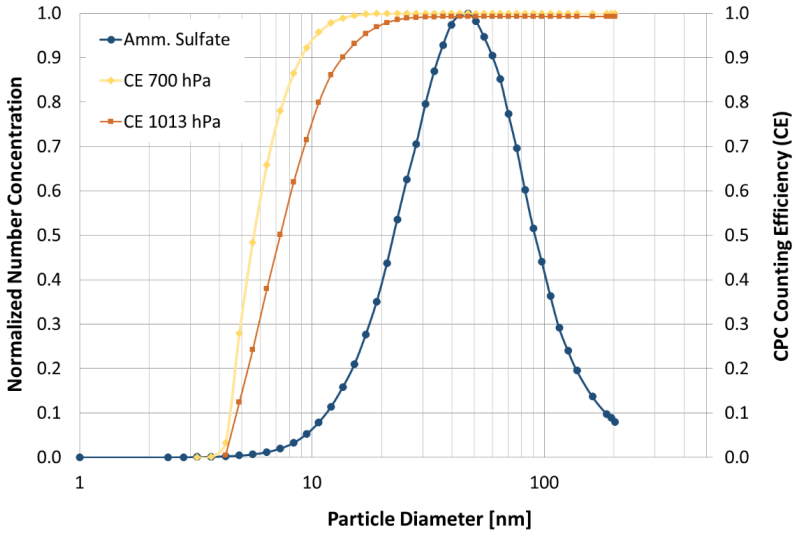

Fig. 56: Normalized size distribution for AS aerosol (blue) and counting efficiencies of the CPC 3772-CEN at 1,013 hPa (orange) and 700 hPa (yellow).

The second case presented in Fig. 57 is from the exhaust emission of a diesel vehicle operated at a test bench, with the distribution again normalized to its modal value. This measurement was made with an Engine Exhaust Particle Sizer (EEPS, Model 3090, TSI Inc.) on a test bench at steady state conditions. Diesel exhaust often has a bimodal size distribution by particle number, with the first mode generated by homogeneous condensation as the exhaust cools and a second mode that mainly consists of solid soot and fly ash particles. The normalized lognormal particle size distribution has its

first mode at 10.7 nm and a second mode at 43.3 nm. In this case the efficiency curve for 700 hPa can be seen to capture almost all of the particles in the first mode. By contrast, the counting efficiency curve at 1,013 hPa cuts through the left shoulder of the first mode at close to half height, so it misses some of that peak. This is different when it comes to the second mode as the CPC has a measurement efficiency of close to 100% at either pressure level for most of these presumably solid particles.

As the type approval of vehicles can also be performed at higher altitude as previously discussed in chapter 2.5.4, this is another very concrete application of CPCs at reduced pressure. It is important to emphasize that vehicle compliance tests during type approval require a highly accurate measurement of the total concentration by the CPC in order to demonstrate compliance with the particle number (PN) emission limit value of the emissions regulations.

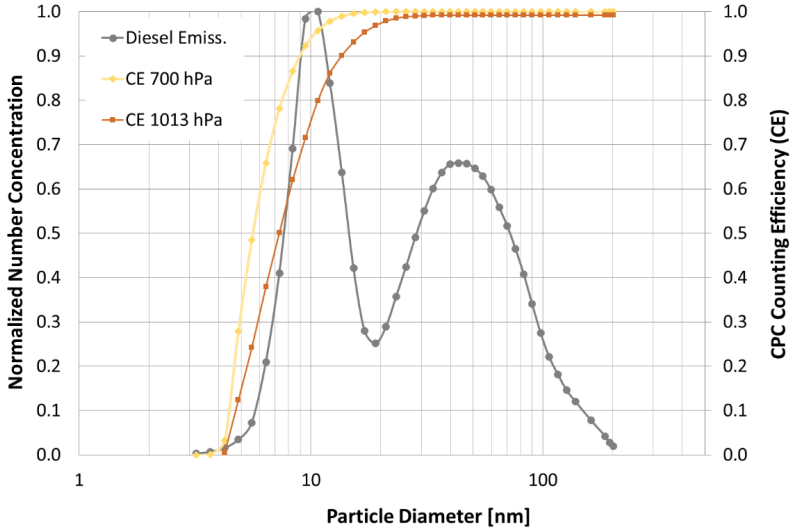

Fig. 57: Normalized size distribution for diesel exhaust (dark grey) and counting efficiencies of the CPC 3772-CEN at 1,013 hPa (orange) and 700 hPa (yellow).

In order to quantify the effect that a shift in the counting efficiency at reduced pressure has on the CPC performance, a simple arithmetical calculation is introduced. The idea behind it is to convolute each of the size distributions with the counting efficiency data for both pressure levels. The CPC's measurement efficiency can be calculated as a weighted average, where the concentration at each size is multiplied by its weight, and then added. In practice this can be done by a point by point multiplication of the normalized particle concentration of the particle size distribution for a given size by the corresponding value of the counting efficiency for the same particle diameter. In order to obtain a total measurement efficiency of the CPC, this has to be done from the

smallest particle size to the largest, and the total has to be divided by the normalized concentration without the counting efficiency applied. This calculation can be expressed by the following equation:

$$\eta_{CPC,Tot} = \frac{\sum_{i=0}^{n} (N_{norm,i} * \eta_{CPC,i})}{\sum_{i=0}^{n} (N_{norm,i})} \quad (6.1)$$

where, $\eta_{CPC,Tot}$ is the total measurement efficiency of the CPC for a given particle size distribution, $N_{norm,i}$ the number concentration normalized to its modal value at particle size *i*, and $\eta_{CPC,i}$ the counting efficiency at that same particle size.

The outcome of this calculation for the ammonium sulfate and diesel exhaust size distributions in the two scenarios is given in Tab. 14. In case of the AS aerosol, the change in the counting efficiency curve from 1,013 hPa to 700 hPa results in a minor increase in the measurement performance. Most of the particles in this distribution are larger than the CPC cut-off sizes at either pressure anyway, so the small chance is due to a slightly higher maximum counting efficiency around the mode of the distribution. The results of that calculation reveal that only 1.4% of the total number of particles are not measured by the CPC at the higher pressure, which is in line with the visual assessment.

Tab. 14: Effective counting efficiencies of the CPC 3772-CEN for the model scenarios.

	1,013 hPa	**700 hPa**	**Delta**
Ammonium Sulfate	98.4%	99.8%	1.4%
Diesel Exhaust	90.8%	97.0%	6.2%
Diesel Exhaust (23 nm cut-off)	99.2%	99.9%	0.7%

There is a more distinct impact caused by the shift in counting efficiency in case of the diesel exhaust aerosol. First of all, it becomes obvious that this model CPC would not be a good choice for this specific measurement as it does not capture close to 100% of all particles at standard conditions. Instead, an ultrafine CPC with a lower nominal cut-off diameter would be a more appropriate choice. In addition, there is an increase of the model 3772-CEN CPC's counting efficiency by a considerable amount of 6.2% when the ambient pressure is reduced to 700 hPa. This is caused by many of the

particles in this distribution being less than 20 nm in size, which is the range where the difference in counting efficiency is most pronounced. With PN emission limit values becoming ever more stringent, a change on that order could make the difference between a vehicle passing or failing an emission type approval test. However, current EU emissions legislations still define a lower cut-off diameter of 23 nm for this test. With this in mind, the results for the diesel emission were also calculated for particles of 23 nm and larger only. As can be seen from the results in Tab. 14, the impact on a CPC with that larger cut-off would be only 0.7% and thus negligible. Therefore, as long as a 23 nm detection limit is required, most of the particles would be counted by a CPC with either counting efficiency curve. Yet, there are several efforts underway to regulate the particle emissions from vehicles down to a lower size limit of 10 nm, notably the three EU-funded research projects on the sub-23 nm methodology (DownToTen, Surreal-23 and PEMs4Nano) that all finished in 2020. In addition, the measurement with a 10 nm detection limit was already included as an option in a Global Technical Regulation of the UN-ECE recently. From this basic analysis it can be seen that ambient pressure has to be considered as an operational condition during the ongoing discussion about a reduction of the current detection limit from 23 nm to 10 nm, even though only solid particles are to be measured per the regulation.

Lastly, it has to be pointed out that the impact of reduced pressure on the performance of a CPC would certainly be different in atmospheric nucleation campaigns as well as atmospheric simulation chamber studies. In such research, mainly monodisperse atmospheric clusters and freshly nucleated particles in the sub-3 nm range are of interest to investigate how new particles are formed. With the peaks of the size distribution near the detection limit of a CPC instrument, any change in the counting efficiency curve would result in a much more significant difference in the CPC count. However, such measurements are not done using CPC models of a full-flow design as investigated in this work. Instead, they require specialized CPCs that are optimized for a sensitivity down to 1 nm. Their lower detection limit has been pushed down to that size with the introduction of two-stage CPC designs. In 1nm-CPCs, the very small particles get activated by using diethylene glycol (DEG) as the working fluid in a first “booster” stage (Iida et al., 2009; Dahlkötter et al., 2016; Kangasluoma et al., 2017). For the past few years, 1nm-CPC instruments have been routinely used in atmospheric and climate research, for example the CPC systems that include a Particle Size Magnifier (PSM, Model A10, Airmodus Ltd.), a Nano Enhancer (Model 3757, TSI Inc.) or similar home-built diethylene glycol (DEG) CPCs (Wimmer et al., 2013). The characterization of their performance at reduced pressure would amount to even more time and effort than spent on the full-flow CPCs investigated in this thesis, with the identification of an appropriate, representative calibration aerosol in the single nanometer range being one of the major challenges to be overcome.

7. Conclusions and Outlook

The objective of this thesis was a comprehensive study to better understand how Condensation Particle Counters (CPC) perform when operated at reduced pressure. Previous studies, although conclusive within themselves, did not demonstrate an agreement on the low-pressure performance of CPCs when compared with each other. Some found that the counting efficiency curves of a CPC investigated shifted to a lower detection limit, while others found larger d_{50} cut-off diameters with decreasing pressure. In this thesis, the research was taken further by combining an in-depth literature analysis, numerical modeling and extensive experiments. The laboratory measurements provided a simultaneous characterization of the performance of two commercially available CPC models, the CPC 3772-CEN and the Sky-CPC 5.411, which were operated with only very minor modifications. Both CPCs were always characterized in parallel at several levels of low pressure that are found during practical applications in real life. Their counting efficiency curves were determined with a high particle size resolution down to a few nanometers, along with their characteristic lower detection limits and asymptotic efficiency characteristics.

The key finding from this work is that while reduced pressure can have a pronounced effect on the counting efficiency of a standard CPC, the exact consequences very much depend on the concrete measurement conditions and the specific CPC design. CPC models in use today differ considerably in their instrumental parameters. This includes the geometry, operating parameters and handling of the working fluid, which all play a role in their performance at reduced pressure. It could be demonstrated that both of the butanol CPCs used in this work are linear instruments with R^2 values larger than 0.9 during valid measurements. It was shown that the slope of the efficiency curve as well as the d_{50} detection limit of a CPC can change depending on the ambient pressure, with the impact being the greatest at very low levels. This is caused by a change of the supersaturation profile inside the condenser section, with lower pressures resulting in different peak saturation values than at standard conditions. That said, only minor differences were observed between the two butanol CPC models in the experiments until a threshold level of reduced pressure was reached. It was established, within experimental uncertainties, that the counting efficiency of these CPCs is largely independent of the ambient pressure between standard conditions and 500 hPa. Both of these specific full-flow CPC models can be used down to 400 hPa with acceptable corrections. Below that pressure, the performance of the CPC 3772-CEN that was not developed for low-pressure operation collapsed. This sudden decrease in the CPC's total measurement efficiency when operated below standard atmospheric pressure largely agrees with findings first reported more than 80 years ago (Schlarb, 1940). The Sky-CPC 5.411, which was custom-designed for operation at reduced pressure, continued to measure accurately at 300 hPa. It even reported acceptable concentration data at a pressure of 200 hPa when the fluctuations seen with high time resolution are averaged out. The conclusion from these calibration

experiments is that there is a distinct minimum pressure level until which a certain CPC model will work reliably. That minimum pressure level depends on its inner geometry, residence time of the aerosol going through the condenser, internal temperatures and other characteristics, and is therefore different for different designs of CPCs. The more than 50% larger temperature difference and the resulting much higher saturation ratio of the Sky-CPC compared to the CPC 3772-CEN are key reasons for the more efficient activation of particles. In fact, the saturation ratio of the CPC 5.41X reaches a peak value that is about a factor of 3 higher than the one of the 3772-CEN. In consequence, the spatial profile of the saturation ratio inside the condenser tube is also very different which results in its better activation probability. This work also suggests that certain CPC models are less suitable or even unsuitable for use at low pressure. The choice of water-based CPC, the model 3783, which was made based on its use in atmospheric monitoring and proven long-term stability in near-road networks, was not adequate for low-pressure experiments. It failed already at ambient pressures between 920 hPa to 930 hPa and cannot be used as an instrument for operation at reduced pressure without modifications. This does not mean that water-based CPCs are unsuitable for use in low-pressure applications in general, though, as the newer, third generation model vWCPC 3789 seems to have overcome these issues (Mei et al., 2020).

A further goal of this research was to investigate if small levels of relative humidity and low pressure combined can have an effect on the CPC performance. Measurements were conducted at several levels of low relative humidity, well below the dew point. Experiments were made between 1 and 40% RH, although the full extent of that range could never be realized at one and the same pressure. Yet in each experiment stable values of relative humidity that were a factor of 5 or 6 different were achieved. Some of the greatest difficulties in this experimental work were due to the ambitious endeavor of doing experiments at reduced pressure and at defined levels of relative humidity at the same time. Combining different aerosol generation methods, low pressure and relative humidity while performing the measurements with three to five particle detectors simultaneously lead to a substantial experimental complexity. It could be demonstrated that there is no apparent influence of such low to moderate levels of relative humidity on the performance of CPCs under reduced pressure conditions. There was no significant shift in the d_{50} detection limit of the CPCs to either larger or smaller diameters due to these levels of relative humidity alone. The maximum differences in the d_{50} visible were less than 1.5 nm, which is within measurement uncertainty at the statistically poor concentrations during some of the experiments and the slight variation of conditions from experiment to experiment, although conditions were always stable within each experiment. It could also be seen that there is no clear effect onto the slope of the counting efficiency in any of the data sets that can be attributed to humidity alone. Results may be quite different when the relative humidity reaches near-condensing conditions – but that was not the scope of this work as it is not likely to occur during the practical applications of interest here.

Furthermore, it was investigated if the choice of aerosol material plays a role during operation at reduced pressure. Accordingly, all the counting efficiency experiments were done with two different aerosol materials representing atmospheric background and urban environments. A recently-developed flame soot generator was introduced as source of particles representative of an urban aerosol to the calibration of CPCs. Since this novel soot generator had not been used for such calibrations before, a comprehensive characterization to determine an operational setting that would allow for its use in the small nanometer size range was done. Even with this optimum setting, however, the particle concentrations of the flame soot aerosol were very low. Statistics were especially poor below 10 nm as the monodisperse sizes needed to determine the counting efficiency curve were obtained by size classifying the soot aerosol with a DMA. This meant that under certain conditions the measurements had to be repeated several times and also that some data sets had to be discarded post experiment. A further aspect was that the natural flickering of the flame lead to a larger fluctuation of the fresh soot aerosol compared to the AS aerosol generated by the much more constant atomizer aerosol generator. This could be seen in a jagged counting efficiency curve also at larger particle sizes up to the CPC's asymptotic efficiency. When comparing the counting efficiency for the flame soot at different pressures for one CPC, the curves agreed well with one another in the steep slope section. While results for the CPC 3772-CEN were again largely similar down to what was found to be its practical limit at 500 hPa, the cut-off size of the Sky-CPC showed a minor difference when reducing the pressure further down to 200 hPa. When comparing the flame soot to ammonium sulfate as calibration aerosol, a slight material dependence was observed as both CPCs responded to a change in particle material with a minor change in their performance. Their d_{50} cut-off size was about 2 nm to 3 nm lower for soot than for ammonium sulfate and also the slope of the curves was slightly steeper for soot than for the AS aerosol. This is very likely due to the fact that the flame soot aerosol consists predominantly of chain agglomerates. The corresponding complex structure and irregular geometry have been shown to enhance the condensation of liquids. It is therefore most probable that the soot's surface properties such as the negative curvature and the contact angle lead to a lower cut-off diameter when it is used as a calibration aerosol also at reduced pressure.

Finally, it is important to consider the impact of low pressure on the total concentration measurement of a CPC. It could be demonstrated that for many low-pressure measurements, apart from those instances when the activation inside the CPC collapses partially or completely, a small shift in the detection limit or in the slope of the counting efficiency curve will only result in minor differences in the total concentration. The exception to that are aerosols that have a distinct nucleation mode at or close to the lower cut-off diameter of the CPC, like in the presence of volatile organic compounds under certain atmospheric conditions or when hot vehicle emissions are cooled down quickly. The latter will be of significance for regulatory measurements when a CPC with a future 10-nm instead of the currently required 23-

nm lower detection limit is used for the PN emissions test. In the last chapter it was shown that a simple arithmetical calculation can be made to quantify the corresponding effect of reduced pressure on the CPC performance. It is recommended to make this simple correction to the total particle number, assuming the aerosol size distribution is known or that one representative for the respective measurement condition can be used. For vehicle homologation, correction factors should be developed for the different engine and vehicle types to be tested. For transient drive cycle measurements at a test rig for vehicle type approval or permanent use at a measurement site of high elevation, it makes sense to simply adjust the condenser and saturator temperatures. With this readjustment the cut-off size of the CPC is shifted back to its nominal value for the respective pressure. It is much more difficult to make an appropriate correction to the total concentration when the ambient pressure experiences a high, rapid variation over time. In-flight measurements with a CPC onboard an aircraft are therefore the most reliable during cruise conditions, while data from the climb or descent have to be examined with caution.

In summary, it could be shown that CPCs are reliable, accurate instruments for the measurement of submicrometer aerosols at moderate to medium levels of reduced pressure. If they should be operated at very low levels of reduced pressure, custom designs optimized for such condition are advisable. For the highest accuracy and legislative purposes, CPCs should be calibrated for their specific application, especially if it requires their operation at pressures below 500 hPa. The surrogate calibration of a certain CPC model at discrete pressure levels can provide some general guidance if an application-specific calibration is not feasible. Such a proxy calibration will be the more meaningful the further the mode of the aerosol size distribution to be measured is away from the CPC's lower-detection limit. For measurements at high altitude under stationary conditions, appropriate calibrations can be determined to adjust the CPC's saturator and condenser temperatures and thereby moving the d_{50} cutoff diameter back to its specified value.

Without doubt, this study is by no means the last chapter in either the calibration or the use of CPCs at reduced pressure. The work documented in this thesis also points to some questions that have not been finally answered. A very important one is the striking difference in the saturation ratio and the unique spatial profile between the two CPCs characterized here, and the effect it has on their performance at low-pressure. Given more time, this could be investigated in greater detail by conducting experiments at different saturation ratios. Ideally it should also be considered if it is possible to simulate the CPC response or to include it in the current adaption of Stolzenburg's numerical model. Adding to the current experiments in this thesis it would also be of interest to perform measurements with the Sky-CPC below 200 hPa to see if its performance also changes greatly at a certain point. This would require a revised experimental setup with more technical complexities to implement. The benefit would be to see if the fluctuations that were observed at 200 hPa get more pronounced

the lower the pressure and also if there is a threshold pressure at which the performance of the Sky-CPC also breaks down.

Last but not least there is a very pragmatic opportunity to carry-out a similarly detailed low-pressure calibration of the third generation of water-based CPCs, such as the MAGIC CPC or the model 3789 vWCPC. The use of water as the CPC's working fluid could put an end to any concerns of flammability that exist when butanol-based CPCs are used onboard aircraft. Especially their certification for use onboard commercial airliners as during IAGOS is becoming increasingly difficult and time-consuming, which would be extremely beneficial to overcome by the use of water-based CPCs.

References

Agarwal, J. K., & Sem, G. J. (1980). Continuous flow, single-particle-counting condensation nucleus counter. *J. Aerosol Sci.*, 11:343-357. https://doi.org/10.1016/0021-8502(80)90042-7.

Agarwal, J. K., Sem, G. J., & Pourprix, M. (1981). A continuous flow CNC capable of counting single particles. *Proceedings of the 9th International Conference on Atmospheric Aerosols, Condensation & Ice Nuclei*, September 1977, 118-122, Galway University Press, Galway, Ireland.

Aitken, J. (1880). On dusts, fogs and clouds. *Nature*, 23 (583): 195-197.

Aitken, J. (1890-1891). On a simple pocket dust-counter. *Proceedings of the Royal Society of Edinburgh*, XVIII, 39-53.

Andersson, J., Giechaskiel, B., Munoz-Bueno, R., Sandbach, E., & Dilara, P. (2007). Particle Measurement Programme (PMP) Light-duty Inter-laboratory Correlation Exercise (ILCE_LD). Final Report, EUR 22775 EN, GRPE-54-08-Rev.1

Banse, D. F., Esfeld, K., Hermann, M., Sierau, B., & Wiedensohler, A. (2001). Particle Counting Efficiency of the TSI CPC 3762 for Different Operation Parameters. *J. Aerosol Sci*., 32:157-161. https://doi.org/10.1016/s0021-8502(00)00060-4.

Berner, A., Lürzer, C. H., Pohl, L., Preining, O. & Wagner, P. (1979). The Size Distribution of the Urban Aerosol in Vienna. *Sci. Total Environ*., 13: 245-261. https://doi.org/10.1016/0048-9697(79)90105-0.

Birmili, W., Sun, J., Weinhold, K., Merkel, M., Rasch, F., Spindler, G., Wiedensohler, A., Bastian, S., Loeschau, G., Schladitz, A., & Quass, U. (2015). Atmospheric aerosol measurements in the German Ultrafine Aerosol Network (GUAN) Part 3: black Carbon mass and particle number concentrations 2009 to 2014. *Gefahrst. Reinhalt. Luft*, 75 (11-12), 479-488.

Bischof, O. F. (2015). Recent Developments in the Measurement of Low Particulate Emissions from Mobile Sources: A Review of Particle Number Legislations. *Emiss. Control Sci. Technol.*, 1: 203-212, 2015. https://doi.org/10.1007/s40825-015-0016-9.

Bischof, O. F., Weber, P., Bundke, U., Petzold, A., & Kiendler-Scharr, A. (2019). Characterization of the Miniaturized Inverted Flame Burner as a Combustion Source to Generate a Nanoparticle Calibration Aerosol. *Emiss. Control Sci. Technol.*, 6: 37-46. https://doi.org/10.1007/s40825-019-00147-w.

Bradbury, N. E., & Meuron, H. J. (1938). The Diurnal Variation of Atmospheric Condensation Nuclei. *Terr. Magn*., 43, 231-240.

Bricard, J. P. G. M., Delattre, P., Madelaine, G., & Pourprix, M. (1976). Detection of ultra-fine particles by means of a continuous flux condensation nuclei counter. In: "*Fine particles*" (Edited by B.Y.H. Liu), Academic Press, New York, 565-580.

Bronkhorst High-Tech B.V. (2018). Operational instructions for digital multibus Mass Flow / Pressure instruments. Instruction manual, doc. no.: 9.17.023AL.

Bundke, U., Berg, M., Houben, N., Ibrahim, A. Fiebig, M., Tettich, F., Klaus, C., Franke, H., & Petzold, A. (2015). The IAGOS-CORE aerosol package: instrument design, operation and performance for continuous measurement aboard in-service aircraft. *Tellus B: Chemical and Physical Meteorology*, 67:1. https://doi.org/10.3402/tellusb.v67.28339.

CEN/TS 16976:2016. Ambient air - Determination of the particle number concentration of atmospheric aerosol; European Committee for Standardization, June 2016.

Chen, T. M., & Chein, H. M. (2006). Generation and Evaluation of Monodisperse Sodium Chloride and Oleic Acid Nanoparticles. *Aerosol Air Qual. Res.*, Vol. 6, No. 3, pp. 305-321, 2006. https://doi.org/10.4209/aaqr.2006.09.0007.

Cofer III, W. R., Anderson, B. E., Winstead, E. L., & Bagwells, D. R. (1998). Calibration and demonstration of a condensation nuclei counting system for airborne measurements of aircraft exhausted particles. *Atmos. Environ.*, 32, 2, 169-177. https://doi.org/10.1016/S1352-2310(97)00318-X.

Coulier, P. J. (1875). Note sur une nouvelle propriété de l'air. *Journal de Pharmacie et de Chimie*, Series 4, 22, 165-173, Paris, France.

Crayford, A., Johnson, M., Marsh, R., Sevcenco, Y., Walters, D., Williams, P., Christie, S., Chung, W., Petzold, A., Ibrahim, A., Delhaye, D., Qincey, P., Bowen, P., Coe, H., Raper, D., & Wilson, C. (2011). SAMPLE III: Contribution to Aircraft Engine PM Certification Requirement and Standard First Specific Contract - *Final Report* EASA.2010.FC.10, European Aviation Safety Agency.

Dahlkötter, F., Krinke, T. J., Tritscher, T., Bischof, O. F., Kykal, C., Werner, A., Weber, A., & Spielvogel, J. (2016). Extending particle size distribution measurements down to 1 nm. *Proceedings of the NOSA Aerosol Symposium 2016*, Aarhus, Denmark, April 4-6. https://doi.org/10.13140/RG.2.1.1845.0324.

EMPA (2010). Technischer Bericht zum Nationalen Beobachtungsnetz für Luftfremdstoffe (NABEL) 2010. Dübendorf, Switzerland. https://doi.org/10.3929/ethz-a-006173107.

Fierz, M., Houle, C., Steigmeier, P., & Burtscher, H. (2011). Design, Calibration, and Field Performance of a Miniature Diffusion Size Classifier. *Aerosol Sci. Technol.*, 45:1, 1-10. https://doi.org/10.1080/02786826.2010.516283.

Fierz, M., Meier, D., Steigmeier, P., & Burtscher, H. (2014). Aerosol Measurement by Induced Currents. *Aerosol Sci. Technol.*, 48:4, 350-357. https://doi.org/10.1080/02786826.2013.875981.

Fierz, M., Scherrer, L., Burtscher, H. (2002). Real-time measurement of aerosol size distributions with an electrical diffusion battery. *J. Aerosol Sci.*, 33: 1049-1060. https://doi.org/10.1016/S0021-8502(02)00057-5.

Fischer, B., Unpublished notes. Personal communication, FZ Jülich, March 2019.

Flagan, R. C. (1999). On Differential Mobility Analyzer Resolution, *Aerosol Sci. Technol.*, 30:6, 556-570. https://doi.org/10.1080/027868299304417.

GAeF (2020). Position paper of the Gesellschaft für Aerosolforschung on understanding the role of aerosol particles in SARS-CoV-2 infection. *Zenodo*, December 18, 2020. https://doi.org/10.5281/zenodo.4350494.

GAW Station Information System (GAWSiS), Repository URL https://gawsis.meteoswiss.ch/GAWSIS/#/ (accessed January 2, 2020).

Giechaskiel, B., & Bergmann, A. (2011a). Validation of 14 used, re-calibrated and new TSI 3790 condensation particle counters according to the UN-ECE Regulation 83. *J. Aerosol Sci.,* 42, 195-203. https://doi.org/10.1016/j.jaerosci.2011.01.002.

Giechaskiel, B., Wang, X., Gilliland, D., & Drossinos, Y. (2011b). The effect of particle chemical composition on the activation probability in n-butanol condensation particle counters. *J. Aerosol Sci.,* 42, 20-37. https://doi.org/10.1016/j.jaerosci.2010.10.006.

Giechaskiel, B., Wang, X., Horn, H. G., Spielvogel, J., Gerhart, C., Southgate, J., Jing, L., Kasper, M., Drossinos, Y., & Krasenbrink, A. (2009). Calibration of Condensation Particle Counters for Legislated Vehicle Number Emission Measurements. *Aerosol Sci. Technol.*, 43:12, 1164-1173. https://doi.org/10.1080/02786820903242029.

Gormley, P. G., & Kennedy, M. (1949). Diffusion from a Stream Flowing through a Cylindrical Tube. *Proc. Roy. Irish Acad.,* Vol. 52, Sect. A, 163-169.

He, M., Dhaniyala, S., & Wagner, M. (2015). Aerosol Filtration with Mobility-Classified Particles: Role of Multiply Charged Particles in Skewing Penetration Measurements, *Aerosol Sci. Technol.*, 49:9, 705-716. https://doi.org/10.1080/02786826.2015.1062467.

Heintzenberg, J., & Ogren, J. A. (1985). On the operation of the TSI-3020 condensation nuclei counter at altitudes up to 10 km. *Atmos. Environ.*, 19, 8, 1385-1387.

Hering, S. V., & Stolzenburg, M. R. (2004). Continuous, Laminar Flow Waterbased Particle Condensation Device and Method. *US Patent 6,712,881*, issued March 30, 2004.

Hering, S. V., & Stolzenburg, M. R. (2005). A Method for Particle Size Amplification by Water Condensation in a Laminar, Thermally Diffusive Flow. *Aerosol Sci. Technol.*, 39, 428-436. https://doi.org/10.1080/027868290953416.

Hering, S. V., Lewis, G. S., Spielman, S. R., Eiguren-Fernandez, A., Kreisberg, N. M., Kuang, C., & Attoui, M. (2017). Detection near 1-nm with a laminar-flow, water-based condensation particle counter. *Aerosol Sci. Technol.*, 51:3, 354-362. https://doi.org/10.1080/02786826.2016.1262531.

Hering, S. V., Spielman, S. R., & Lewis, G. S. (2014). Moderated, Water-Based, Condensational Particle Growth in a Laminar Flow. *Aerosol Sci. Technol.*, 48:4, 401-408. https://doi.org/10.1080/02786826.2014.881460.

Hermann, M. (2000). Development and application of an aerosol measurement system for use on commercial aircraft. *PhD thesis*, University of Leipzig.

Hermann, M., & Wiedensohler, A. (2001). Counting efficiency of condensation particle counters at low-pressures with illustrative data from the upper troposphere. *J. Aerosol Sci.*, 32: 975-991. https://doi.org/10.1016/S0021-8502(01)00037-4.

Hermann, M., Adler, S., Caldow, R., Stratmann, F., & Wiedensohler, A. (2005). Pressure-Dependent Efficiency of a Condensation Particle Counter Operated with FC-43 as Working Fluid. *J. Aerosol Sci.,* 36: 1322-1337. https://doi.org/10.1016/j.jaerosci.2005.03.002.

Hermann, M., Wehner, B., Bischof, O. F., Han, H.-S., Krinke, T. J., Liu, W., Zerrath, A. F., & Wiedensohler, A. (2007). Particle counting efficiencies of new TSI condensation particle counters. *J. Aerosol Sci.,* 38: 674-682. https://doi.org/10.1016/j.jaerosci.2007.05.001.

Hillamo, R. E., & Kauppinen, E. I. (1991). On the Performance of the Berner Low Pressure Impactor. *Aerosol Sci. Technol.*, 14:1, 33-47. https://doi.org/10.1080/02786829108959469.

Hinds, W.C. (1999). *Aerosol Technology: Properties, Behavior, and Measurement of Airborne Particles* (2nd Edition). Wiley, 1999.

Iida, K., Stolzenburg, M. R., & McMurry, P. H. (2009). Effect of working fluid on Sub-2 nm particle detection with a laminar flow ultrafine condensation particle counter. *Aerosol Sci. Technol*. 43:1, 81-96. https://doi.org/10.1080/02786820802488194.

ISO 27891 (2015). Aerosol particle number concentration - Calibration of condensation particle counters, International Organization for Standardization, February 2015.

Joint Committee for Guides in Metrology (JCGM), International vocabulary of metrology - Basic and general concepts and associated terms (VIM), 3rd edition, 2008 version with minor corrections, 200, 2012.

Kangasluoma, J., Hering, S., Picard, D., Lewis, G., Enroth, J., Korhonen, F., Kulmala, M., Sellegri, K., Attoui, M., & Petäjä, T. (2017). Characterization of three new condensation particle counters for sub-3 nm particle detection during the Helsinki CPC workshop: The ADI versatile water CPC, TSI 3777 nano enhancer and boosted TSI 3010. *Atmos. Meas. Tech.,* 10 (6), 2271-2281. https://doi.org/10.5194/amt-10-2271-2017.

Kangasluoma, J., Kuang, C., Wimmer, D., Rissanen, M. P., Lehtipalo, K., Ehn, M., Worsnop, D. R., Wang, J., Kulmala, M., & Petäjä, T. (2014). Sub-3 nm Particle Size and Composition-Dependent Response of a Nano-CPC Battery. *Atmos. Meas. Tech.*, 7:689-700. https://doi.org/10.5194/amt-7-689-2014.

Kazemimanesh, M., Dastanpour, R., Baldelli, A., Moallemi, A., Thomson, K. A., Jefferson, M. A., Johnson, M. R., Rogak, S. N., & Olfert, J. S. (2019). Size, effective density, morphology, and nanostructure of soot particles generated from buoyant turbulent diffusion flames. *J. Aerosol Sci.*, 132: 22-31. https://doi.org/10.1016/j.jaerosci.2019.03.005.

Keady, P. B., Quant, F. R., & Sem, G. J. (1988). Two New Condensation Particle Counters: Design and Performance. Poster presentation at the 7th Annual Meeting of AAAR, Chapel Hill, NC, USA.

Knutson, E. O., & Sinclair, D. (1979). Experience in Sampling Urban Aerosol with the Sinclair Diffusion Battery and Nucleus Counter. In Proc.: "*Advances in Particle Sampling and Measurement*" (Edited by W. B. Smith), EPA-600/7-79-065, 98-120, U.S. Environmental Protection Agency, Asheville, NC.

Kousaka, Y., Niida, T., Okuyama, K., & Tanaka, H. (1982). Development of a Mixing-Type Condensation Nucleus Counter. *J. Aerosol Sci.*, 13: 231-240. https://doi.org/10.1016/0021-8502(82)90064-7.

Kulkarni, P., Baron, P. A., & Willeke, K. (2011). Aerosol Measurement: Principles, Techniques, and Applications (Third Edition). John Wiley & Sons, Inc. https://doi.org/10.1002/9781118001684.

Kulmala, M., Mordas, G., Petäjä, T., Grönholm, T., Aalto, P. P. Vehkamäki, H., Hienola, A. I., Herrmann, E., Sipilä, M., Riipinen, I., Manninen, H. E., Hämeri, K., Stratmann, F., Bilde, M., Winkler, P. M., Birmili, W., & Wagner, P. E. (2007). The Condensation Particle Counter Battery (CPCB): A New Tool to Investigate the Activation Properties of Nanoparticles. *J. Aerosol Sci.*, 38: 289-304. https://doi.org/10.1016/j.jaerosci.2006.11.008.

Kupc, A., Bischof, O. F., Beeston, M., Tritscher, T., Krinke, T. J., & Wagner, P. E. (2013). Laboratory Characterization of a New Nano Water-Based CPC 3788 and

Performance Comparison to an Ultrafine Butanol-Based CPC 3776. *Aerosol Sci. Technol.* 47:2, 183-191. https://doi.org/10.1080/02786826.2012.738317.

Liu, B. Y. H., & Pui, D. Y. H. (1974). A submicron aerosol standard and the primary, absolute calibration of the condensation nuclei counter. *J. Colloid Interface Sci.*, Vol. 47, No. 1, 155-171, April 1974.

Liu, W., Osmondson, B. L., Bischof, O. F., & Sem, G. J. (2005). Calibration of Condensation Particle Counters. *SAE Transactions,* Paper 2005-01-0189. https://doi.org/10.4271/2005-01-0189.

Mamakos, A. (2016). Methodology to quantify the ratio of multiple-to single-charged fractions acquired in aerosol neutralizers. *Aerosol Sci. Technol.* 50:4, 183-191. https://doi.org/10.1080/02786826.2016.1153034.

Maricq, M. M., Podsiadlik, D. H., & Chase, R. E. (2000). Size Distributions of Motor Vehicle Exhaust PM: A comparison Between ELPI and SMPS Measurements. *Aerosol Sci. Technol*., 33: 239-260. https://doi.org/10.1080/027868200416231.

Marple, V. A., Rubow, K. L., & Behm, S. M. (1991). A Microorifice Uniform Deposit Impactor (MOUDI): Description, Calibration, and Use. *Aerosol Sci. Technol*., 14: 434-446. https://doi.org/10.1080/02786829108959504.

Marple, V.A. (2004). History of Impactors - The First 110 Years. *Aerosol Sci. Technol*., 38:3, 247-292. https://doi.org/10.1080/02786820490424347.

Marshall, I., & Sandbach, E. (2007). Particle Number Counter Calibration/Validation Procedures. *Report to the Department for Transport*, AEA Energy & Environment, ED47382004/PNC Issue Number 5, December 2007.

McMurry, P. H. (2000). A review of atmospheric aerosol measurements. *Atmos. Environ*., 34, 1959-1999. https://doi.org/10.1016/S1352-2310(99)00455-0.

McMurry, P. H. (2003). Aerosols | Observations and Measurements. Chapter in: "*Encyclopedia of Atmospheric Sciences*" (Edited by James R. Holton), 20-34, Academic Press. https://doi.org/10.1016/B0-12-227090-8/00048-8.

Mei, F., Havlicek, M., Pekour, M., Tiwari, A., Tomlinson, J., Schmid, B., Bischof, O. F., & Roth, P. (2020). Operation of a condensation particle counter under low-pressure conditions. Platform presentation at AAAR 38th Annual Conference, October 6, 2020, http://aaarabstracts.com/2020/.

Mertes, S., Schröder, F., & Wiedensohler, A. (1995). The Particle Detection Efficiency Curve of the TSI-3010 CPC as a Function of the Temperature Difference between Saturator and Condenser. *Aerosol Sci. Technol.*, 23:2, 257-261. https://doi.org/10.1080/02786829508965310.

Mohr, M., & Lehmann, U. (2003). Comparison study of particle measurement systems for future type approval application. Research report No-202779, Swiss contribution to GRPE particle measurement programme (GRPE-PMP CH5).

Mulcey, P. (1976). Contribution à l'étude de l'aérosol stratosphérique. *Thèse de doctorat*, Université Pierre et Marie Curie Paris 6, le 3 juin 1976.

Nolan, P., & Pollak, L. (1945). The Calibration of a Photo-Electric Nucleus Counter. *Proc.Royal Irish Acad., Section A: Mathematical and Physical Sciences*, 51, 9-31. http://www.jstor.org/stable/20488468.

Noone, K. J., & Hansson, H.-C. (1990). Calibration of the TSI 3760 condensation nucleus counter for nonstandard operating conditions. *Aerosol Sci. Technol.*, 13:4, 478-485, https://doi.org/10.1080/02786829008959462.

Pelzer, J., Bischof, O. F., van den Brink, W., Fierz, M., Isherwood, H., Gnewuch, H., Knecht, A., Krinke, T., & Zerrath, A. (2010). Geräte zur Messung der Anzahlkonzentration von Nanopartikeln. *Gefahrstoffe – Reinhalt. Luft*, 70, 11/12, 469-477.

Penner, J. E., Zhou, C., Garnier, A., & Mitchell, D. L. (2018). Anthropogenic Aerosol Indirect Effects in Cirrus Clouds. *J. Geophys. Res. Atmos*. 2018 Oct 27; 123(20): 11652-11677. https://doi.org/10.1029/2018JD029204.

Petzold, A., Marsh, R., Johnson, M., Miller, M., Sevcenco, Y., Delhaye, D., Ibrahim, A., Williams, P., Bauer, H., Crayford, A., Bachalo, W. D., & Raper, D. (2011). Evaluation of Methods for Measuring Particulate Matter Emissions from Gas Turbines. *Environ. Sci. Technol.*, 45, 3562-3568. https://doi.org/10.1021/es103969v.

Petzold, A., Stein, C., Nyeki, S., Gysel, M., Weingartner, E., Baltensperger, U., Giebl, H., Hitzenberger, R., Döpelheuer, A., Vrchoticky, S., Puxbaum, H., Johnson, M., Hurley, C. D., Marsh, R., & Wilson, C. W. (2003). Properties of jet engine combustion particles during the PartEmis experiment: Microphysics and Chemistry. *Geophys. Res. Lett*., 30, 1719. https://doi.org/10.1029/2003GL017283.

Petzold, A., Thouret, V., Gerbig, C., Zahn, A., Brenninkmeijer, C. A. M., Gallagher, M., Hermann, M., Pontaud, M., Ziereis, H., Boulanger, D., Marshall, J., Nédélec, P., Smit, H. G. J., Friess, U., Flaud, J.-M., Wahner, A., Cammas, J.-P., Volz-Thomas, A., & IAGOS TEAM (2015). Global-scale atmosphere monitoring by in-service aircraft - current achievements and future prospects of the European Research Infrastructure IAGOS. *Tellus B: Chemical and Physical Meteorology*, 67:1. https://doi.org/10.3402/tellusb.v67.28452.

Picard, D., Attoui, M., & Sellegri K. (2019). B3010: a boosted TSI 3010 condensation particle counter for airborne studies. *Atmos. Meas. Tech*., 12, 2531-2543. https://doi.org/10.5194/amt-12-2531-2019.

Pollak, L. W., & Metnieks, A. L. (1960). The influence of pressure and temperature on the counting of condensation nuclei. *Geofisica Pura e Applicata*, 47, 123-141. https://doi.org/10.1007/BF01992490.

Pui, D. Y. H., & Lui, B. Y. H. (1998). Advances in instrumentation for atmospheric aerosol measurement. *Phys. Scr.,* 37, 2, 252. https://doi.org/10.1088/0031-8949/37/2/012.

Scheibel, H. G., & Porstendörfer, J. (1983). Generation of monodisperse Ag- and NaCl-aerosols with particle diameters between 2 and 300 nm. *J. Aerosol Sci*., 14: 2, 113-126. https://doi.org/10.1016/0021-8502(83)90035-6.

Schlarb, G. (1940). Untersuchungen über Kondensationskerne und Leichtionen in künstlich klimatisierten Räumen. *Bioklimatische Beiblätter*, Braunschweig, 7, 86-105.

Schröder, F., & Ström, J. (1997). Aircraft measurements of sub micrometer aerosol particles (> 7 nm) in the midlatitude free troposphere and tropopause region. *Atmos. Res.* 44: 3-4, 333-356. https://doi.org/10.1016/S0169-8095(96)00034-8.

Seifert, M., Tiede, R., Schnaiter, M., Linke, C., Möhler, O., Schurath, U., & Ström, J. (2004). Operation and performance of a differential mobility particle sizer and a TSI 3010 condensation particle counter at stratospheric temperatures and pressures. *J. Aerosol Sci*., 35, 981-993. https://doi.org/10.1016/j.jaerosci.2004.03.002.

Sem, G. J. (2002). Design and performance characteristics of three continuous-flow condensation particle counters: a summary. *Atmos. Res*. 62: 3-4, 267-294. https://doi.org/10.1016/S0169-8095(02)00014-5.

Sem, G. J., Bischof, O. F., & Kittelson, D. B. (2010). Review of Particle Size Distribution Measurements of Engine Exhaust Before 1985. Chapter in: "*Aerosol Science and Technology: History and Reviews*" (Edited by David S. Ensor), RTI Press. https://doi.org/10.3768/rtipress.2011.bk.0003.1109.

Shaddix, C. R., & Smyth, K. C. (1996). Laser-induced incandescence measurements of soot production in steady and flickering methane, propane, and ethylene diffusion flames. *Combustion and Flame*, Vol. 107, 4, 418-452. https://doi.org/10.1016/S0010-2180(96)00107-1.

Shin, W. G., Pui, D. Y. H., Fissan, H., Neumann, S., & Trampe, A. (2007). Calibration and numerical simulation of Nanoparticle Surface Area Monitor (TSI Model 3550 NSAM). *J Nanopart Res*., 9, 61-69. https://doi.org/10.1007/s11051-006-9153-y.

Stein, C., Schröder, F., & Petzold, A. (2001). The Condensation Particle Size Analyzer: A New Instrument for the Measurement of Ultrafine Aerosol Size Distributions. *J. Aerosol Sci*., 32, S381-S382. https://doi.org/10.1016/S0021-8502(21)00175-0

Steiner, G., Orzan, M., Nagler, I., Petrakakis, E., Selimovic, M., Tauber, C., & Tettich, F. (2018). Improving airborne nanoparticle and cluster detection with the butanol based laminar flow condensation nuclei counters Grimm 5.403 and 5.412. Presentation at Aerosol Technology 2018, Bilbao, Spain, June 20, 2018.

Stipe, C. B., Higgins, B. S., Lucas, D., Koshland, C. P., & Sawyer, R. F. (2005). Inverted co-flow diffusion flame for producing soot. *Review of Scientific Instruments* 76, 023908. https://doi.org/10.1063/1.1851492.

Stolzenburg, M. R. (1988). An Ultrafine Aerosol Size Distribution Measuring System. *Ph.D. Thesis*, University of Minnesota, Minneapolis, Minnesota, USA, July 1988.

Stolzenburg, M. R., & McMurry, P. H. (1991). An Ultrafine Aerosol Condensation Nucleus Counter. *Aerosol Sci. Technol*., 14:1, 48-65. https://doi.org/10.1080/02786829108959470.

Takegawa, N., & Sakurai, H. (2011). Laboratory Evaluation of a TSI Condensation Particle Counter (Model 3771) Under Airborne Measurement Conditions. *Aerosol Sci. Technol.*, 45:2, 272-283. https://doi.org/10.1080/02786826.2010.532839.

Tröstl, J., Tritscher, T., Bischof, O. F., Horn, H.-G., Krinke, T. J., Baltensperger, U., & Gysel, M. (2015). Fast and Precise Measurement in the sub-20 nm Size Range using a Scanning Mobility Particle Sizer. *J. Aerosol Sci*., 87: 75-87. https://doi.org/10.1016/j.jaerosci.2015.04.001.

TSI Inc., Model 3068B Aerosol Electrometer, User's Manual P/N 6007222, Revision C, January 2016.

TSI Inc., Model 3076 Constant Output Atomizer, Instruction Manual P/N 1933076, Revision J, June 2005.

TSI Inc., Model 3783 Environmental Particle Counter Monitor Operation and Service Manual P/N 6003653, Revision E, September 2015.

TSI Inc., Model 3790 Engine Exhaust Condensation Particle Counter Operation and Service Manual P/N 1933802, Revision B, January 2007.

UN-ECE (2015). Regulation no. 83, Revision 5, 22 Jan 2015, United Nations - Economic Commissions for Europe.

VDI 3489 Part 2, Particulate matter measurement - Methods for characterizing and monitoring test aerosols - Continuous flow condensation nucleus counter, December 1995.

VDI 3867 Part 2, Measurement of particulate matter in ambient air - Methods for characterizing test aerosols - Determination of the particle number concentration and particle size distribution - Condensation Particle Counter (CPC), February 2008.

Verheggen, B., Cozic, J., Weingartner, E., Vana, M., Aalto, P., Hirsikko, A., Kulmala, M., Bischof, O. F., & Baltensperger, U. (2006). Observations of Atmospheric Nucleation Events in the Lower Free Troposphere. Poster EGU06-A-07606. *Geophysical Research Abstracts*, Vol. 8, 07606.

Vincent, J. H. (1995). *Aerosol Science for Industrial Hygienists* (1st Edition), Pergamon, Oxford, 1995.

Wang, S. C., & Flagan, R.C. (1990). Scanning Electrical Mobility Spectrometer. *Aerosol Sci. Technol*., 13:2, 230-240. https://doi.org/10.1080/02786829008959441.

Weigel, R., Hermann, M., Curtius, J., Voigt, C., Walter, S., Böttger, T., Lepukhov, B., Belyaev, G., & Borrmann, S. (2009). Experimental characterization of the COndensation Particle counting System for high altitude aircraft-borne application. *Atmos. Meas. Tech.,* 2, 243-258. https://doi.org/10.5194/amt-2-243-2009.

Weingartner, E., Baltensperger, U., & Burtscher, H. (1995). Growth and structural change of combustion aerosols at high relative humidity. *Environ. Sci. Technol.*, 29, 2982-2986. https://doi.org/10.1021/es00012a014.

Wiedensohler, A. (1988). An approximation of the bipolar charge distribution for particles in the submicron size range. *J. Aerosol Sci.* 19:3, 387-389. https://doi.org/10.1016/0021-8502(88)90278-9.

Wiedensohler, A., Lütkemeier, E., Feldpausch, M., & Helsper, C. (1986). Investigation of the Bipolar Charge Distribution at Various Gas Conditions. *J. Aerosol Sci.*, 17:3, 413-416. https://doi.org/10.1016/0021-8502(86)90118-7.

Wiedensohler, A., Orsini, D., Covert, D. S., Colmann, D., Cantrell, W., Havlicek, M., Brechtel, F. J., Russell, L. M., Weber, R. J., Gras, J., Hudson, J. G., & Litchy, M. (1997). Intercomparison study of the size-dependent counting efficiency of 26 condensation particle counters. *Aerosol Sci. Technol.*, 27:2, 224-242. https://doi.org/10.1080/02786829708965469.

Wilson, J. C., Hyun, J. H., & Blackshear, E. D. (1983). The function and response of an improved stratospheric condensation nucleus counter. *J. Geophys. Res*. 88, 6781. https://doi.org/10.1029/JC088iC11p06781.

Wimmer, D., Lehtipalo, K., Franchin, A., Kangasluoma, J., Kreissl, F., Kürten, A., Kupc, A., Metzger, A., Mikkilä, J., Petäjä, T., Riccobono, F., Vanhanen, J., Kulmala, M., & Curtius, J. (2013). Performance of diethylene glycol-based particle counters in the sub-3 nm size range. *Atmos. Meas. Tech*., 6, 1793-1804, https://doi.org/10.5194/amt-6-1793-2013.

Winkler, P. M., Hienola, A., Steiner, G., Hill, G., Vrtala, A. Reischl, G. P., Kulmala, M., & Wagner, P. E. (2008). Effects of seed particle size and composition on heterogeneous nucleation of *n*-nonane. *Atmos. Res*. 90: 2-4, 187-194. https://doi.org/10.1016/j.atmosres.2008.02.001.

Zhang, R., Khalizov, A. F., Pagels, J., Zhang, D., Xue, H., & McMurry, P. H. (2008). Variability in Morphology, Hygroscopicity, and Optical Properties of Soot Aerosols during Atmospheric Processing. *Proc. Natl. Acad. Sci. USA*, 105: 30, 10291-10296. https://doi.org/10.1073/pnas.0804860105.

Zhang, Z. Q., & Liu, B. Y. H. (1991). Performance of TSI 3760 Condensation Nuclei Counter at Reduced Pressures and Flow Rates. *Aerosol Sci. Technol.*, 15:4, 228-238. https://doi.org/10.1080/02786829108959530.

Zhang, Z. Q., & Liu, B.Y.H. (1990). Dependence of the performance of TSI 3020 condensation nucleus counter on pressure, flow rate, and temperature. *Aerosol Sci. Technol.*, 13:4, 493-504. https://doi.org/10.1080/02786829008959464.

List of Tables

List of Figures

Band / Volume 566
Cirrus clouds in the extratropical tropopause and lowermost stratosphere region
I. Bartolomé García (2022), iii, 155 pp
ISBN: 978-3-95806-610-6

Band / Volume 567
Stationary and Transient Behaviour of Polymer Electrolyte Fuel Cells
Y. Shi (2022), viii, 172 pp
ISBN: 978-3-95806-611-3

Band / Volume 568
14th Carolus Magnus Summer School on Plasma and Fusion Energy Physics
D. Reiser (Ed.), (2022), 207 pp
ISBN: 978-3-95806-613-7

Band / Volume 569
Spectral induced polarization of calcite precipitation in porous media
S. Izumoto (2022), xviii, 106 pp
ISBN: 978-3-95806-614-4

Band / Volume 570
Technische und ökonomische Bewertung der Polymer-Elektrolyt-Membran Elektrolyse
S. M. Saba (2022), IV, 263 pp
ISBN: 978-3-95806-615-1

Band / Volume 571
Advanced Sintering of Garnet-Based Ceramic Composite Cathodes for All-Solid-State Lithium Batteries
M. Ihrig (2022), VIII, 160 pp
ISBN: 978-3-95806-616-8

Band / Volume 572
Developing an integrated value-based institutional framework for analyzing nexus governance challenges – the case study of Germany
C. Märker (2022), 290 pp
ISBN: 978-3-95806-617-5

Band / Volume 573
Ecological sanitation via thermophilic co-composting of humanure and biochar as an approach to climate-smart agriculture
D. Castro Herrera (2022), XVIII, 127 pp
ISBN: 978-3-95806-622-9

Band / Volume 574
Towards 3D crosshole GPR full-waveform inversion
A. Mozaffari (2022), viii, 122 pp
ISBN: 978-3-95806-623-6

Band / Volume 575
Investigations of the atmospheric OH, HO2 and RO2 radical chemical budgets and their impact on tropospheric ozone formation in a rural area in West-Germany in the JULIAC 2019 campaign
C. Cho (2022), 182 pp
ISBN: 978-3-95806-625-0

Band / Volume 576
Thermochemische Beständigkeit von Carbonat-Keramik-Membranen für die CO_2-Abtrennung in Wassergas-Shift-Reaktoren
U. Gude (2022), X, 176, LXIII pp
ISBN: 978-3-95806-626-7

Band / Volume 577
Neue Ziele auf alten Wegen?
Strategien für eine treibhausgasneutrale Energieversorgung bis zum Jahr 2045
D. Stolten, P. Markewitz, T. Schöb, F. Kullmann, S. Risch, T. Groß, M. Hoffmann, D. Franzmann, T. Triesch, S. Kraus, R. Maier, B. Gillessen, H. Heinrichs, N. Pflugradt, T. Grube, J. Linssen, L. Kotzur (2022), VI, 81 pp
ISBN: 978-3-95806-627-4

Band / Volume 578
Improving stationary and mobile cosmic ray neutron soil moisture measurements
Assessment of the cosmic ray neutron uncertainty
and the potential of the thermal neutron signal
J. C. Jakobi (2022), xxiii, 137 pp
ISBN: 978-3-95806-628-1

Band / Volume 579
Application-Specific Calibration of Condensation Particle Counters under Low Pressure Conditions
O. B. F. Bischof (2022), ix, 137 pp
ISBN: 978-3-95806-629-8

Energie & Umwelt / Energy & Environment
Band / Volume 579
ISBN 978-3-95806-629-8

Mitglied der Helmholtz-Gemeinschaft

JÜLICH
Forschungszentrum